Máster Universitario en Física y Matemáticas

Trabajo de fin de Máster

Facultad de ciencias

Interacting Anyons in a one-dimensional optical lattice

María del Pilar Martín Clavero

Supervised by: Alberto Rodríguez González

July 2025

Máster Universitario en Física y Matemáticas

Trabajo de fin de Máster

Facultad de ciencias

Interacting Anyons in a one-dimensional optical lattice

María del Pilar Martín Clavero

Supervised by: Alberto Rodríguez González

July 2025

Abstract

This thesis is devoted to the study of the structural properties of the ground state of anyonic matter in one dimension, governed by the *Anyonic-Hubbard model*, simulated by a modified version of the Bose-Hubbard Hamiltonian in which the tunneling strengths become occupation dependent.

In order to describe quantum many-body systems of interacting particles, we acquire some of the most important notions on the *second quantization formalism*. We define the *Fock space* and its associated field operators, as well as their commutation algebra and their action on *Fock states*. The latter formalism is used to construct the general form of a many-body Hamiltonian in second quantization, particularizing to derive the *Bose-Hubbard Hamiltonian*, and to analyze the emergence of Mott insulating and superfluid phases. The importance of understanding the structural properties in Fock space of many-body states is remarked, and the concept of *multifractality* is introduced.

Having understood these fundamental concepts, which are initially applied to bosons, the possibility of *fractional statistics* in low dimensional systems is discussed, giving rise to particles with intermediate statistics between bosonic and fermionic, called *anyons*. The Anyonic-Hubbard model is presented, whose physics can be emulated by means of bosonic operators, using a modified version of the Bose-Hubbard Hamiltonian including a *statistical angle*, which determines the anyonic behavior of the system. The method by which the Anyonic-Hubbard model can be experimentally implemented is described, as well as some of the most interesting results obtained with anyons in the laboratory.

We then perform a series of numerical simulations and analytical calculations to study the properties of the ground state of the anyonic system. First, an approximate phase diagram delimiting the Mott insulator and superfluid phases as functions of the statistical angle is obtained using *mean field theory*.

In order to understand the Fock space structure of the ground state, we calculate numerically some *generalized fractal dimensions* as functions of the system parameters, and further obtain an analyitical expression of the generalized fractal dimensions in the strongly-interacting regime using perturbation theory.

An extensive analysis of the dependence of the ground state generalized fractal dimensions on interaction strength, statistical angle and particle density, provides strong evidence of the existence of multifractality, which characterizes the structural changes of the state when modifying the system parameters, and serves to reveal the emergence of Mott insulating and superfluid phases in the anyonic system.

Finally, the evolution of the generalized fractal dimensions when changing particle interaction is studied to determine whether it encodes the information of the critical point of

the Mott insulator to superfluid phase transition, and to establish to which extent this approach can provide an accurate description of the dependence of the transition point on the statistical angle.

Keywords: Bose-Hubbard Hamiltonian, anyons, generalized fractal dimensions, localization, Fock space, Anyonic-Hubbard Hamiltonian, Mott insulator, superfluid.

Resumen

Este trabajo está dedicado al estudio de las propiedades estructurales del estado fundamental de materia anyonica en una dimensión, gobernada por el *modelo Anyonic-Hubbard*, simulado a través de una versión modificada del Hamiltoniano de Bose-Hubbard en la que la fuerza de tunneling es dependiente del número de ocupación.

Para poder describir sistemas cuánticos de muchos cuerpos con interacción, primero adquirimos los conocimientos imprescindibles acerca del formalismo conocido como *segunda cuantización*. Definimos el *espacio de Fock* y sus operadores de campo asociados, así como su álgebra de conmutación y su operación sobre los *estados de Fock*. Este formalismo se utiliza para construir la forma general de un Hamiltoniano en segunda cuantización para un sistema de muchos cuerpos, particularizando esta construcción para el Hamiltoniano de Bose-Hubbard, para el cual analizamos la aparición de las fases de aislante de Mott y estado superfluido. Remarcamos la importancia del estudio de las propiedades estructurales de los estados de muchos cuerpos en el espacio de Fock, e introducimos el concepto de *multifractalidad*.

Una vez que estos conceptos fundamentales han sido comprendidos, que en un principio se aplican solo a sistemas bosónicos, se discute la posibilidad de la existencia de *estadística fraccionaria* en sistemas de dimensión baja, que dan lugar a partículas con estadística intermedia entre bosónica y fermiónica, conocidas como *anyones*. Se presenta el modelo Anyonic-Hubbard, cuya física puede emularse utilizando una versión modificada del Hamiltoniano de Bose-Hubbard en el que se incluye un *ángulo estadístico*, encargado de determinar el comportamiento anyonico del sistema. Se describe el método que permite la implementación experimental del modelo Anyonic-Hubbard, así como algunos de los resultados más interesantes a los que estos experimentos con anyones en el laboratorio han dado lugar.

Después, procedemos al desarrollo de una serie de simulationes numéricas y de cálculos analíticos para estudiar las propiedades del estado fundamental del sistema anyonico. Primero, utilizando la *teoría de campo medio* se obtiene un diagrama de fases aproximado, en el que se representa el límite entre las fases de asilante de Mott y superfluida como funciones del ángulo estadístico.

Con el propósito de comprender la estructura del estado fundamental en el espacio de Fock, calculamos numéricamente algunas *dimensiones fractales generalizadas* como función de los distintos parámetros del sistema, y posteriormente se obtiene una expresión analítica para dichas dimensiones fractales generalizadas en el límite de altas interacciones, utilizando teoría de perturbaciones.

Un análisis extensivo de la dependencia de las dimensiones fractales generalizadas en el estado fundamental con la fuerza de tunneling, ángulo estadístico y densidad de partículas da como resultado una clara evidencia de la existencia de multifractalidad, que caracteriza los cambios estructurales en el estado cuando se modifican los parámetros del sistema, y que sirve para revelar la aparición de fases de aislante de Mott y superfluidas en el sistema anyonico.

Finalmente, la evolución de las dimensiones fractales generalizadas cuando se varía la interacción entre partículas es estudiada con el objetivo de determinar si dicha evolución contiene información sobre el punto crítico de la transición entre las fases de aislante de Mott y superfluida, así como hasta qué punto este tratamiento es capaz de proporcionar una descripción precisa de la dependencia del punto de transición con el ángulo estadístico.

Palabras clave: Hamiltoniano Bose-Hubbard, anyones, dimensiones fractales generalizadas, localización, espacio de Fock, Hamiltoniano Anyonic-Hubbard, aislante de Mott, superfluido.

Contents

Abstract **i**

Resumen **iii**

1 Introduction **1**
- 1.1 Scientific context . . . 1
- 1.2 Objectives and thesis structure . . . 3

2 System of interacting bosons **5**
- 2.1 Second quantization formalism . . . 5
  - 2.1.1 Creation and annihilation operators. Fock space . . . 5
  - 2.1.2 Quantization of the single-particle wavefunction . . . 7
  - 2.1.3 Field operators in different bases . . . 8
  - 2.1.4 Many body Hamiltonian in second quantization . . . 10
- 2.2 The Bose-Hubbard Hamiltonian . . . 12
  - 2.2.1 Symmetries of the Bose-Hubbard Hamiltonian . . . 16
  - 2.2.2 Mott insulator to superfluid phase transition . . . 17
- 2.3 Characterization of the eigenstate structure: Multifractality . . . 22

3 Anyons in low dimensions **29**
- 3.1 Fractional statistics . . . 29
- 3.2 Lattice anyons in one dimension . . . 33
  - 3.2.1 Anyonic-Hubbard model . . . 33
  - 3.2.2 Experimental realization . . . 37

4 Physical properties of the anyonic ground state **43**
- 4.1 Superfluid to Mott insulator transition: Mean-field calculation . . . 43
- 4.2 Multifractality in the Anyonic-Hubbard ground state . . . 47
  - 4.2.1 Ground state structure and multifractality versus J/U for different values of θ . . . 49
  - 4.2.2 Perturbation theory . . . 51
  - 4.2.3 Evolution of the generalized fractal dimensions with particle density and statistical angle . . . 58
- 4.3 Mott insulator to superfluid transition via multifractality: Estimation of the critical point . . . 61

5 Conclusions **69**

Bibliography **71**

A Anyonic-Hubbard Hamiltonian in terms of bosonic operators. Jordan-Wigner transformation. **75**

B Perturbation theory calculation of the ground state **81**

B.1 First-order correction 82

B.2 Second-order correction 83

C Numerical resources **89**

List of Figures

1.1 Single-site resolution of Mott shells . . . 2

2.1 One-dimensional optical lattice . . . 12
2.2 Boundary conditions . . . 13
2.3 Wannier states in an optical lattice . . . 13
2.4 Scheme of the Bose-Hubbard Hamiltonian . . . 16
2.5 Mott lobes of the Bose-Hubbard Hamiltonian for integer density . . . 23
2.6 Generalized fractal dimensions D_q as functions of q. . . . 25
2.7 Finite-size generalized fractal dimensions $\tilde{D}_q$ in the ground state of the BHH at unit density as functions of J/U, for different values of q. . . . 26
2.8 Squared amplitudes as a function of the basis index for a system with $L = 7$ and $\nu = 1$ for two different tunneling strengths. . . . 27

3.1 Relative motion of two identical particles in three dimensions . . . 31
3.2 Relative motion of two identical particles in two dimensions . . . 31
3.3 Some possible paths of two particles in two dimensions, with and without interchanges. . . . 32
3.4 Single-particle spectrum and group velocity as functions of the single-particle momenta in a one-dimensional system with anyonic excitations. . . 32
3.5 Different paths followed by two particles in one dimension, with and without crossings. . . . 33
3.6 Illustration of the phase acquired by anyons . . . 35
3.7 Phase acquisition for anyons hopping along closed paths in Fock space. . . 36
3.8 Realization of anyons in one dimension . . . 38
3.9 Experimental sequence with the AHH . . . 39
3.10 Quantum walks of two anyons for $U = 0$ . . . 39
3.11 Interferometric picture of the Fock state evolution . . . 41
3.12 Quantum walks of two anyons for $U \neq 0$ . . . 41
3.13 Anyonic transport as a function of θ and U. . . . 42

4.1 Mott lobes for different values of θ obtained with mean-field theory . . . 48
4.2 Critical points $(J/U)_c$ for the Mott insulator to superfluid phase transition obtained from mean-field theory . . . 49
4.3 Generalized fractal dimensions $\tilde{D}_1$, $\tilde{D}_2$ and $\tilde{D}_\infty$ versus J/U for different lattice sizes and statistical angles, for fixed integer density $\nu = 1$. . . . 50
4.4 Ground state intensities $|\varphi_{j(\mathbf{n})}|^2$ versus basis index $j(\mathbf{n})$. . . . 52
4.5 Comparison between perturbation theory and exact diagonalization for different J/U values and lattice sizes as a function of θ. . . . 56

4.6 Comparison between perturbation theory and exact diagonalization for different θ values and lattice sizes as a function of J/U. 57
4.7 $\tilde{D}_1$ and $\tilde{D}_\infty$ comparison between perturbation theory and exact diagonalization for different θ values as a function of J/U, for $L = N = 5$ and $L = N = 7$. 58
4.8 Density plots of $\tilde{D}_1$ as a function of J/U and the density ν, for different statistical angles. 59
4.9 $\tilde{D}_1$ versus density ν for $L = 7$ and different J/U values and statistical angles 60
4.10 $\tilde{D}_1$ versus J/U for different statistical angles and lattice sizes. 61
4.11 $\tilde{D}_1$ versus J/U and θ for integer densities $\nu = 1$ and $\nu = 2$, using hard wall boundary conditions. 62
4.12 $\tilde{D}_1$ and its derivative versus J/U for $\theta = 0$ and different sizes. Scaling law of the position of the derivative maximum. 64
4.13 $\tilde{D}_1$ and its derivative versus J/U for $\theta = 0.02\pi$ and different sizes. Scaling law of the position of the derivative maximum. 66
4.14 $\tilde{D}_1$ and its derivative versus J/U for $\theta = 0.04\pi$ and different sizes. Scaling law of the position of the derivative maximum. 67
4.15 Position of the maximum for the derivative of $\tilde{D}_1$ as function of L, for several values of the statistical angle θ. 68

List of Tables

2.1 Estimations of the critical point from theoretical and experimental studies. 23

4.1 Intensities contributing to $|\phi_{gs}|^2$, $|\langle \mathbf{n}|\phi_{gs}\rangle|^2$, and their multiplicities 55
4.2 Information on the Padé fits of Fig. 4.12. 63
4.3 Information on the Padé fits of Fig. 4.13. 66

C.1 Computational resources required to obtain the ground state of Hamiltonian (3.13) for different L at unit density by exact diagonalization. 89

1 | Introduction

1.1 Scientific context

Strongly correlated quantum systems represent a frequent object of study in diverse fields, such as physics or chemistry. Such highly interacting systems are extremely non-trivial, and generally do not admit an analytical solution [1, 2]. For this reason, advanced numerical techniques are required in order to comprehend these many-body systems, which usually demand resources that scale exponentially with the number of constituents (i.e., particles), rendering greatly difficult to make theoretical advances in the understanding of the system's physics.

Since theoretical studies are often limited, state-of-the-art experimental methods have recently enabled reliable simulations of strongly correlated systems. In this way, configurations of ultracold atoms in optical potentials provide a useful tool to mimic complex many-body systems [3–5]. For instance, these ultracold atoms can play the role of electrons in a solid crystal, which is simulated by the optical lattice [6]. The high degree of controllability of this experimental platform allows to observe and measure many different phenomena that otherwise would be rather inaccessible in a real solid due to undesired effects, such as disorder, or simply the extremely reduced length and time scales involved.

Ultracold atoms in optical lattices have been used to implement paradigmatic many-body Hamiltonians, the Bose-Hubbard model (describing interacting bosons) being the prominent one. With this quantum simulation, several bosonic macroscopic phenomena may be experimentally studied. Particularly, it was observed that the ground state of the Bose-Hubbard system, by varying the interparticle interaction, transitions from a Mott insulator to a superfluid [7–9]. In this case, advanced microscopy techniques [10, 11] allow the extraction of high-resolution images of the system's single-site configuration, as for instance the ones shown in Fig. 1.1, where the structures known as *Mott shells* are displayed [12].

Besides bosonic systems, other archetypic fermionic models, such as the Fermi-Hubbard Hamiltonian, have also been realized with ultracold atoms [13, 14]. However, recent experimental works demonstrate that possibilities are not reduced to just fermionic and bosonic systems [15, 16]. In fact, theoretical approaches have for long concluded that quantum theory must allow, at least in low dimensional systems, the existence of particles with intermediate statistics between fermionic and bosonic, which are called *anyons* [17–20]. At first, the existence of these particles was believed to be restricted to two-dimensional systems, however it was later shown that fractional statistics may also emerge in one dimension [20, 21].

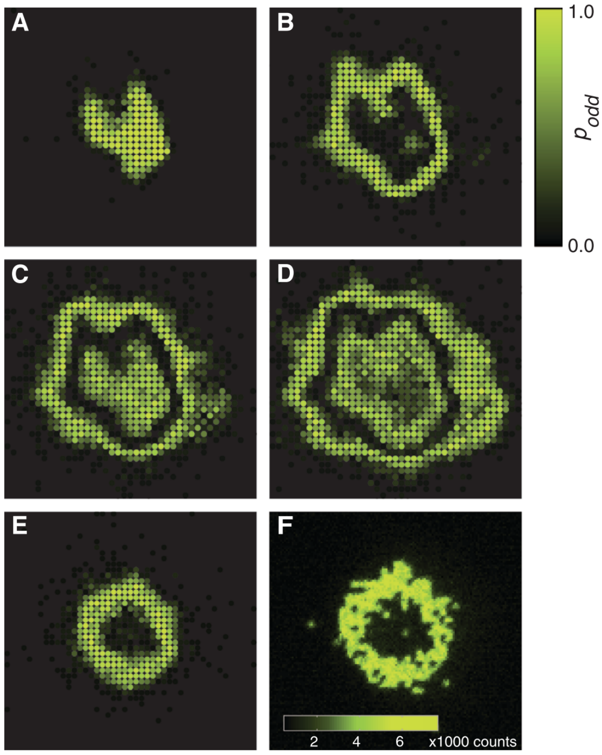

Figure 1.1: Single-site resolution of Mott shells obtained with fluorescence imaging, using ultracold atoms in an optical lattice. Image taken from Ref. [12]

Remarkably, anyons are not restricted to theoretical proposals based on quantum statistics theory but can also be observed in the laboratory, for example in systems exhibiting the so called *fractional quantum Hall effect* [19, 20]. Moreover, one experimental work has been carried out in a system analogous to the Bose-Hubbard model but describing anyons, referred to as the Anyonic-Hubbard model (although restricted to only two particles), which was implemented with ultracold atoms in a one-dimensional optical lattice [15]. The latter experiment and some theoretical approaches [22–25] have been useful to unveil some properties of the Anyonic-Hubbard model, such as the predicted existence of the ground state Mott insulating and superfluid phases, in analogy with the phenomena observed for the Bose-Hubbard model.

In order to understand the physics of strongly correlated quantum many-body systems, many theoretical approaches are devoted to the study of their energy spectra and the structure of the corresponding eigenstates, since these fundamentally determine the dynamical response of the system and may also reveal the emergence of different macroscopic phases. Particularly, the multifractal formalism provides detailed information regarding the structure of many-body eigenstates, and has been successfully employed to characterize quantum phase transitions [26–28] as well as the appearance of ergodic (chaotic) and non-ergodic phases [29–33] in quantum many-body systems. However, multifractality has not yet been studied in anyonic models, and thus will be one of the main topics analyzed in this work.

1.2 Objectives and thesis structure

The purpose of this work is to study the Mott insulator to superfluid phase transition in the one-dimensional Anyonic-Hubbard model, as well as to determine whether the structure of the system's ground state encodes information of the critical point for which the transition occurs. For this purpose, we analyze the emergence of *multifractality* in the ground state by studying numerically and analitically the evolution of the *generalized fractal dimensions* with the system parameters, including interaction strength, statistical phase θ and particle density.

In Chapter 2, we give the fundamental ideas regarding the second quantization formalism, introducing Fock space as well as creation and annihilation operators. Then, we describe the procedure by which one can quantize the single-particle wavefunction, and the concept of *field operators* and their expression in different bases. These operators are used to build a general many-body Hamiltonian in second quantization. Particularly, we derive the Bose-Hubbard Hamiltonian and explain the physical meaning of each of its terms, as well as its symmetries. We also discuss the emergence of a Mott insulator to superfluid phase transition in the Bose-Hubbard ground state. Finally, the concept of *multifractality* is introduced and related to the main structural properties of the eigenstates of a system.

In Chapter 3 we introduce the existence of a particle with statistics beyond bosonic and fermionic, which receives the name of *anyon*. In order to do this, we postulate the possibility of having *fractional statistics* for two and one-dimensional systems via topological arguments. We present the model ruling systems formed by anyons, the *Anyonic-Hubbard model*, for which we write the standard Hamiltonian and then derive the form of a modified Bose-Hubbard model describing the same physics. After elaborating on the symmetries of the system, the experimental implementation of the model is described along with the main experimental results.

In Chapter 4 we perform a series of numerical simulations and analytical calculations that allow us to understand the structural properties of the ground state of the system and their macroscopic manifestations. First, we make use of *mean-field theory* to determine an approximate phase diagram of the θ-dependent Bose-Hubbard model, from which we intend to obtain the system parameters that define the border between the Mott insulator and superfluid phases.

We numerically analyze the emergence of multifractality in the system's ground state. For this purpose, we fix the statistical angle characterizing the anyonic behavior of the particles, and modify the tunneling strength to study the evolution of the generalized fractal dimensions.

Afterwards, we look for an approximate analytical expression, valid in the strong interacting limit, of the ground state of the system, which is in turn used to derive an analytical description of the generalized fractal dimensions, whose validity is established by comparing against exact numerical results.

Further numerical simulations study the evolution of the generalized fractal dimensions with particle density, statistical angle and tunneling strength from different points of view, relating the observations to the possible emergence of Mott insulating and superfluid phases in the system, and in connection with previous results reported in literature.

In the last part of Chapter 4 we determine whether the evolution of the generalized fractal dimensions can be used to determine the critical point of the Mott insulator to superfluid phase transition.

Finally, in Chapter 5 we summarize the main conclusions that can be drawn from the results obtained throughout the work. Detailed technical derivations of certain analytical results, as well as useful information on the numerical simulations are provided in several appendices at the end of the document.

2 | System of interacting bosons

The aim of this chapter is to introduce the main ideas of the *second quantization formalism*, and then use them to derive the form of the Bose-Hubbard Hamiltonian. In the following, we will explain the concept of *multifractality* and its relevance to understanding the structure of the eigenstates of a system.

2.1 Second quantization formalism

2.1.1 Creation and annihilation operators. Fock space

In order to describe many-body systems, it is usual to draw on the *second quantization* formalism [1], which consists in making use of operators rather than wavefunctions. For the purpose of understanding such formalism, we will first introduce the *Fock space*.

For a system formed by N indistinguishable particles, the Fock space is a collection of Hilbert spaces,

$$\mathcal{H} = \mathcal{H}_0 \oplus \mathcal{H}_1 \oplus \mathcal{H}_2 \oplus \ ... \ \oplus \mathcal{H}_N \oplus \ ... \ , \tag{2.1}$$

where $\mathcal{H}_N$ is the Hilbert space for N identical particles. Hence, a general element in Fock space takes the form

$$|\Psi\rangle = \sum_{N=0}^{\infty} c_N |\psi_N\rangle, \quad \text{for } |\psi_N\rangle \in \mathcal{H}_N. \tag{2.2}$$

The states $|\psi_N\rangle$ with different particle number N are orthogonal. Thus,

$$\langle\psi_M|\psi_N\rangle = 0 \text{ for } M \neq N. \tag{2.3}$$

The space with 0 particles, $\mathcal{H}_0$, has only one element, $|0\rangle$, usually referred to as the vacuum. It is now a good point to remark the difference between the vacuum, the state corresponding to having 0 particles, and the null ket, $|\varnothing\rangle = 0$, which is the state which has all $c_N = 0$ in Eq. (2.2).

A general element in Fock space can be described as a time-independent set of occupation numbers,

$$|\mathbf{n}\rangle \equiv |n_1, n_2, ..., n_N, ...\rangle, \tag{2.4}$$

which indicates there are n_l particles in a certain single-particle state $|l\rangle$, and must fulfill

$$\langle n_1, n_2, ..., n_N, ...|n'_1, n'_2, ..., n'_N, ...\rangle = \delta_{n_1,n'_1}\delta_{n_2,n'_2}...\delta_{n_N,n'_N}..., \tag{2.5}$$

$$\sum_{n_1,n_2,...} |n_1, n_2, ..., n_N, ...\rangle\langle n_1, n_2, ..., n_N, ...| = \mathbb{I} \tag{2.6}$$

to span an orthonormal basis of $\mathcal{H}$.

The kets of Eq. (2.4) can be constructed systematically after defining a set of operators $\hat{d}_l^{(\dagger)}$ associated with the chosen single-particle states $|l\rangle$, obeying[1]

$$[\hat{d}_l, \hat{d}_k]_\pm = [\hat{d}_l^\dagger, \hat{d}_k^\dagger]_\pm = 0, \tag{2.7}$$

$$[\hat{d}_l, \hat{d}_k^\dagger]_\pm = \delta_{lk}, \tag{2.8}$$

where one chooses the commutation algebra to describe bosons and the anticommutation algebra to describe fermions. Then, the number operator is defined as

$$\hat{n}_l \equiv \hat{d}_l^\dagger \hat{d}_l, \tag{2.9}$$

which is non-negative and self adjoint, and thus obeys

$$\hat{n}_l|n_l\rangle = n_l|n_l\rangle, \quad n_l \geq 0. \tag{2.10}$$

In this section we will restrict ourselves to the bosonic case. Hence, we will work with the commutation algebra, and we will rename our creation/annihilation operators as $\hat{d}_l^{(\dagger)} \equiv \hat{b}_l^{(\dagger)}$. Consequently, our commutation algebra reads

$$[\hat{b}_l, \hat{b}_k] = [\hat{b}_l^\dagger, \hat{b}_k^\dagger] = 0, \tag{2.11a}$$

$$[\hat{b}_l, \hat{b}_k^\dagger] = \delta_{lk}. \tag{2.11b}$$

It is easy to prove that

$$[\hat{n}_l, \hat{b}_k] = -\delta_{lk}\hat{b}_l, \tag{2.12a}$$

$$[\hat{n}_l, \hat{b}_k^\dagger] = \delta_{lk}\hat{b}_l^\dagger, \tag{2.12b}$$

$$[\hat{n}_l, \hat{n}_k] = 0. \tag{2.12c}$$

By making use of these commutation relations, one can deduce the action of the operators $\hat{b}_l^{(\dagger)}$ on the eigenstates $|n_l\rangle$ of the corresponding number operator,

$$\hat{b}_l^\dagger|n_l\rangle = \sqrt{n_l+1}|n_l+1\rangle, \tag{2.13}$$

$$\hat{b}_l|n_l\rangle = \sqrt{n_l}|n_l-1\rangle. \tag{2.14}$$

From the latter expressions, one can reason that there must exist a state $|0\rangle$ such that $\hat{b}_l|0\rangle = 0$, otherwise $\hat{n}_l$ could have negative eigenvalues, which is not possible since $\hat{n}_l$ is a non-negative operator. As a consequence, the eigenvalues n_l of the number operators must be non-negative integers, $n_l \in \mathbb{N}_0$. Hence, the eigenvalues n_l can be associated with the occupancy of the single-particle state $|l\rangle$, and Eqs. (2.13) and (2.14) indicate that the

[1] Recall the definition of the commutator ($-$) and anticommutator ($+$), $[A, B]_\pm = AB \pm BA$. We shall be using also $[A, B]$ to refer to the commutator.

operators $\hat{b}_l$ and $\hat{b}_l^\dagger$ destroy and create, respectively, a particle in that state. Consequently, the state $|n_l\rangle$ is built using

$$|n_l\rangle = \frac{1}{\sqrt{n_l!}}(\hat{b}_l^\dagger)^{n_l}|0\rangle, \tag{2.15}$$

and the operator $\hat{n}_l$ is hence referred to as the number operator.

Since the number operators of different single-particle states always commute, it is possible to diagonalize them simultaneously. Thus, in view of Eq. (2.15), it can be concluded that one may construct the states of Eq. (2.4) as the tensor product of the eigenstates of the number operators,

$$|n_1, n_2, ..., n_N, ...\rangle = |n_1\rangle \otimes |n_2\rangle \otimes \; ... \; \otimes |n_N\rangle \otimes \; ... \; , \tag{2.16}$$

which are usually called *Fock states*. The creation/annihilation and number operators act on Fock states as

$$\hat{b}_l^\dagger|n_1, n_2, ..., n_N, ...\rangle = \sqrt{n_l + 1}\; |n_1, n_2, ..., n_l + 1, ..., n_N, ...\rangle, \tag{2.17}$$

$$\hat{b}_l|n_1, n_2, ..., n_N, ...\rangle = \sqrt{n_l}\; |n_1, n_2, ..., n_l - 1, ..., n_N, ...\rangle, \tag{2.18}$$

$$\hat{n}_l|n_1, n_2, ..., n_N, ...\rangle = n_l\; |n_1, n_2, ..., n_l, ..., n_N, ...\rangle. \tag{2.19}$$

2.1.2 Quantization of the single-particle wavefunction

The second quantization formalism presented in 2.1.1 can be understood as emerging from the quantization of the single-particle wavefunction [1].

In Quantum Mechanics, one can expand a single-particle state in a complete basis,

$$|\psi(t)\rangle = \sum_m \langle m|\psi(t)\rangle\; |m\rangle \equiv \sum_m c_m(t)|m\rangle. \tag{2.20}$$

In this basis, the Schrödinger equation reads

$$i\hbar\; \dot{c}_n(t) = \sum_m \langle n|H|m\rangle c_m(t), \tag{2.21}$$

$$i\hbar\; \dot{c}_n^*(t) = -\sum_m \langle m|H|n\rangle c_m^*(t), \tag{2.22}$$

where H denotes the single-particle Hamiltonian.

One can now write the energy of the state $|\psi(t)\rangle$ as a function of the c_n coefficients,

$$H(\mathbf{c}, \mathbf{c}^*) \equiv \langle H\rangle_{\psi(t)} = \sum_{l,m} c_m^* \langle m|H|l\rangle c_l. \tag{2.23}$$

Using Eqs. (2.21), (2.22) and (2.23), it follows that the equations of motion for c_n and c_n^* are

$$\dot{c}_n = \frac{\partial H(\mathbf{c}, \mathbf{c}^*)}{\partial(i\hbar\; c_n^*)}, \quad i\hbar\; \dot{c}_n^* = -\frac{\partial H(\mathbf{c}, \mathbf{c}^*)}{\partial(c_n)}, \tag{2.24}$$

which can be seen as the classical equations of motion

$$\dot{q}_n = \frac{\partial H}{\partial p_n}, \quad \dot{p}_n = -\frac{\partial H}{\partial q_n} \tag{2.25}$$

of the canonically conjugated variables $q_n \equiv c_n$ and $p_n \equiv i\hbar\, c_n^*$.

In order to quantize these variables, one only has to take the amplitudes c_n and c_n^* to be operators,

$$c_n \longrightarrow \hat{b}_n, \quad i\hbar\, c_n \longrightarrow i\hbar\, \hat{b}_n^\dagger, \tag{2.26}$$

and apply the canonical quantization rule turning the Poisson brackets into commutators,

$$\{q_n, p_m\} = \delta_{nm} \longrightarrow [\hat{q}_n, \hat{p}_m] = i\hbar\, \delta_{nm}, \tag{2.27}$$

leading to

$$\begin{aligned}
[\hat{b}_n, \hat{b}_m] &= [\hat{b}_n^\dagger, \hat{b}_m^\dagger] = 0, \\
[\hat{b}_n, \hat{b}_m^\dagger] &= \delta_{nm},
\end{aligned}$$

which corresponds to the commutation algebra previously introduced.

In view of Eqs. (2.23) and (2.26), the single-particle Hamiltonian in second quantization reads

$$\hat{H} = \sum_{n,m} \hat{b}_m^\dagger \langle m|H|n\rangle \hat{b}_n, \tag{2.28}$$

in terms of the matrix elements of the single-particle Hamiltonian H in first quantization.

Using this new form of the Hamiltonian, it is easy to check that the Heisenberg equations of motion for the operators $\hat{b}_k$ match the time evolution of the single-particle amplitudes. In other words,

$$i\hbar\, \dot{\hat{b}}_l(t) = \sum_n \langle l|H|n\rangle \hat{b}_n(t), \tag{2.29}$$

$$i\hbar\, \dot{\hat{b}}_l^\dagger(t) = -\sum_n \langle n|H|l\rangle \hat{b}_n^\dagger(t). \tag{2.30}$$

From this point on, will refer to the second quantized creation/annihilation operators as *field operators*.

2.1.3 Field operators in different bases

In the same way as a single-particle state can be written in different orthonormal bases,

$$|\psi\rangle = \sum_r c_r |r\rangle = \sum_s \tilde{c}_s |\tilde{s}\rangle, \tag{2.31}$$

$$\tilde{c}_s = \langle \tilde{s}|\psi\rangle = \sum_r \langle \tilde{s}|r\rangle\langle r|\psi\rangle = \sum_r \langle \tilde{s}|r\rangle c_r, \tag{2.32}$$

one can use the same unitary transformation to express the field operators that destroy/create particles in a different basis,

$$\hat{f}_s = \sum_r \langle \tilde{s}|r\rangle \hat{d}_r. \tag{2.33}$$

The operators $\hat{f}_s^\dagger$ and $\hat{f}_s$, respectively, create and destroy a particle in the single-particle state $|\tilde{s}\rangle$. Analogously, the operators $\hat{d}_r^\dagger$ and $\hat{d}_r$ create and destroy a particle in the single-particle state $|r\rangle$.

The operators in the new basis obey

$$[\hat{f}_s, \hat{f}_r^\dagger]_\pm = \sum_{r,r'} \langle \tilde{s}|r\rangle\langle r'|\tilde{t}\rangle [\hat{d}_r, \hat{d}_{r'}^\dagger]_\pm = \sum_{r,r'} \langle \tilde{s}|r\rangle\langle r'|\tilde{t}\rangle \delta_{rr'} = \langle \tilde{s}|\tilde{t}\rangle = \delta_{st}. \tag{2.34}$$

Thus, unitary basis transformations preserve the commutation or anticommutation algebra.

A particularly relevant single-particle basis is the position basis $\{|x\rangle\}$. Recall that, for a $D-$dimensional system,

$$|\psi\rangle = \int d^D x \; \langle x|\psi\rangle |x\rangle = \int d^D x \; \psi(x)|x\rangle, \tag{2.35}$$

where

$$\langle x'|x\rangle = \delta^D(x - x') \; , \quad \int d^D x |x\rangle\langle x| = \mathbb{I}.$$

As before, we can write

$$\psi(x) \equiv \langle x|\psi\rangle = \sum_r \langle x|r\rangle c_r, \tag{2.36}$$

which in terms of the field operators reads

$$\hat{\psi}(x) = \sum_r \langle x|r\rangle \hat{d}_r \equiv \sum_r \phi_r(x)\hat{d}_r, \tag{2.37}$$

where $\phi_r(x) \equiv \langle x|r\rangle$ is the representation of $|r\rangle$ in real space (i.e., the wavefunction of $|r\rangle$). We denote the creation/annihilation fields in the continuum real space basis $\{|x\rangle\}$ by $\hat{\psi}^{(\dagger)}(x)$, which destroy (create) a particle at position x, i.e., in the state $|x\rangle$.

One can invert Eq. (2.37) to obtain

$$\hat{d}_r = \int d^D x \; \phi_r^*(x)\hat{\psi}(x), \tag{2.38}$$

$$\hat{d}_r^\dagger = \int d^D x \; \phi_r(x)\hat{\psi}^\dagger(x). \tag{2.39}$$

Following the same procedure as in Eq. (2.34) and using (2.37), the commutation algebra in real space reads

$$[\hat{\psi}(x), \hat{\psi}^\dagger(y)]_\pm = \delta^D(x - y), \tag{2.40a}$$

$$[\hat{\psi}(x), \hat{\psi}(y)]_\pm = [\hat{\psi}^\dagger(x), \hat{\psi}^\dagger(y)]_\pm = 0. \tag{2.40b}$$

From the number operators in a given discrete basis, we define the *total particle number operator* as

$$\hat{N} = \sum_l \hat{n}_l = \sum_l \hat{d}_l^\dagger \hat{d}_l. \tag{2.41}$$

In the real space basis,

$$\hat{N} = \int d^D x \int d^D x' \sum_l \hat{\psi}^\dagger(x)\langle x|l\rangle\langle l|x'\rangle\hat{\psi}(x') = \int d^D x \; \hat{\psi}^\dagger(x)\hat{\psi}(x), \tag{2.42}$$

from which one can immediately identify the particle density operator

$$\hat{n}(x) \equiv \hat{\psi}^\dagger(x)\hat{\psi}(x). \tag{2.43}$$

It is straightforward to demonstrate that the latter operators verify[2]

$$[\hat{n}(x), \hat{\psi}(y)] = \pm[\hat{\psi}^\dagger(x), \hat{\psi}(y)]_\mp \; \hat{\psi}(x) = -\delta^D(x-y)\; \hat{\psi}(y), \tag{2.44a}$$

$$[\hat{n}(x), \hat{n}(y)] = [\hat{n}(x), \hat{\psi}^\dagger(y)\hat{\psi}(y)] = 0. \tag{2.44b}$$

2.1.4 Many body Hamiltonian in second quantization

In Sec. 2.1.2, we saw that the single-particle Hamiltonian could be written in the form of Eq. (2.28). In terms of the field operators $\hat{d}_r^{(\dagger)}$ associated with a discrete single particle basis $\{|r\rangle\}$, such Hamiltonian takes the form

$$\hat{H}_0 = \sum_{r,m} \hat{d}_m^\dagger \langle m|H_0|r\rangle \hat{d}_r, \tag{2.45}$$

which ensures that the dynamics of the fields coincides with the one for the single-particle wavefunction amplitudes, and where $\langle m|H_0|r\rangle$ are the matrix elements of the single particle Hamiltonian H_0 in first quantization.

One may choose the basis provided by the single-particle eigenstates $H_0|\alpha\rangle = \epsilon_\alpha|\alpha\rangle$, such that $\hat{f}_\alpha^\dagger|0\rangle = |1_\alpha\rangle$. Then,

$$\hat{H}_0 = \sum_\alpha \epsilon_\alpha \hat{f}_\alpha^\dagger \hat{f}_\alpha = \sum_\alpha \epsilon_\alpha \hat{n}_\alpha. \tag{2.46}$$

Consequently, one can see that the Hamiltonian of non-interacting particles is the sum of the different terms associated with the occupancy of the single-particle eigenstates. Thus, the eigenstates of $\hat{H}_0$ are the tensor products of the corresponding number operators.

One can express the single-particle Hamiltonian in the continuum basis using the relations obtained in Eqs. (2.38) and (2.39), which lead to

$$\hat{H}_0 = \int d^D x \int d^D y \; \hat{\psi}^\dagger(x)\langle x|H_0|y\rangle\hat{\psi}(y).$$

For a standard single particle Hamiltonian

$$H_0 = \frac{p^2}{2m} + U(x), \tag{2.47}$$

including kinetic and potential energy $U(x)$, one has

$$\langle x|H_0|y\rangle = \left(-\frac{\hbar}{2m}\nabla_x^2\delta^D(x-y) + U(x)\delta^D(x-y)\right) = \langle y|H_0|x\rangle,$$

[2]Recall that $[A,B] = A[B,C]_\mp \pm [A,C]_\mp B$.

and

$$\hat{H}_0 = \int d^D x\ \hat{\psi}^\dagger(x) \left[-\frac{\hbar^2}{2m} \nabla_x^2 + U(x) \right] \hat{\psi}(x). \tag{2.48}$$

We have written the single-particle Hamiltonian. The only step left to obtain the complete second quantization many-body Hamiltonian is to derive the interaction term. Let us recall the classical expression for a two-body interaction energy,

$$V_{\text{int}} = \frac{1}{2} \sum_{i \neq j} U(x_i, x_j) = \frac{1}{2} \sum_{i,j} U(x_i, x_j) - \frac{1}{2} \sum_{i} U(x_i, x_i),$$

where the interaction energy of each particle pair is invariant under particle exchange, i.e., $U(x_i, x_j) = U(x_j, x_i)$.

If we take the continuum limit,

$$V_{\text{int}} = \frac{1}{2} \int d^D x \int d^D y\ U(x, y)\ n(x) n(y) - \frac{1}{2} \int d^D x\ U(x, x)\ n(x).$$

Quantizing the latter expression and inserting Eqs. (2.43) and (2.44), one obtains

$$\begin{aligned}
\hat{V}_{\text{int}} &= \frac{1}{2} \int d^D x \left\{ \int d^D y\ U(x, y)\ \hat{n}(x)\ \hat{n}(y) - U(x, x)\ \hat{n}(x) \right\} \\
&= \frac{1}{2} \int d^D x \int d^D y\ U(x, y) \left\{ \hat{n}(x)\ \hat{n}(y) - \hat{n}(x) \delta^D(x - y) \right\} \\
&= \frac{1}{2} \int d^D x \int d^D y\ U(x, y) \left\{ \hat{n}(x)\ \hat{n}(y) - \hat{\Psi}^\dagger(x) \hat{\Psi}(x)\ \delta^D(x - y) \right\} \\
&= \frac{1}{2} \int d^D x \int d^D y\ U(x, y) \left\{ \hat{n}(x)\ \hat{n}(y) + \hat{\Psi}^\dagger(x) [\hat{n}(y), \hat{\Psi}(x)] \right\},
\end{aligned}$$

which immediately leads to the second quantized form of the interaction in terms of the fields in real space,

$$\hat{V}_{\text{int}} = \frac{1}{2} \int d^D x \int d^D y\ U(x, y)\ \hat{\psi}^\dagger(x) \hat{\psi}^\dagger(y) \hat{\psi}(y) \hat{\psi}(x). \tag{2.49}$$

The two-body interaction term may also be expressed in terms of field operators in a discrete basis. Using the relation given in Eq. (2.37) and its self-adjoint, one can derive

$$\hat{V}_{\text{int}} = \frac{1}{2} \sum_{m,l,r,s} \int d^D x \int d^D y\ U(x, y) \langle m, l | x, y \rangle \langle x, y | s, r \rangle d_m^\dagger d_l^\dagger d_r d_s \Rightarrow \tag{2.50}$$

$$\hat{V}_{\text{int}} \equiv \frac{1}{2} \sum_{m,l,r,s} \langle m, l | U | s, r \rangle d_m^\dagger d_l^\dagger d_r d_s, \tag{2.51}$$

where the above matrix element is defined as

$$\langle m, l | U | s, r \rangle \equiv \int d^D x \int d^D y\ U(x, y) \phi_m^*(x) \phi_l^*(y) \phi_r(y) \phi_s(x). \tag{2.52}$$

We will regard the full many body Hamiltonian in second quantization as the contributions from the energy of the single-particle modes and a two-body interaction term,

$$\hat{H} = \hat{H}_0 + \hat{V}_{\text{int}}. \tag{2.53}$$

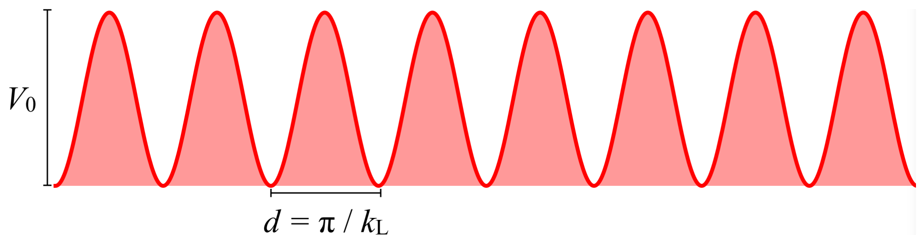

Figure 2.1: Schematic representation of the one-dimensional optical lattice with lattice constant $d = \lambda_L$ and depth V_0, taken from Ref. [34].

2.2 The Bose-Hubbard Hamiltonian

The purpose of this section is to describe the Hamiltonian of a one-dimensional system consisting of bosons trapped in a lattice potential. A one-dimensional optical lattice can be experimentally created by retroreflection of a monochromatic laser beam of frequency ω_L, which is set up in a particular way that produces an effective lattice potential given by

$$V_{\mathrm{latt}}(x) = V_0 \sin^2 (k_L x), \tag{2.54}$$

where $k_L = 2\pi/\lambda_L$, with λ_L the laser beam wavelength [34]. V_0 characterizes the depth of the lattice, which has lattice constant

$$d_L = \lambda_L/2, \tag{2.55}$$

as represented in Fig. 2.1

The single-particle Hamiltonian H_0 of a particle of mass m subjected to the potential provided by the optical lattice in (2.54) reads

$$H_0(x) = \frac{-\hbar^2}{2m}\nabla_x^2 + \mathrm{V}_{\mathrm{latt}}(x). \tag{2.56}$$

Note that the latter single-particle Hamiltonian exhibits the same periodicity as the lattice, and thus, $H_0(x) = H_0(x + d_L)$.

In order to fully specify the conditions under which the Hamiltonian is going to be studied, one has to give the considered boundary conditions, for which two options are valid. One of them is *hard wall boundary conditions* (HWBC), which connect sites 1 and L of the lattice to a wall, as represented in Fig. 2.2(b). Unless otherwise specified, we will assume that our system has *periodic boundary conditions* (PBC). That is, we will consider that our system wavefunction, $\varphi(x)$, verifies $\varphi(x) = \varphi(x + Ld_L)$, where Ld_L is the length of the lattice and L is the number of sites. This condition is equivalent to considering that the lattice site $L+1$ is the site 1, as shown by Fig. 2.2(a).

Bloch's theorem states that, for a periodic Hamiltonian, the solutions of Schrödinger's equation, $\varphi_q^n(x)$, are given by the product of a plane wave e^{iqx} and a periodic function $u_q^n(x)$ whose periodicity is the one of the Hamiltonian potential. Hence,

$$H_0(x)\varphi_q^n(x) = \epsilon_q^n \varphi_q^n(x) \;\Rightarrow\; \varphi_q^n(x) = e^{iqx} u_q^n(x), \tag{2.57}$$

where n is the band index and q denotes the quasimomentum associated with the peri-

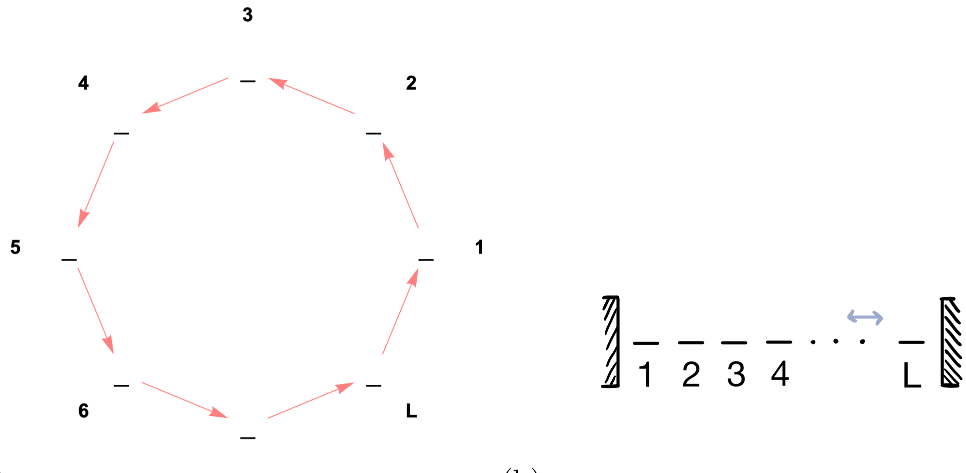

(a) (b)

Figure 2.2: Schematic representation of (a) Periodic boundary conditions, where sites 1 and L are connected, and (b) hard wall boundary conditions, on a lattice formed by L sites.

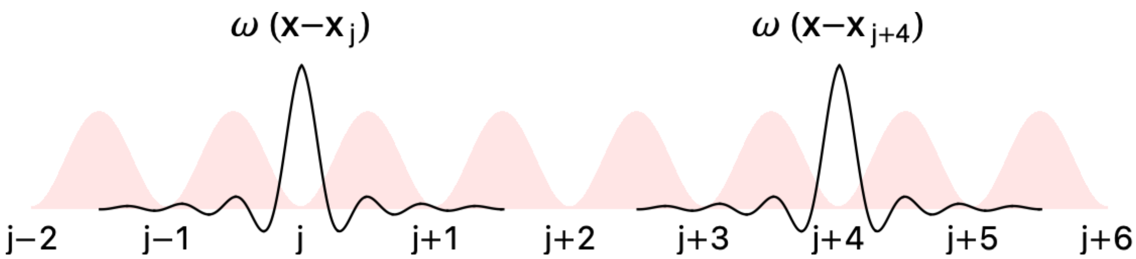

Figure 2.3: Representation of two Wannier states in an optical lattice , centered at lattice sites j and $j+4$. It can be seen that both states only differ in a spatial translation.

odicity of the lattice. Without loss of generality, we can restrict the values of q to those belonging to the first Brillouin Zone (1BZ), and thus $q \in [0, 2\pi/d_L)$.

The functions $\varphi_q^n(x)$ are extended throughout the lattice. However, the *Wannier basis* can be more useful when it comes to working with bosons in a lattice potential. The states of this basis are localized states, i.e., they are wavefunctions localized in a small region of the lattice and centered at a determined site, as represented in Fig. 2.3. The states forming the Wannier basis (named *Wannier states*), denoted by $w^n(x - x_j)$, can be written in terms of the Bloch states,

$$w^n(x - x_j) = \frac{1}{\sqrt{L}} \sum_{q \in 1\mathrm{BZ}} e^{-iqx_j} \varphi_q^n(x). \tag{2.58}$$

One can see that such states are localized around the center of the lattice site j, $x_j = j\, d_L$. An inversion of Eq. (2.58) leads to

$$\varphi_q^n(x) = \frac{1}{\sqrt{L}} \sum_j e^{iqx_j} w^n(x - x_j). \tag{2.59}$$

Once we have presented the main properties of the wavefunction of a periodic single-particle Hamiltonian, we are ready to derive the second quantized Hamiltonian describing an ultracold gas of interacting bosons in a one-dimensional lattice. Using the expressions shown in the previous section, one has

$$\hat{H} = \frac{1}{2}\int dx \int dx' \; \hat{\psi}^\dagger(x)\hat{\psi}^\dagger(x')U(x,x')\hat{\psi}(x)\hat{\psi}(x') + \int dx \; \hat{\psi}^\dagger(x)H_0(x)\hat{\psi}(x), \tag{2.60}$$

where $U(x,x')$ is the interaction function between two bosons of mass m located at positions x and x', and $H_0(x)$ is the single-particle Hamiltonian function given in Eq. (2.56). Lastly, the operators $\hat{\psi}(x)$ and $\hat{\psi}^\dagger(x)$ are the bosonic field operators in the position basis.

First, we specify the interaction term. We will consider a contact interaction given by

$$U(x,x') = g \; \delta(x-x'). \tag{2.61}$$

In first Born approximation, one can see that the value of g corresponds to

$$g = \frac{4\pi\hbar^2}{m}a_s, \tag{2.62}$$

where a_s is the scattering length of the contact potential [2].

For convenience, we choose to write the Hamiltonian in the on-site single-particle Wannier basis given in Eq. (2.58), and for this purpose we have to expand the field operators in such basis,

$$\hat{\psi}(x) = \sum_n \sum_{j=1}^{L} \hat{b}_j^n w^n(x-x_j), \tag{2.63}$$

where

$$\hat{b}_j^n := \int dx \; \hat{\psi}(x)[w^n(x-x_j)]^* \tag{2.64}$$

is an operator that annihilates a boson in the $n-$th band Wannier state around the position $x_j = j \; d_L$. Such operators verify

$$[\hat{b}_i^n, \hat{b}_j^{n'\dagger}] = \delta_{ij}\delta_{nn'}, \quad [\hat{b}_i^n, \hat{b}_j^{n'}] = [\hat{b}_i^{n\dagger}, \hat{b}_j^{n'\dagger}] = 0. \tag{2.65}$$

Assuming the optical lattice is deep enough, one can see that the Wannier basis can be restricted to the first band ($n = 1$), since it is enough to describe the low-energy physics. Hence, the n index will no longer be necessary. Using the relation given in Eq. (2.63) one can see that the Hamiltonian of Eq. (2.60) takes the form

$$\hat{H} = -\sum_{i,j=1}^{L} J_{ij} \; \hat{b}_i^\dagger \hat{b}_j + \frac{1}{2}\sum_{i,j,k,l=1}^{L} U_{ijkl} \; \hat{b}_i^\dagger \hat{b}_j^\dagger \hat{b}_k \hat{b}_l, \tag{2.66}$$

where

$$U_{ijkl} \equiv \langle ij|U|lk\rangle = \frac{4\pi\hbar^2}{m}a_s \int dx \; w^*(x-x_i)w^*(x-x_j)w(x-x_k)w(x-x_l) \tag{2.67}$$

and

$$J_{ij} = -\int dx \; w^*(x-x_i)\left[V_{\text{latt}}(x) - \frac{\hbar^2}{2m}\nabla_x^2\right] w(x-x_j). \tag{2.68}$$

Since we are considering highly localized single particle states, the largest matrix element U_{ijkl} is given by the interaction between bosons in the same lattice site. Thus, the dominant interaction term is given by

$$U \equiv \frac{4\pi\hbar^2}{m} a_s \int dx \; |w(x)|^4. \tag{2.69}$$

Therefore, we can approximate $U_{ijkl} \approx U\delta_{ij}\delta_{il}\delta_{ik}$, and the interaction term of the Hamiltonian reduces to

$$\hat{H}_U \equiv \frac{U}{2}\sum_{i=1}^{L} \hat{n}_i(\hat{n}_i - 1). \tag{2.70}$$

Lastly, one can separate the diagonal and off-diagonal terms of the first contribution in (2.66). The diagonal terms correspond to the on-site energies, which are the same for all the sites of the lattice, and read

$$-\sum_{i}^{L} J_{ii} \; \hat{b}_i^\dagger \hat{b}_i = \epsilon \sum_{i=1}^{L} \hat{n}_i, \tag{2.71}$$

where $\epsilon = J_{ii}$ is the on-site energy of any single-particle state.

Similarly, J_{ij} characterizes the tunneling strength with which a boson moves from site i to site j of the lattice. Again, as we are taking highly localized single particle states, only tunneling to nearest neighbours is considered. As a consequence, the tunneling term reduces to

$$-\sum_{i \neq j}^{L} J_{ij} \; \hat{b}_i^\dagger \hat{b}_j \approx -J \sum_{\langle i,j \rangle}^{L} \; \hat{b}_i^\dagger \hat{b}_j, \tag{2.72}$$

where $\langle i,j \rangle$ denotes pairs of sites $\{i,j\}$ that differ in one site, i.e., $j = i \pm 1$. The off-diagonal contributions are then given by

$$\hat{H}_J \equiv -J \sum_{i}^{L} \; (\hat{b}_i^\dagger \hat{b}_{i+1} + \hat{b}_{i+1}^\dagger \hat{b}_i). \tag{2.73}$$

After putting together the diagonal and off-diagonal terms of the tunneling contribution with the interaction term, one obtains the form of the Bose-Hubbard Hamiltonian (BHH) in the Wannier basis, which reads [4, 35–37]

$$\hat{H}_{BH} = -J \sum_{\langle i,j \rangle}^{L} \; \hat{b}_i^\dagger \hat{b}_j + \frac{U}{2} \sum_{i=1}^{L} \hat{n}_j(\hat{n}_j - 1) + \epsilon \sum_{i=1}^{L} \hat{n}_i. \tag{2.74}$$

Therefore, one can conclude that the Hamiltonian ruling the system formed by bosons trapped in a lattice potential consists of three terms, illustrated in Fig. 2.4.

- *Tunneling term*

  The term $-J\sum_{\langle i,j \rangle}^{L} \hat{b}_i^\dagger \hat{b}_j$ is controlled by the *tunneling strength*, J. The operator $\hat{b}_i^\dagger \hat{b}_j$ annihilates a boson on site j, and creates it on site i. Since the sum over i, j only considers nearest neighbours, this term describes tunneling of bosons from one site of the lattice to one of the two adjacent ones.

- *On-site interaction term*

  The second part of the Hamiltonian is $\frac{U}{2}\sum_{i=1}^{L} \hat{n}_j(\hat{n}_j - 1)$, which is ruled by the

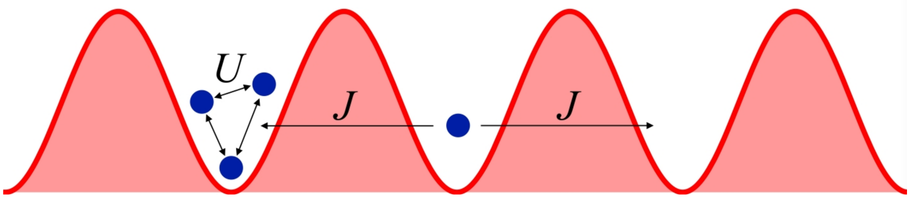

Figure 2.4: Schematic representation of a Bose-Hubbard model, taken from Ref. [34].

interaction strength U and describes the energy the system acquires when more than one boson occupies the same lattice site. Hence, this term accounts for all pairs of bosons interacting on each lattice site.

- *On-site energy term*

  The last term takes into account the energy a boson gains just by occupying a Wannier state, whose total corresponds to $\epsilon \sum_{i=1}^{L} \hat{n}_i$. Since the total particle number is preserved (this fact will be discussed later), this term only adds a constant to the Hamiltonian, and may therefore be neglected.

2.2.1 Symmetries of the Bose-Hubbard Hamiltonian

The Bose-Hubbard Hamiltonian introduced above exhibits several symmetries, which are presented here.

- Total particle number conservation

  Recall the form of the total particle number operator defined in Eq. (2.41). It is easy to demonstrate that the commutator $[\hat{H}_{BH}, \hat{N}] = 0$, which implies that the expectation value $\langle \hat{N} \rangle$ remains constant. In other words, the total particle number is conserved.

  Because of this symmetry, the Bose-Hubbard Hamiltonian can be diagonalized independently in subspaces of fixed particle number. It is now a good point to remark that the dimension of the Hilbert space of the system, $\mathcal{N}$, is determined by the number of sites L and the number of particles N, reading

$$\mathcal{N} = \binom{N+L-1}{L}. \tag{2.75}$$

  Hence, for a system with constant particle density $\nu \equiv N/L$, the dimension of the Hilbert space grows exponentially with N or L.

- Time-reversal symmetry

  The Hamiltonian matrix is real and symmetric in the on-site Fock basis $\{|\mathbf{n}\rangle\}$, which implies that the BHH is invariant under the action of the antiunitary time-reversal operator, $\hat{T}$.

- Parity symmetry

  Let us define the *parity* operator Π as the operator acting on Fock states as follows

$$\Pi|n_1, n_2, ..., n_{L-1}, n_L\rangle = |n_L, n_{L-1}, ..., n_2, n_1\rangle. \tag{2.76}$$

Thus, the parity operator performs a reflection with respect to the center of the lattice, and verifies

$$\Pi\Pi^\dagger = \mathbb{I}, \quad \Pi^2 = \mathbb{I}. \tag{2.77}$$

In other words, the parity operator is unitary and self-adjoint.

Under the action of Π, the creation/annihilation operators transform as follows,

$$\Pi \hat{b}_j^{(\dagger)} \Pi^\dagger = \hat{b}_{L-j+1}^{(\dagger)}, \tag{2.78}$$

which immediately leads to

$$\Pi \hat{n}_j \Pi^\dagger = \hat{n}_{L-j+1}. \tag{2.79}$$

From the latter expressions, it is straightforward to see that

$$\Pi \hat{H}_{\mathrm{BH}} \Pi^\dagger = \hat{H}_{\mathrm{BH}}, \tag{2.80}$$

which means the Bose-Hubbard Hamiltonian is invariant under reflection symmetry.

- Translational invariance

  Since we are considering periodic boundary conditions, our system exhibits invariance under discrete spatial translations. In other words, the Bose-Hubbard Hamiltonian is invariant under the action of the operator P, which acts on Fock states as

$$P|n_1, n_2, ..., n_L\rangle = |n_L, n_1, n_2, ..., n_{L-1}\rangle. \tag{2.81}$$

  The operator P is unitary,

$$PP^\dagger = P^\dagger P = \mathbb{I}, \tag{2.82}$$

  but it is not self-adjoint.

  One can also obtain the form of the annihilation and creation operators transformed under spatial translations,

$$P \hat{b}_j^{(\dagger)} P^\dagger = \hat{b}_{j+1}^{(\dagger)}, \tag{2.83}$$

  from which one can easily deduce

$$P \hat{H}_{BH} P^\dagger = \hat{H}_{BH}. \tag{2.84}$$

  Consequently, the Bose-Hubbard Hamiltonian is invariant under spatial translations.

Once the main features the Bose-Hubbard Hamiltonian have been understood, one is in a position to study some of the most important physical properties of such system.

2.2.2 Mott insulator to superfluid phase transition

In order to understand the properties of the ground state of the Hamiltonian derived in Eq. (2.74), we are going to discuss the two analytical solutions of the Hamiltonian, which correspond to limiting cases of the ratio of the tunneling to interaction strength.

Limit $J/U \to \infty$.

In this limit, the interaction term can be neglected and the Hamiltonian is reduced to

$$\hat{H}_J = -J \sum_{i=1}^{L} (\hat{b}_i^\dagger \hat{b}_{i+1} + \hat{b}_{i+1}^\dagger \hat{b}_i). \tag{2.85}$$

The solution of this Hamiltonian requires a change of basis in the creation/annihilation operators from the Wannier basis to the Bloch basis. We will use a different set of single-particle modes,

$$\hat{d}_k := \sqrt{\frac{1}{L}} \sum_{j=1}^{L} e^{-ikx_j}\ \hat{b}_j, \quad k \in 1\text{BZ}, \tag{2.86}$$

where the operator $d_k^{(\dagger)}$ destroys (creates) a boson in a Bloch mode characterized by a momentum k. One can invert this relation to obtain

$$\hat{b}_j = \sqrt{\frac{1}{L}} \sum_{k \in 1\text{BZ}} e^{ikx_j}\ \hat{d}_k, \quad j = 1, ..., L. \tag{2.87}$$

The last relation can be inserted in Eq. (2.85), giving

$$\hat{H}_J = -J \sum_{k \in 1\text{BZ}} 2\cos(kd)\ \hat{d}_k^\dagger \hat{d}_k, \tag{2.88}$$

where d is the lattice constant, and

$$kd = \frac{2\pi}{L}\, m, \text{ with } \ m = 0, ..., L-1. \tag{2.89}$$

The eigenstates of $\hat{H}_J$ are then Fock states for the new operators $\hat{\tilde{n}}_k \equiv \hat{d}_k^\dagger \hat{d}_k$, and their eigenenergies are constructed from the single-particle energies

$$\varepsilon_k \equiv -2J\cos(kd)\,. \tag{2.90}$$

The latter expression allows us to obtain the form of the ground state, since it can be seen that the lowest energy configuration is the one corresponding to all bosons occupying the state with $k = 0$. Thus,

$$|\psi_{gs}\rangle = \frac{(\hat{d}_0^\dagger)^N}{\sqrt{N!}}|0\rangle, \tag{2.91}$$

which has an associated energy

$$E_{gs} = -2JN. \tag{2.92}$$

Note that this ground state corresponds to having each boson delocalized over the lattice.

Limit $J/U \to 0$

When taking this limit, the Hamiltonian is dominated by the interaction term,

$$\hat{H}_U = \frac{U}{2} \sum_{j=1}^{L} \hat{n}_j(\hat{n}_j - 1). \tag{2.93}$$

The eigenstates in this limit are the Fock states of the on-site densities,

$$|\mathbf{n}\rangle \equiv |n_1, n_2, ..., n_L\rangle, \tag{2.94}$$

which have eigenenergies

$$E_{\mathbf{n}} = \frac{U}{2}\sum_{j=1}^{L} n_j(n_j - 1). \tag{2.95}$$

In the case where we have integer filling, the ground state corresponding to this limit is the one where the bosons are distributed in a way which ensures the interaction is the lowest possible. This configuration is the one where all the lattice sites have the same number of bosons, corresponding to $N/L \equiv \nu$. In other words,

$$|\Phi_{gs}\rangle = |\nu, \nu, ..., \nu\rangle, \tag{2.96}$$

whose corresponding energy is

$$\varepsilon_{gs} = \frac{U}{2}L\ \nu(\nu - 1). \tag{2.97}$$

In this case, the ground state corresponds to having bosons localized at the lattice sites.

In view of the ground state energy (2.97), it is easy to demonstrate that in the strongly interacting limit tunneling is suppressed, since it would cost a high energy increment. In order to understand this, let us start from the ground state and let one boson tunnel. This process requires an energy cost

$$\Delta E = \frac{U}{2}(\nu + 1)\nu + \frac{U}{2}(\nu - 1)(\nu - 2) - 2\ \frac{U}{2}\nu(\nu - 1) = U. \tag{2.98}$$

Since we are working in the strongly interacting limit, $U/J \gg 1$, this energy increment is very high. As a result, matter flow across the system is suppressed, i.e., an insulating behavior emerges as a consequence of the high interaction strength. Therefore, in this limit, the system is said to be a *Mott insulator*. Note that for non-integer density, a Mott insulator cannot exist, since there can be tunneling events at zero energy cost.

At integer filling ν, the ground state of the Bose-Hubbard Hamiltonian undergoes a quantum phase transition in the thermodynamic limit between a gapped *Mott insulator* phase and a gapless *superfluid* phase, as a function of J/U [4, 35–37]. Let us discuss the main features of both phases.

Superfluidity is a feature that characterizes a quantum fluid that can flow without experiencing friction. In order to understand superfluitidy, it is necessary to introduce the concept of *superfluid fraction*, f_s. For this purpose, we have to work in the thermodynamic limit. In other words, we need to take the limit

$$L \to \infty, \quad N \to \infty, \quad \frac{N}{L} = \text{const}. \tag{2.99}$$

When a quantum mechanical system is subjected to a drag force, as for example moving walls, the normal part of the system will move along with the walls. However, the part called superfluid fraction f_s remains at rest. There are expressions, detailed in Ref. [34], that provide a way to calculating the superfluid fraction,

$$f_s = f_s^{(1)} - f_s^{(2)}, \tag{2.100}$$

$$f_s^{(1)} = -\frac{1}{2JN}\langle\phi_0|\hat{H}_J|\phi_0\rangle, \quad f_s^{(2)} = \frac{1}{JN}\sum_{n\neq 0}\frac{|\langle\phi_0|\hat{W}|\phi_n\rangle|^2}{E_n - E_0}, \quad \text{and} \tag{2.101}$$

$$\hat{H}_J = -J\sum_{j=1}^{L}\left(\hat{b}_{j+1}^\dagger\hat{b}_j + \hat{b}_j^\dagger\hat{b}_{j+1}\right), \quad \hat{W} = -iJ\sum_{j=1}^{L}\left(\hat{b}_{j+1}^\dagger\hat{b}_j - \hat{b}_j^\dagger\hat{b}_{j+1}\right). \tag{2.102}$$

In the latter expressions, $|\phi_0\rangle$ denotes the ground state of the BHH, and $|\phi_n\rangle$ refers to any eigenstate, with energies E_0 and E_n, respectively. Note that $f_s^{(1)}$ provides an upper bound for the total superfluid fraction.

With the definition of f_s, it is possible to characterize the ground state of the BHH as a superfluid in the regime $J/U \to \infty$. It was already explained that the ground state of the system in this limit is the one which has all bosons occupying the state with quasimomentum $k = 0$, $|\Psi_{gs}\rangle \equiv |N, 0, ..., 0\rangle$ [Eq. (2.91)]. The first excited state, $|\psi_{exc}\rangle$, will be the one with all bosons in states with $k = 0$ but one, which occupies a state with the first $k \neq 0$ allowed,

$$|\psi_{exc}\rangle = |N-1, 1, 0, ..., 0\rangle. \tag{2.103}$$

The energy gap between these two states is, according to Eqs. (2.92) and (2.90),

$$\Delta^{(sf)} = 2J\left[1 - \cos\left(\frac{2\pi}{L}\right)\right]. \tag{2.104}$$

Since we are taking the thermodynamic limit, $L \to \infty$, this gap vanishes.

In order to calculate the superfluid fraction, it is convenient to rewrite the operators from Eq. (2.102) in terms of the operators $\hat{d}_k$. For this purpose, we insert the relation (2.87) in the expressions for $\hat{H}_J$ and $\hat{W}$, and obtain

$$\hat{H}_J = -2J\sum_{k\in 1ZB}\cos(kd)\;\hat{d}_k^\dagger\hat{d}_k, \tag{2.105}$$

$$\hat{W} = 2J\sum_{k\in 1ZB}\sin(kd)\;\hat{d}_k^\dagger\hat{d}_k. \tag{2.106}$$

Using the latter expressions, one obtains

$$f_s^{(1)} = \frac{1}{N}\sum_{k\in 1ZB}\cos(kd)\,\langle\Psi_{gs}|\hat{d}_k^\dagger\hat{d}_k|\Psi_{gs}\rangle = 1, \tag{2.107}$$

$$f_s^{(2)} = \frac{4J}{N}\sum_{n\neq gs}\frac{|\langle\phi_n|\sum_{k\in 1ZB}\sin(kd)\,\hat{d}_k^\dagger\hat{d}_k|\Psi_{gs}\rangle|^2}{E_n - E_{gs}} = 0, \tag{2.108}$$

which lead to a total superfluid fraction

$$f = f_s^{(1)} - f_s^{(2)} = 1. \tag{2.109}$$

Hence, it seems natural to say that the ground state of the BHH, in the limit $J/U \to \infty$, is in a gapless superfluid (SF) phase.

In the opposite limit, where $J/U \to 0$, the system forms a Mott insulator. In fact, it can be seen that the superfluid fraction f_s is vanishing in this limit, leading to a Mott insulator phase (MI). Recall the expression for the ground state of the BHH in the no tunneling regime, given by Eq. (2.96), which corresponds to all lattice sites occupied by the same number of bosons ν. In this case, the first contribution of the superfluid fraction $f_s^{(1)}$ is 0, since

$$\hat{b}^\dagger_{j+1}\hat{b}_j|\phi_{gs}\rangle \propto |\nu,\nu,...,\underbrace{\nu-1}_{j},\underbrace{\nu+1}_{j+1},...,\nu,\nu\rangle \Rightarrow \langle\phi_{gs}|\hat{b}^\dagger_{j+1}\hat{b}_j|\phi_{gs}\rangle = 0. \tag{2.110}$$

But it was already mentioned that $f_s^{(1)}$ provides an upper bound for the superfluid fraction. Thus, since f_s has to be non-negative, $f_s = 0$.

The two phases of the system exist on the two limiting cases for the ratio J/U. In the thermodynamic limit, there is a value of J/U, which we will name the *critical point* $(J/U)_c$, at which the transition occurs, such that $f_s = 0$ for $J/U < (J/U)_c$ and $f_s \neq 0$ otherwise [36].

Apart from the superfluid fraction, there are other quantities that distinguish between the two phases, as for instance the on-site density fluctuations. In any phase, $\langle\hat{n}_j\rangle = \nu$ in a uniform lattice. However, the on-site density fluctuations are different depending on the phase

$$\mathrm{var}(\hat{n}_j) \equiv \langle\hat{n}_j^2\rangle - \langle\hat{n}_j\rangle^2 \begin{cases} \sim \nu & \text{in the SF phase ,} \\ \to 0 & \text{in the Mott insulator phase.} \end{cases} \tag{2.111}$$

The transition takes place because a change in the structure of the ground state emerges, and this change can be monitored via the *correlation length*, ξ, which characterizes the decay of the off-diagonal elements of the *one-particle density matrix*, given by the matrix elements $\langle\hat{b}^\dagger_j\hat{b}_i\rangle$. Thus, the correlation length is defined as

$$\langle\hat{b}^\dagger_j\hat{b}_{j+r}\rangle_{gs} \sim e^{r/\xi}, \quad \text{for } r \neq 0. \tag{2.112}$$

Within the Mott insulator phase, $(J/U) < (J/U)_c$, ξ is finite and independent of the system size. However, for a $D-$dimensional system, ξ diverges at the transition as [36]

$$\xi \sim \exp\left(\frac{\text{const.}}{\sqrt{(J/U)_c - (J/U)}}\right), \quad \text{for } D = 1, \tag{2.113}$$

$$\xi \sim |(J/U)_c - (J/U)|^{-\alpha}, \quad \text{for } D > 1, \tag{2.114}$$

where α is known as the *critical exponent*, whose value depends on D. For instance, it is known that $\alpha \simeq 2/3$ for $D = 2$, and $\alpha \simeq 1/2$ in $D \geq 3$. Thus, the correlation length provides another tool to characterize both phases, since in the Mott insulator phase it takes finite values whereas in the superfluid phase it diverges.

The facts presented above indicate that the critical point of the transition depends both on the dimensionality and on particle density. This transition was observed experimentally for the first time in 2002, using a gas of ultracold atoms in a three-dimensional optical lattice [8]. Later, experimental advances in microscopy techniques have even allowed to visualize directly the bosonic density distribution in both phases with single-site resolution [12].

The transition can also take place by changing the particle density in the system. To understand this, one needs to consider the Bose-Hubbard Hamiltonian in the *grand canonical ensemble*. This is, we take the expression for the BHH and allow the total particle number to vary by adding a term proportional to the chemical potential μ,

$$\hat{K}_{BH} = -J\sum_{i}^{L}(\ \hat{b}_i^{\dagger}\hat{b}_{i+1} + \hat{b}_{i+1}^{\dagger}\hat{b}_i) + \frac{U}{2}\sum_{i=1}^{L}\hat{n}_i(\hat{n}_i - 1) - \mu\hat{N}. \tag{2.115}$$

Although an exact description of the phase diagram for this Hamiltonian is not known, it is possible to obtain information about it in the limit $J/U \to 0$. Then,

$$\hat{K}_{BH} \xrightarrow[J/U\to 0]{} \frac{U}{2}\sum_{i=1}^{L}\hat{n}_i(\hat{n}_i - 1) - \mu\sum_{i=1}^{L}\hat{n}_i, \tag{2.116}$$

from which one can see that in this limit the lattice sites are decoupled. In order for the configuration with ν bosons per site to be the ground state, the energy K of the system must verify $K(\nu) < K(\nu \pm 1)$. This condition is fulfilled if

$$\frac{U}{2}\ \nu(\nu-1) - \mu\nu < \begin{cases} \frac{U}{2}(\nu+1)\nu - \mu(\nu+1) & \\ & \Rightarrow \\ \frac{U}{2}(\nu-1)(\nu-2) - \mu(\nu-1) & \end{cases} \begin{array}{l} \mu < U\nu, \\ \\ \mu > U(\nu-1). \end{array} \tag{2.117}$$

Together, the latter expressions give the condition

$$\nu - 1 < \mu/U < \nu. \tag{2.118}$$

This yields the conclusion that, for $J/U \to 0$, there is a finite range of μ/U for which the system remains in the configuration with ν bosons per site.

Using different perturbation methods in one dimension, the phase diagram μ/U versus J/U has been estimated, as represented in Fig.2.5, where we show results obtained with second-order *strong coupling expansion* (SCE), described in Ref. [34], and *mean field theory*, which will be discussed in following sections. It can be seen that for non-integer densities the Mott insulator phase, colored in pink in the figure, does not exist, and thus the system remains in the superfluid regime for all values of J/U. The SCE method has been proven to provide a better approximation than mean field theory. However, both techniques show the same qualitative results, since in both cases the Mott lobes depend on the density ν, and seem to exhibit lower values of the critical point for greater integer fillings.

Several theoretical and experimental studies have provided estimates of the critical point for different integer fillings, as shown in Table 2.1. In particular, we note that in one dimension for $\nu = 1$, the critical point is $(J/U)_c \approx 0.3$.

2.3 Characterization of the eigenstate structure: Multifractality

In this section the concept of *multifractality* will be presented, as well as its relevance as a method of characterizing the Mott-insulator to superfluid transition.

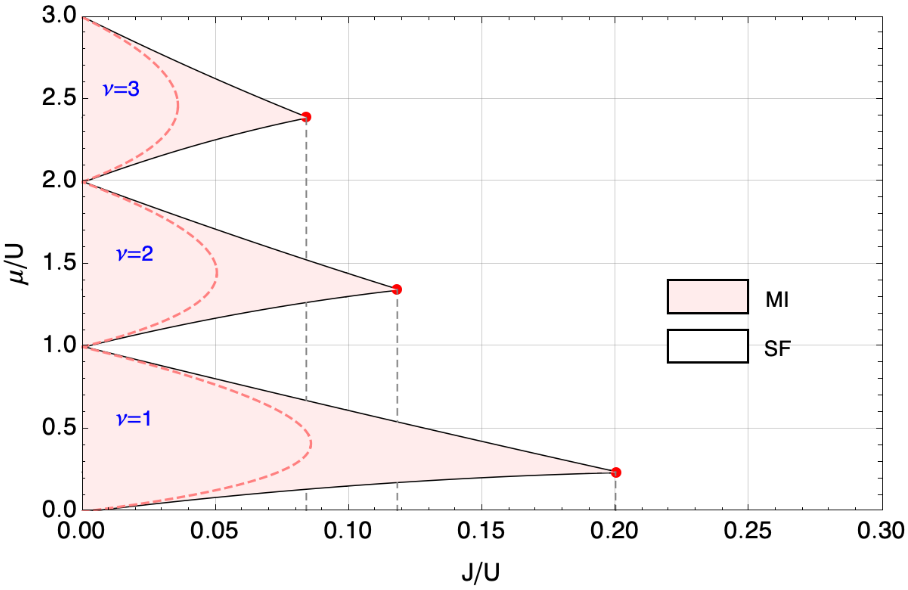

Figure 2.5: Mott lobes of the Bose-Hubbard Hamiltonian for different values of integer density ν, as a function of μ/U and J/U. The black lines indicate the border between the Mott insulator and the superfluid phases calculated with strong-coupling expansion, whereas the dashed pink was obtained using mean field theory. The red dots indicate the critical points obtained with SCE.

ν	Theoretical $(J/U)_c$	Theoretical $(J/U)_c$	Experimental $(J/U)_c$
1	0.3049 ± 0.0001	0.305 ± 0.001	0.297 ± 0.01
2	0.1790 ± 0.0003	0.180 ± 0.001	–
3	0.12697 ± 0.00002	–	–

Table 2.1: Estimations of the critical point from theoretical and experimental studies for different densities. Results shown in each columns are extracted, from left to right, from Refs. [38], [39] and [7].

Imagine that we are working with a Hilbert space of dimension $\mathcal{N}$. In order to understand the concept of multifractality, we will start expanding a wavefunction $|\Psi\rangle$ in a given basis $\{|j\rangle\}$,

$$|\Psi\rangle = \sum_{j=1}^{\mathcal{N}} \psi_j |j\rangle. \tag{2.119}$$

The q-moments R_q of the distribution of $|\psi_j|^2$ are defined as

$$R_q := \sum_{j=1}^{\mathcal{N}} |\psi_j|^{2q}, \text{ for } \ q \in \mathbb{R}^+. \tag{2.120}$$

The distribution of probabilities $|\psi_j|^2$ is said to be *multifractal* if its q-moments obey the scaling law

$$R_q \sim \mathcal{N}^{-\tau_q}, \text{ for } \ \mathcal{N} \to \infty, \tag{2.121}$$

where the τ_q functions must be non-linearly dependent on q. As the R_q depend on the chosen basis, multifractality is, in general, basis dependent.

Multifractality is usually characterized by a set of variables called *generalized fractal dimensions* (GFDs), defined as

$$D_q := \frac{\tau_q}{q-1}. \tag{2.122}$$

Any generalized fractal dimension can be obtained by making use of the fact that any $\mathcal{N}$-dependent prefactor $h(\mathcal{N})$ on the right hand side of Eq.(2.121) must become irrelevant as $\mathcal{N} \to \infty$. In such case,

$$R_q = h(\mathcal{N})\ \mathcal{N}^{-(q-1)D_q} \tag{2.123}$$

$$\Rightarrow \frac{\log R_q}{\log \mathcal{N}} \frac{1}{1-q} = \frac{\log h(\mathcal{N})}{\log \mathcal{N}} \frac{1}{1-q} + D_q, \tag{2.124}$$

and therefore

$$D_q = \lim_{\mathcal{N}\to\infty} \frac{1}{1-q} \frac{\log R_q}{\log \mathcal{N}} \equiv \lim_{\mathcal{N}\to\infty} \tilde{D}_q, \tag{2.125}$$

where we used that

$$\lim_{\mathcal{N}\to\infty} \frac{\log h(\mathcal{N})}{\log \mathcal{N}} = 0,$$

and we have defined the finite-size GFDs as

$$\tilde{D}_q = \frac{1}{1-q} \frac{\log R_q}{\log \mathcal{N}}. \tag{2.126}$$

The dimensions D_q then determine the asymptotic scaling of the moments of the distribution of intensities $|\psi_j|^2$ with the dimensionality $\mathcal{N}$ of Hilbert space.

For finite $\mathcal{N}$, there are three specially relevant cases for $\tilde{D}_q$, which correspond to $q = 1, 2$ and ∞,

$$\tilde{D}_1 = \lim_{q\to 1} \tilde{D}_q = -\frac{\sum_{j=1}^{\mathcal{N}} |\psi_j|^2 \log |\psi_j|^2}{\log \mathcal{N}}, \tag{2.127}$$

$$\tilde{D}_2 = -\frac{\log \sum_{j=1}^{\mathcal{N}} |\psi_j|^4}{\log \mathcal{N}}, \tag{2.128}$$

$$\tilde{D}_\infty = -\frac{\log \left(|\psi_j|^2_{\max}\right)}{\log \mathcal{N}}. \tag{2.129}$$

The relevance of the GFDs relies on the fact that they allow one to understand the localization properties in Hilbert space of the state $|\Psi\rangle$, as can be easily demonstrated. For a state that becomes fully extended in Hilbert space, the occupation probability will be of the form $|\psi_j|^2 \propto \mathcal{N}^{-1}$ for all j. This yields

$$R_q = \sum_{j=1}^{\mathcal{N}} |\psi_j|^{2q} \propto \mathcal{N}^{-(q-1)} \tag{2.130}$$

$$\Rightarrow D_q = 1 \text{ for all } q. \tag{2.131}$$

In this case, the states are said to be *ergodic extended*, as they participate equally of all basis elements.

On the other hand, a state is said to be *localized* if only a fixed finite number of basis states contribute to its expansion, i.e., the state only covers a fixed finite region of Hilbert

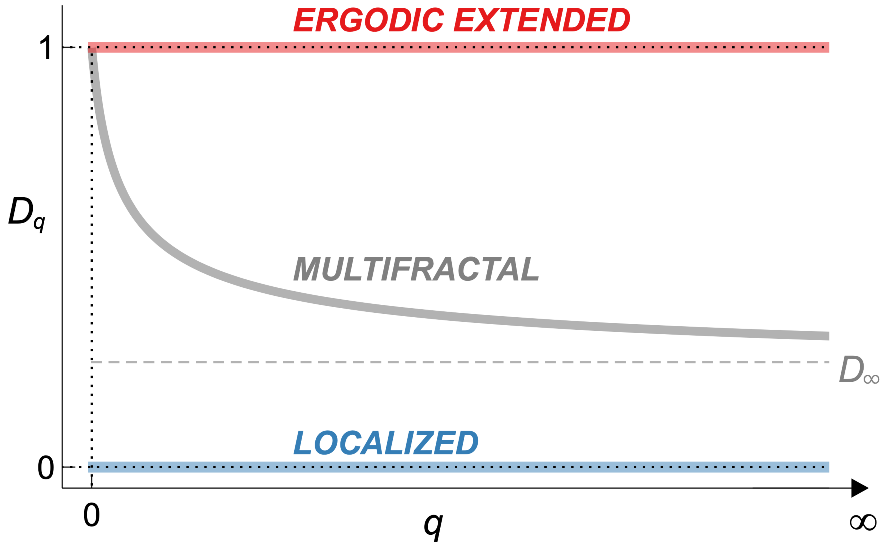

Figure 2.6: Generalized fractal dimensions D_q as functions of q for three different types of states.

space. In this case, a saturation of R_q as $\mathcal{N} \to \infty$ will eventually occur,

$$R_q \propto \mathcal{N}^0 \Rightarrow D_q = 0 \text{ for } q > 0. \tag{2.132}$$

Lastly, if the GFDs exhibit a dependence on q, $0 \leq D_q \leq 1$, the states are said to be *multifractal*. One can also prove that the GFDs are always monotonically decreasing functions of q [30]. Figure 2.6 shows the dependence of D_q on q for the different categories of states described above.

It has already been remarked that between all the GFDs, three cases are specially relevant as for the information they provide, which correspond to $q = 1, 2$ and ∞. Due to its connection with the Shannon information entropy, $-\sum_j |\psi_j|^2 \ln |\psi_j|^2$, the generalized fractal dimension D_1 is known as the *information dimension*, since $D_1 \ln \mathcal{N} \sim -\sum_j |\psi_j|^2 \ln |\psi_j|^2$. The dimension D_2 rules the growth of the participation ratio, given by R_2^{-1}. Lastly, for the case $q = \infty$ only the maximum value of the intensities, $\mathrm{p_{max}} \equiv \max(|\psi_j|^2)$ is relevant for the calculation of R_q, and the dimension D_∞ is given by $D_\infty = -\log_{\mathcal{N}} \mathrm{p_{max}}$.

Multifractality has been proven to be relevant for the study of quantum many-body systems. The quantum states of such systems exhibit a complex structure in Fock space, which can be studied using this formalism. Multifractality has become a useful tool in several works, where it has been possible to study phase transitions [27, 28] and the emergence of quantum chaos [29, 31–33].

The multifractal properties of the Bose-Hubbard Hamiltonian ground state in the Fock basis were shown to carry a distinctive signature of the transition from superfluid to Mott insulator. In Ref. [28], they manage to relate changes in the values of the dimensions D_q with the phase transition.

Figure 2.7 shows the evolution of various $\tilde{D}_q$ as functions of the tunneling strength $\eta \equiv (J/U)$ for a Bose-Hubbard model, using different lattice sizes L. In this representation, it can be seen that the finite-size GFDs take almost vanishing values for low values J/U, and as the tunneling strength is increased, the values of $\tilde{D}_q$ start to grow. As we have discussed

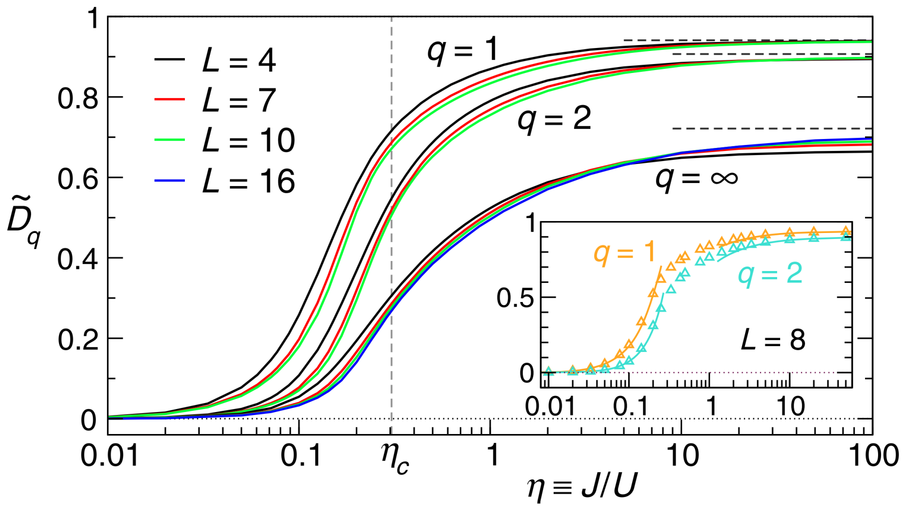

Figure 2.7: Finite-size generalized fractal dimensions $\tilde{D}_q$ in the ground state of the BHH at unit density as functions of J/U, for different values of q and lattice sizes, taken from Ref. [28].

during this chapter, this changing value of the GFDs is a manifestation of changes in the ground state structure. Such structure starts being highly-localized in Fock space in the limit $J/U \to 0$, leading to a Mott-insulator phase, and ends as a superfluid in the opposite regime, characterized for being largely delocalized in Fock space. In order to illustrate this relation between the GFDs and the eigenstate structure, we represent the ground state intensities $|\varphi_j|^2$ as functions of the basis index j, for two values of J/U with a noticeable different value of the $\tilde{D}_q$ associated. We choose, for a system with $L = 7$, the values $J/U = 0.08$ and $J/U = 2$, and represent our squared amplitudes in Fig. 2.8. It can be seen that, for the case $J/U = 0.08$, the state is localized in Fock space, since there is one amplitude dominating the others, which are negligible, corresponding to the mentioned expected structure when the values of D_q are close to 0 for any q. On the other hand, for the case $J/U = 2$, greater values of D_q were observed for every q, and it corresponds to a ground state that is highly delocalized over the lattice, since there is a large region of Fock space in which the intensities take comparable, non-negligible values.

In the forthcoming chaperts, the multifractal formalism will be used to study the properties of a modified version of the BHH suitable to describe a system of anyons.

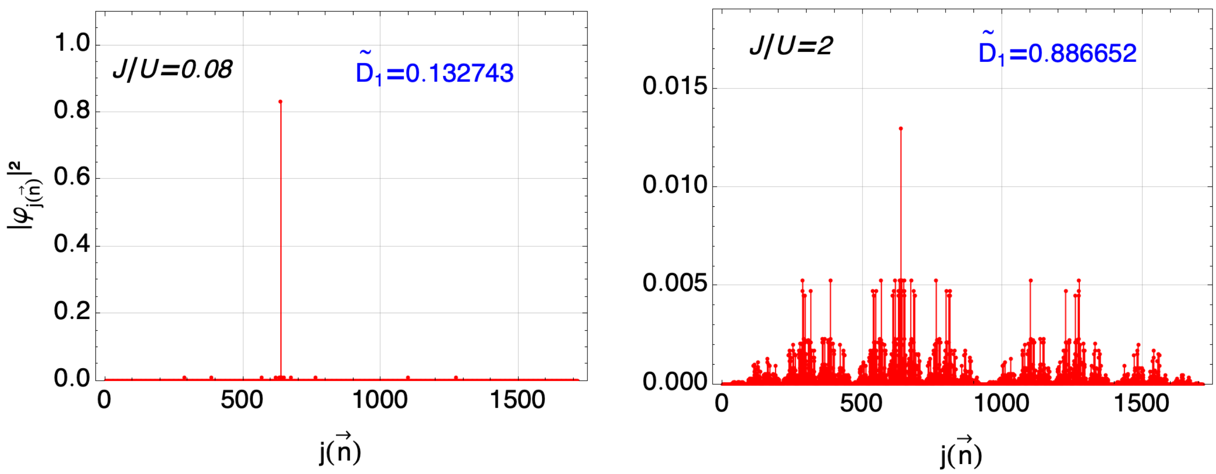

Figure 2.8: Ground state intensities in the on-site Fock basis as functions of the basis index for the BHH with $L = 7$ and $\nu = 1$ for two different tunneling strengths known to have noticeably different values of the corresponding $\tilde{D}_q$.

3 | Anyons in low dimensions

In this chapter we present the *Anyonic-Hubbard model.* For this purpose, we first introduce the concept of *fractional statistics*, which leads to the existence of a different type of particle from fermions and bosons, called *anyons.* Then, we describe a system formed by these anyons occupying a one-dimensional lattice, ruled by the Anyonic-Hubbard model, as well as the method by which it is possible to probe experimentally the properties of the anyonic system using ultracold atoms in optical potentials.

3.1 Fractional statistics

In this section we discuss how, making use of topological arguments, the possibility of particles with intermediate statistics between bosonic and fermionic can be deduced, following the discussions of Refs. [20] and [19].

When working with identical particles in three dimensions, quantum theory distinguishes between two types of particles, depending on the phase the wavefunction acquires when two of them exchange positions: If the wavefunction acquires a phase $\theta = \pi$ after such exchange, identical particles are referred to as *fermions.* On the other hand, if the acquired phase is $\theta = 0$, particles receive the name of *bosons.* The consequence of this phase acquisition results in fermions obeying *Pauli's exclusion principle*, which forces them to occupy different quantum states as, for example, different electronic orbitals to produce elements in the periodic table. In contrast, bosons show a preference for occupying the same quantum state, which is manifested, for instance, in degenerate atoms in a Bose-Einstein condensate.

In order to understand the origin of this distinction, we consider a system formed by N identical particles at positions $\mathbf{r}_1, \mathbf{r}_2, ..., \mathbf{r}_N$. The amplitude of such configuration is given by the many-particle wavefunction $\Psi(\mathbf{r}_1, \mathbf{r}_2, ..., \mathbf{r}_N)$. The amplitude which differs only by a single particle permutation is $\Psi' \equiv \Psi(\mathbf{r}_2, \mathbf{r}_1, ..., \mathbf{r}_N)$. However, since we are dealing with indistinguishable particles, these two amplitudes must obey

$$|\Psi'|^2 = |\Psi|^2 \tag{3.1}$$

in order for both wavefunctions to describe the same physical situation, which is equivalent to saying

$$\Psi' = p\Psi, \tag{3.2}$$

where p is a simple phase $p = e^{i\theta}$. One can perform a second exchange, having as a result an amplitude that we will name Ψ'', so that $\Psi'' \equiv p^2\Psi(\mathbf{r}_1, \mathbf{r}_2, ..., \mathbf{r}_N)$. By requiring the wavefunction to be single-valued, one has $\Psi'' = \Psi$, leading to

$$p = \pm 1. \tag{3.3}$$

The argument presented above apparently allows for only two types of identical particles depending on the acquired phase after the position exchange of two of them: The first corresponding to a phase $\theta = 0$, and the second with an associated phase $\theta = \pi$. However, a more careful analysis will help us to reason that in lower dimensions this is no longer the case.

Although we are used to thinking that the quantity that determines the physics of a system of identical particles is the permutation eigenvalue p, it turns out that what actually rules the physics is the phase $\eta = e^{i\theta}$ that arises from the adiabatic transport of two particles along a path that gives an actual physical exchange.

For the purpose of understanding the statistics of the system, we define a configuration space C^d as a set of points in Nd dimensions, which represents the positions of the N particles in d spatial dimensions. In this space, all points connected by permutations describe physically equivalent configurations. Correspondingly, such points may be identified as geometrically the same, and hence particle exchange paths in this space can be thought of as closed paths. Furthermore, we exclude the cases where more than one particle can be located at the same position, assuming, e.g., that they suffer some hard-core repulsion. For simplicity we will only consider two particles and only track their relative coordinate $\mathbf{r}$ recalling that, in C^d, $\mathbf{r} = -\mathbf{r}$. Our purpose is to obtain the constraints on the statistical phase η.

Let us start with the case $d = 3$, where closed paths can be classified in three types, as shown in Fig. 3.1. Since we are excluding the points corresponding to having more than one particle at the same spatial location, $\mathbf{r} = 0$ is forbidden and we can fix a value of $|\mathbf{r}|$ without loss of generality. Hence, we can think of two particles moving in three spatial dimensions relative to one another at a fixed separation. In such case, the resulting manifold, P_2, is a spherical surface with opposite points identified as the same. Figure 3.1A shows a path which does not involve any particle exchange. All of the paths from this class can be shrunk by a continuous deformation to a point, and thus the acquired phase has to be 1 in this case. Figure 3.1B represents a single exchange of the two particles (i.e., taking $\mathbf{r}$ to $-\mathbf{r}$), associated with a path that cannot be reduced to a point without cutting, receiving an η phase. Lastly, in Fig. 3.1C a path representing two exchanges is shown. This last path can be continuously deformed on the sphere into the trivial path, the one with no exchanges. Since its phase has to be η^2 and is topologically equivalent to the path in 3.1A, η^2 must be equal to one. As a consequence, the values of η are restricted to ± 1, which is in accordance with Eq. (3.3). Topological arguments thus yield the conclusion that, in three dimensions, two exchanges of particles are equivalent to none, leading to the existence of only bosons, with $\eta = 1$ ($\theta = 0$), and fermions, corresponding to $\eta = -1$ ($\theta = \pi$).

When dimensions are reduced to two, possibilities are not reduced to $\theta = 0$ or $\theta = \pi$ for the acquired phase, but rather to a continuum of statistical phases, giving rise to *fractional statistics*. In this case, the manifold P_1 of our configuration space is reduced to a circle, as represented in Fig. 3.2. After having a look at this representation, one can deduce that a single exchange path (taking the relative coordinate from $\mathbf{r}$ to -$\mathbf{r}$) cannot be

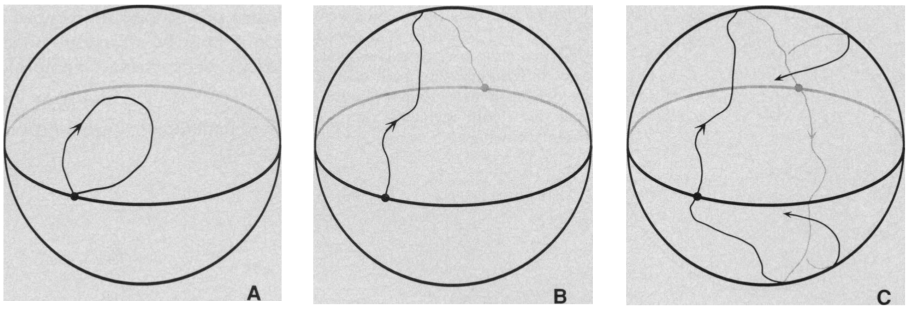

Figure 3.1: Paths showing relative motion of two identical particles in three dimensions by tracking their relative coordinate $\mathbf{r}$, taken from Ref. [19]. (**A**) shows a path which does not involve an exchange. (**B**) represents a path that involves one exchange. (**C**) is a path where two exchanges occur.

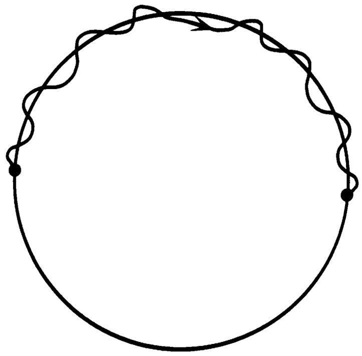

Figure 3.2: Path showing relative motion involving the exchange of two identical particles in two dimensions by tracking their relative coordinate $\mathbf{r}$, taken from Ref. [19].

deformed into a point without cutting, but neither can two exchanges. In fact, there is no $n \neq 0$ number of exchanges that can be continuously shrunk to a point in P_1, and hence there is no restriction for the value of η. In other words, in two dimensions it is possible to assign any value to the acquired phase due to exchange, giving rise to fractional statistics. The particles associated with such statistics are called *anyons*, whose wavefunction is characterized by acquiring a phase $e^{i\theta}$, with $\theta \in [0, 2\pi)$, under the position exchange of two identical particles.

Another point of view can be helpful to understand the different possibilities regarding to the particle statistics that arise in two-dimensional systems. In this case, we only need to imagine two particles in two dimensions that follow paths with or without exchanges, as depicted in Fig. 3.3. Each of the paths has a different *winding number* w, which corresponds to the total number of times that the path the moving particle follows travels counterclockwise around the other particle. From left to right, we have, first, an exchange of the two particles with $w = 0$, which corresponds to a phase $e^{i\theta}$. Then, the same exchange is represented, but the followed path is different, since the moving particle forms a closed loop around the other, and thus has $w = 1$. Because this configuration has been reached by performing three consecutive exchanges, the acquired phase is $e^{3i\theta}$. The third path shows a different situation, in which the final configuration is equal to the initial one, since the particles do not change their relative positions, and thus no exchange is performed. Because the motion of the particle does not perform any closed loop around the other, the followed path has $w = 0$ and no phase is acquired. The

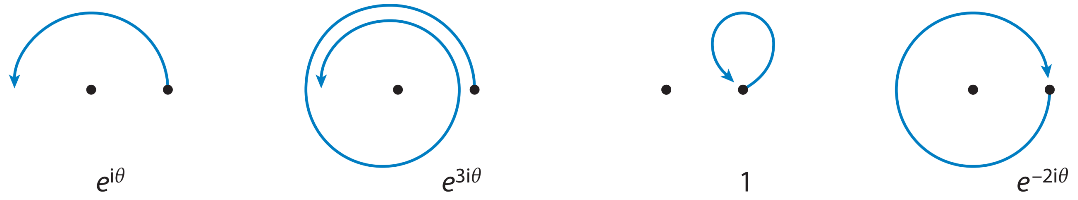

Figure 3.3: Some possible paths of two particles in two dimensions, with and without interchanges, taken from Ref. [20].

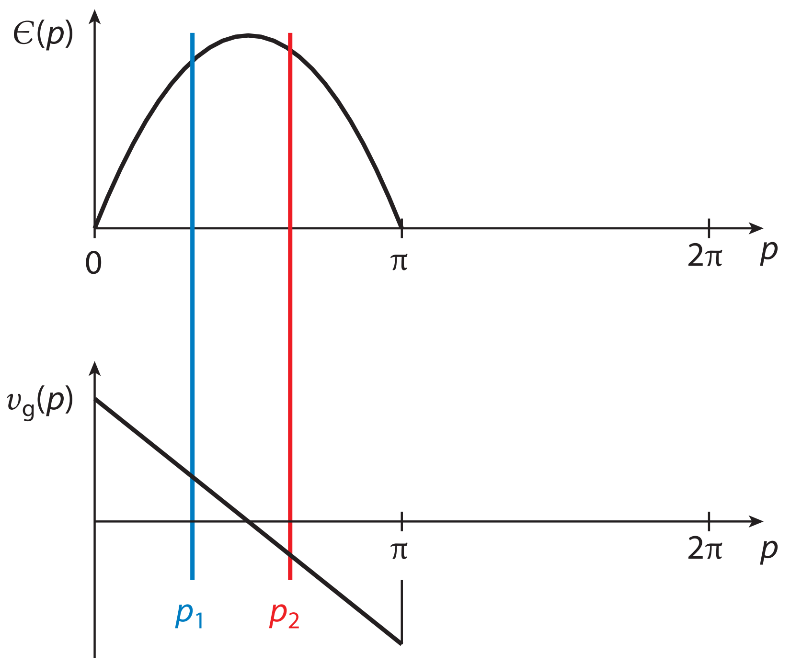

Figure 3.4: Single-particle spectrum and group velocity as functions of the single-particle momenta in a one-dimensional system with anyonic excitations, taken from Ref. [20].

fourth path corresponds to the same final configuration, which is however achieved by the moving particle performing one closed clockwise loop around the other one, and thus with $w = -1$. As this is the path corresponding to two consecutive exchanges, the acquired phase is $e^{-2i\theta}$. It becomes clear from this representation that every path leading to the same final configuration is topologically distinct from the others, since different winding numbers are associated with them. This latter approach will help us to understand the possibility of observing fractional statistics in one dimension, which in principle was only proposed formally as a generalization of Pauli's exclusion principle [21].

For the purpose of deducing the existence of anyons in one dimension using topological arguments, we will imagine a chain formed by particles with periodic boundary conditions, i.e., forming a circle. It has been seen that for certain one-dimensional systems that exhibit anyonic excitations, only half of the Brillouin zone for the momenta of the quasi-particles is allowed [20], which leads to having a single-particle spectra $\epsilon(p)$ that is always concave or always convex. As a result, the group velocity $v_g(p) = \partial_p\ \epsilon(p)$ is either monotonically decreasing or monotonically increasing with the single-particle momentum, respectively, as illustrated in Fig. 3.4. If we think of a system with only two excitations with momenta p_1 and p_2 with $p_2 > p_1$, such that the single-particle spectrum is concave

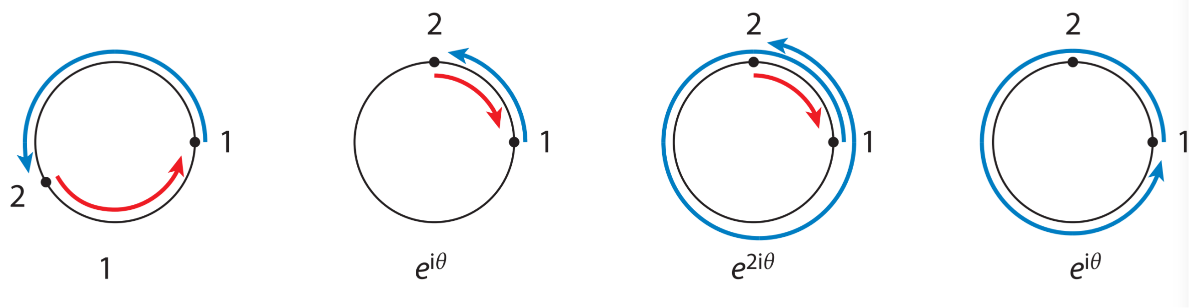

Figure 3.5: Different paths followed by two particles in one dimension, with and without crossings, taken from [20].

and thus $v_g(p_1) > v_g(p_2)$, we will have that the excitation with momentum p_1 is always faster than the other (taking the counterclockwise direction as positive). In this case, crossings can only occur unidirectionally, and consequently paths with different number of crossings are topologically different, since the associated winding number is different, as can be seen in Fig. 3.5. From left to right, the following situations are illustrated: First, two particles move so that no crossing takes place, and hence $w = 0$ (no global phase is acquired). In the next representation, the positions of the two particles are exchanged by performing a crossing, thus with $w = 1$ and, consequently, acquiring a phase $e^{i\theta}$. In the third scheme the same final configuration is achieved, but in this case particle 1 performs and additional loop around the other, carrying with itself thus a phase $e^{2i\theta}$. Finally, a situation where the starting configuration coincides with the final one is represented (the positions do not end up exchanged), but the followed path is such that particle 1 performs a closed loop around the other, thus giving an acquired phase $e^{i\theta}$. Hence, it is seen that in such one dimensional system those paths with different winding (crossing) number are not equivalent, and thus the possibilities for the statistical angle θ are again a continuum rather than only 0 and π, thus allowing us to refer to our particles as anyons.

Models of one-dimensional systems with fractional statistics have recently been proposed on a discrete lattice [23], finding an experimental realization with cold atoms in optical lattices [15], and will be the subject of study throughout this work.

3.2 Lattice anyons in one dimension

3.2.1 Anyonic-Hubbard model

Here we describe a model for a system analogous to the one presented in Sec. 2.2, with the only difference that the particles we deal with will now be anyons, instead of bosons.

Recall that bosons were defined as those particles whose creation and annihilation operators obey the commutation relations given by (2.11a) and (2.11b). Similarly, lattice anyons in one dimension are defined by the generalized commutation relations

$$\hat{a}_j \hat{a}_k^\dagger - e^{i\theta \, \mathrm{sgn}(j-k)} \hat{a}_k^\dagger \hat{a}_j = \delta_{jk}, \tag{3.4a}$$

$$\hat{a}_j \hat{a}_k - e^{-i\theta \, \mathrm{sgn}(j-k)} \hat{a}_k \hat{a}_j = 0, \tag{3.4b}$$

where $\theta \in [0, \pi]$. The operators $\hat{a}_j^\dagger$ and $\hat{a}_j$ create and destroy, respectively, an anyon on site j. The sign function is such that $\mathrm{sgn}(0) = 0$, hence, two particles on the same site behave as ordinary bosons for any value of θ, since imposing $j = k$ gives

$$\hat{a}_j\hat{a}_j^\dagger - e^{i\theta\ \mathrm{sgn}(j-j)}\hat{a}_j^\dagger\hat{a}_j = [\hat{a}_j, \hat{a}_j^\dagger] = 1,$$
$$\hat{a}_j\hat{a}_j - e^{-i\theta\ \mathrm{sgn}(j-j)}\hat{a}_j\hat{a}_j = [\hat{a}_j, \hat{a}_j] = 0,$$

which correspond to the commutation relations for bosons, recovered for the case $\theta = 0$,

$$\hat{a}_j\hat{a}_k^\dagger - e^{i0\ \mathrm{sgn}(j-k)}\hat{a}_k^\dagger\hat{a}_j = [\hat{a}_j, \hat{a}_k^\dagger] = \delta_{jk},$$
$$\hat{a}_j\hat{a}_k - e^{-i0\ \mathrm{sgn}(j-k)}\hat{a}_k\hat{a}_j = [\hat{a}_j, \hat{a}_k] = 0,$$

for all j, k.

Analogously, anyons with $\theta = \pi$ are *pseudofermions*, as they behave like bosons on-site and fermions off-site. In other words,

$$\hat{a}_j\hat{a}_k^\dagger - e^{i\pi\ \mathrm{sgn}(j-k)}\hat{a}_k^\dagger\hat{a}_j = \begin{cases} [\hat{a}_j, \hat{a}_k^\dagger]_+ = 0 & \text{for } j \neq k, \\ [\hat{a}_j, \hat{a}_j^\dagger] = 0, \end{cases}$$
$$\hat{a}_j\hat{a}_k - e^{-i\pi\ \mathrm{sgn}(j-k)}\hat{a}_k\hat{a}_j = \begin{cases} [\hat{a}_j, \hat{a}_k]_+ = 0 & \text{for } j \neq k, \\ [\hat{a}_j, \hat{a}_j] = 0. \end{cases}$$

Thus, pseudofermions obey the anticommutation algebra off-site (as fermions) and the commutation algebra on-site (as bosons).

The commutation algebra defined above leads to the desired behavior for anyons, as illustrated in Fig. 3.6. In this representation, the initial situation corresponds to having one anyon located at site j and another at site k (with $j < k$), i.e., the initial state is

$$\hat{a}_j^\dagger\hat{a}_k^\dagger|0\rangle. \tag{3.8}$$

One can act on this distribution with $\hat{a}_i^\dagger\hat{a}_k$, which destroys an anyon in site k and creates it in site $i < j$,

$$\hat{a}_i^\dagger\hat{a}_k\ (\hat{a}_j^\dagger\hat{a}_k^\dagger|0\rangle). \tag{3.9}$$

We can use the commutation relation in (3.4a) to write $\hat{a}_k\hat{a}_j^\dagger = e^{i\theta\mathrm{sgn}(k-j)}\hat{a}_j^\dagger\hat{a}_k$, so that the latter expression results

$$\hat{a}_i^\dagger\hat{a}_k\ \hat{a}_j^\dagger\hat{a}_k^\dagger|0\rangle = \hat{a}_i^\dagger e^{i\theta\mathrm{sgn}(k-j)}\hat{a}_j\hat{a}_k\hat{a}_k^\dagger|0\rangle = \hat{a}_i^\dagger e^{i\theta\mathrm{sgn}(k-j)}\hat{a}_j(1-\hat{n}_k)|0\rangle = e^{i\theta}\hat{a}_i^\dagger\hat{a}_j^\dagger|0\rangle. \tag{3.10}$$

which corresponds to the process shown in the upper panel of Fig. 3.6, from which it is easy to see that this tunneling to the left process is equivalent to exchanging the particles, and it gives a global phase $e^{i\theta}$. These leftwards hopping processes are the equivalent to the braiding paths typically used for anyons in two-dimensional systems, illustrated in 3.6. Thus, the commutation algebra presented above gives the behavior described for anyons, in which a particle exchange gives a phase determined by the statistical angle θ. If one takes the situation where the exchange is performed by tunneling to the right, which is depicted in the lower panel of Fig.3.6 (and its two-dimensional equivalence in the right panel), then using an analogous procedure one will straightforwardly find that the

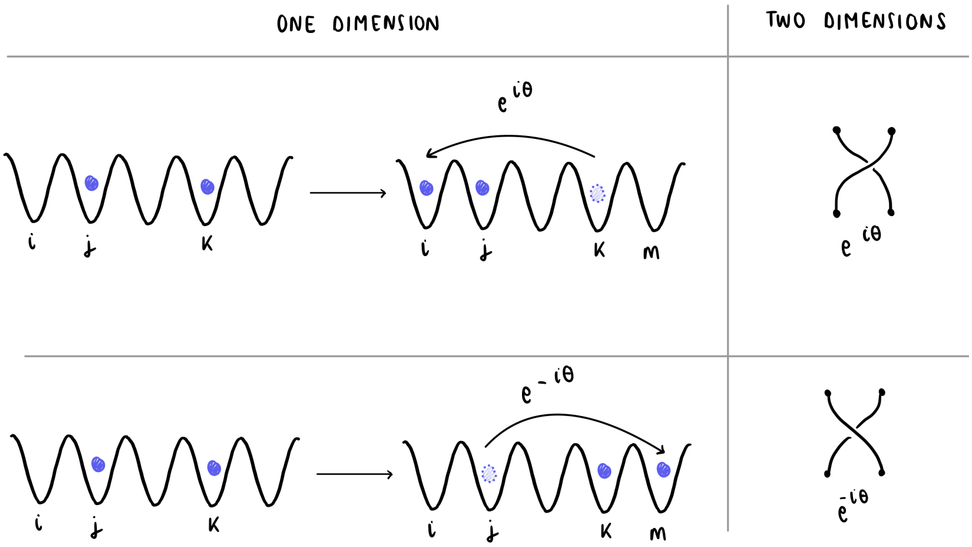

Figure 3.6: Illustration of the phase acquired by anyons performing tunneling processes in different directions, according to Eqs. (3.4).

acquired phase corresponds, in this case, to $e^{-i\theta}$.

The commutation algebra that defines anyons in Eq.(3.4) is explicitly constructed in the Wannier basis to ensure the desired anyonic behavior on the lattice. However, its invariance under unitary basis transformations does not ensue, as it is the case for the canonical bosonic/fermionic commutation/anticommutation algebras.

In terms of the introduced anyonic field operators, the Anyonic-Hubbard Hamiltonian (AHH) reads

$$\hat{H}^a = -J\sum_{j=1}^{L}(\hat{a}_j^\dagger \hat{a}_{j+1} + \hat{a}_{j+1}^\dagger \hat{a}_j) + \frac{U}{2}\sum_{j=1}^{L}\hat{n}_j(\hat{n}_j - 1), \tag{3.11}$$

$\hat{n}_j = \hat{a}_j^\dagger \hat{a}_j$ being the anyonic number operator and including a nearest-neighbour tunneling term, as well as an on-site interaction, analogously to the Bose-Hubbard Hamiltonian (BHH) of Eq. (2.74). It is possible to recast $\hat{H}^a$ in terms of fully bosonic operators using a *Jordan-Wigner transformation*, which relates bosonic operators $\hat{b}_j^{(\dagger)}$ to the anyonic operators $\hat{a}_j^{(\dagger)}$,

$$\hat{a}_j = \hat{b}_j \exp\left(i\theta\sum_{i=1}^{j-1}\hat{n}_i\right), \tag{3.12a}$$

$$\hat{n}_i = \hat{a}_i^\dagger \hat{a}_i = \hat{b}_i^\dagger \hat{b}_i, \tag{3.12b}$$

with $\hat{n}_i$ the number operator for both types of particles. Since $\hat{n}_i$ is the same for anyons and bosons, the total particle number operator $\hat{N}$ will be the same as well. By inserting the Anyon-Boson mapping in Eq.(3.11), one can rewrite the Hamiltonian $\hat{H}^a$ in terms of bosonic operators (a detailed calculation is presented in Appendix A),

$$\hat{H}_\theta = -J\sum_{j=1}^{L}(\hat{b}_j^\dagger \hat{b}_{j+1} e^{i\theta\hat{n}_j} + e^{-i\theta\hat{n}_j}\hat{b}_{j+1}^\dagger \hat{b}_j) + \frac{U}{2}\sum_{j=1}^{L}\hat{n}_j(\hat{n}_j - 1). \tag{3.13}$$

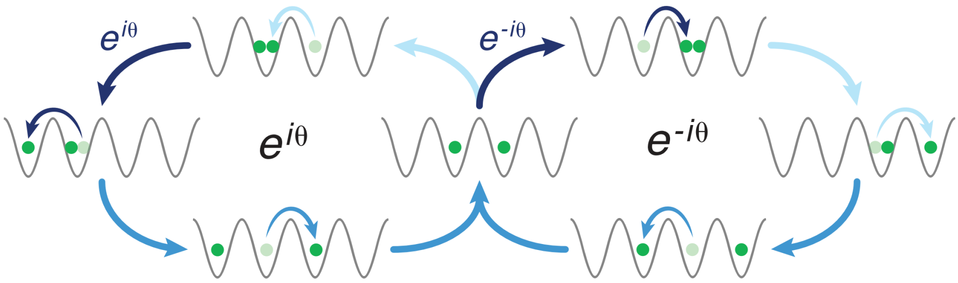

Figure 3.7: Phase acquisition for anyons hopping along closed paths in Fock space, taken from Ref. [15]

The latter expression corresponds to a modified version of Eq. (2.74), where the tunneling amplitudes are occupation-dependent. Thus, $\hat{H}_\theta$ describes bosons with occupation-dependent amplitude $Je^{i\theta n_j}$ for hopping processes from right to left, and $Je^{-i\theta n_j}$ for hopping processes from left to right. Figure 3.7 represents these two anyonic tunneling possibilities, which are well mimicked by the Hamiltonian $\hat{H}_\theta$. It can be noticed that the system holds a certain "memory" of the path followed by the bosons to achieve a certain final configuration, as the acquired phase changes when so does the followed path.

The Hamiltonian presented in Eq. (3.13) exhibits properties that in some cases differ from the ones of the original BHH from Eq. (2.74). In the following, we discuss the main features of $\hat{H}_\theta$, and compare them with those of $\hat{H}_{BH}$. We will start discussing the symmetries of the Hamiltonian $\hat{H}_\theta$:

- Total particle number conservation

  It is straightforward to demonstrate that the Hamiltonian of Eq. (3.13) verifies $[\hat{H}_\theta, \hat{N}] = 0$, where $\hat{N}$ is the total particle number operator. This property is common for both $\hat{H}_\theta$ and $\hat{H}_{BH}$.

  Similarly, the dimensionality of the Anyonic-Hubbard model $\mathcal{N}$ exhibits the same dependence on the number of particles N and lattice sites L as the BHH, and thus follows Eq. (2.75).

- Time reversal symmetry

  Unlike the BHH, the Hamiltonian $\hat{H}_\theta$ is not invariant under the action of the time-reversal operator $\hat{T}$. In other words, the presence of the complex occupation-dependent tunneling strengths breaks time reversal symmetry.

- Parity symmetry

  Using the transformations of the creation/annihilation and number operators given in Eqs. (2.78) and (2.79), it is easy to demonstrate that the transformation of $\hat{H}_\theta$ under the parity operator, $\Pi\hat{H}_\theta\Pi^\dagger$ does not leave the Hamiltonian invariant. In other words, $\Pi\hat{H}_\theta\Pi^\dagger \neq \hat{H}_\theta$, since the occupation-dependent tunneling strengths break parity symmetry.

- Translational invariance

  Just like we did for the BHH, periodic boundary conditions are assumed and, consequently, one can use the transformations given by (2.83) to see that the system described by $\hat{H}_\theta$ remains invariant under spatial translations, i.e., $P\hat{H}_\theta P^\dagger = \hat{H}_\theta$.

In contrast to the Bose-Hubbard Hamiltonian, $\hat{H}_\theta$ does not have an analytical solution for the case where $U = 0$, but only for the case where $J = 0$. The occupation-dependent tunneling strengths, containing the operators $e^{\pm i\theta\hat{n}_j}$, stop the tunneling term from being a one-particle observable, as it was for the BHH. Thus, the non-interacting anyonic system is already highly non-trivial.

On the other hand, the Jordan-Wigner transformation from Eq.(3.12) leaves the energy spectrum invariant, i.e., both forms of the Hamiltonian describing the anyonic system, $\hat{H}^a$ and $\hat{H}_\theta$ share the same eigenenergies. Similarly, the intensities of the eigenstates of $\hat{H}^a$ and $\hat{H}_\theta$ in the on-site Fock basis both coincide, since the transformation from Eq.(3.12) only adds a phase to the states $|\mathbf{n}\rangle$. In other words, the eigenstates of $\hat{a}_j\hat{a}_j^\dagger$ and $\hat{b}_j\hat{b}_j^\dagger$ only differ by a phase. Let the eigenstate of $\hat{H}^a$ with eigenvalue E be denoted by $|\psi_E\rangle$ and, analogously, the eigenstate of $\hat{H}_\theta$ with the same eigenvalue is represented by $|\phi_E\rangle$. If we denote the Jordan-Wigner transformation by Q, we have

$$Q(\hat{H}^a|\psi_E\rangle = E|\psi_E\rangle) \Rightarrow \hat{H}_\theta \underbrace{(Q|\psi_E\rangle)}_{|\phi_E\rangle} = E \underbrace{(Q|\psi_E\rangle)}_{|\phi_E\rangle} \tag{3.14}$$

$$\tag{3.15}$$

and

$$|\phi_E\rangle = Q\sum_{\mathbf{n}} {}_a\langle\mathbf{n}|\psi_E\rangle|\mathbf{n}\rangle_a = \sum_{\mathbf{n}} {}_a\langle\mathbf{n}|\psi_E\rangle\; Q|\mathbf{n}\rangle_a = \sum_{\mathbf{n}} {}_a\langle\mathbf{n}|\psi_E\rangle\; e^{i\beta}|\mathbf{n}\rangle_b, \tag{3.16}$$

where only here we distinguish between the anyonic $\{|\mathbf{n}\rangle_a\}$ and the bosonic $\{|\mathbf{n}\rangle_b\}$ Fock bases for clarity. Therefore,

$$|{}_a\langle\mathbf{n}|\psi_E\rangle|^2 = |{}_b\langle\mathbf{n}|\phi_E\rangle|^2. \tag{3.17}$$

As a consequence, all the properties and observables that are entirely determined by these intensities in the anyonic model can be directly measured using the bosonic system.

3.2.2 Experimental realization

The lattice anyons introduced above are not just a theoretical proposal. Interestingly, the modified bosonic Hamiltonian from Eq. (3.13) has been very recently engineered in the laboratory with ultracold bosons in an optical lattice, and the properties of a system of two interacting anyons could be directly probed. Here, we discuss the basic experimental procedure followed and some of the results reported in Ref. [15].

Concerning the engineering of the AHH, the first step consists in realizing the Bose-Hubbard model with density-dependent phase. This is achieved by modulating the amplitude of a tilted lattice with three frequency components to induce occupation-dependent tunneling strengths, as shown in Fig. 3.8. The assembly consists in a lattice set up in the presence of a magnetic field gradient, resulting in a lattice in which the on-site energies are shifted by an energy E. As a consequence of this shift, tunneling is suppressed, since it becomes off-resonant in energy. In order to restore tunneling in the system, the lattice depth is modulated by three frequencies, all of them with amplitude δV. These frequencies correspond, individually, to the energy necessary for a boson to tunnel from one site

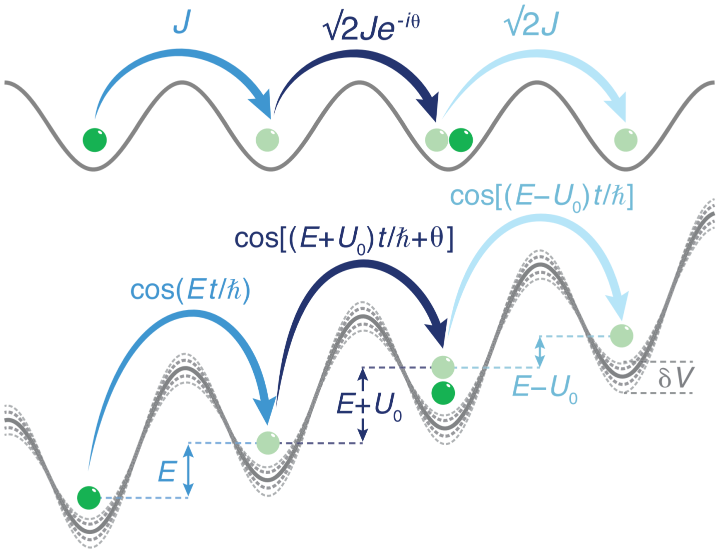

Figure 3.8: Realization of anyons in one dimension. The AHH (3.11) is realized in a tilted optical lattice, whose depth is modulated by three different frequencies responsible for inducing tunneling. The offset phase θ of the frequency component with energy $E + U_0$ realizes the density-dependent phase of Hamiltonian (3.13). Image taken from Ref. [15].

to one of the adjacent ones, according to the occupancy of the origin and destination sites [40]. Thus, the first frequency is $E/\hbar$, and is associated with the required energy for a boson to tunnel from a singly-occupied site to an adjacent empty site (see the leftmost hopping process illustrated in Fig. 3.8). Similarly, the second frequency corresponds to the one needed to induce tunneling of a boson occupying a lattice site in which there are no other bosons to an adjacent site, where another boson is located (which corresponds to the middle hopping process in Fig. 3.8). This frequency takes the value $(E+U_0)/\hbar$, where U_0 is the energy gained when two bosons occupy the same lattice site, i.e., is the energy associated with the interaction between pairs of bosons. The final driving frequency, $(E - U_0)/\hbar$ is the one which induces the remaining tunneling process. It corresponds the energy capable of causing tunneling of a boson that occupies a doubly-occupied lattice site to another site where the occupation is null (see rightmost tunneling process in Fig. 3.8). The amplitude δV of modulation determines J, hence enabling specific tunneling events, and the introduction of an offset θ in the frequency component $(E+U_0)/\hbar$ with respect to components $E/\hbar$ and $(E-U_0)/\hbar$ leads to the emergence of the desired density-dependent phase in the two particle system, and therefore the statistical phase of the original anyonic model. This method is an example of *Floquet engineering*, which consists in modifying the properties of a quantum system by dint of external driving fields [41].

Experimental runs implement the sequence presented in Fig. 3.9. A sample of a Mott insulator of ^{87}Rb is used, as shown in 3.9(1). Particularly, the experiment starts with two columns of atoms of such sample. Each of the rows in 3.9(2) are copies of the same system, corresponding to the scheme where two atoms are placed in two contiguous sites of a lattice. Then, all of the copies are tilted so that tunneling is suppressed [3.9(3)], and then the depth of the lattice is modulated by three frequencies capable of inducing tunneling [3.9(4)], as explained previously. The system is let to evolve and fluorescence imaging is used to make projective measurements on the on-site Fock basis after a desired evolution time of each of the copies of the system [3.9(5)]. Then, an average over all copies

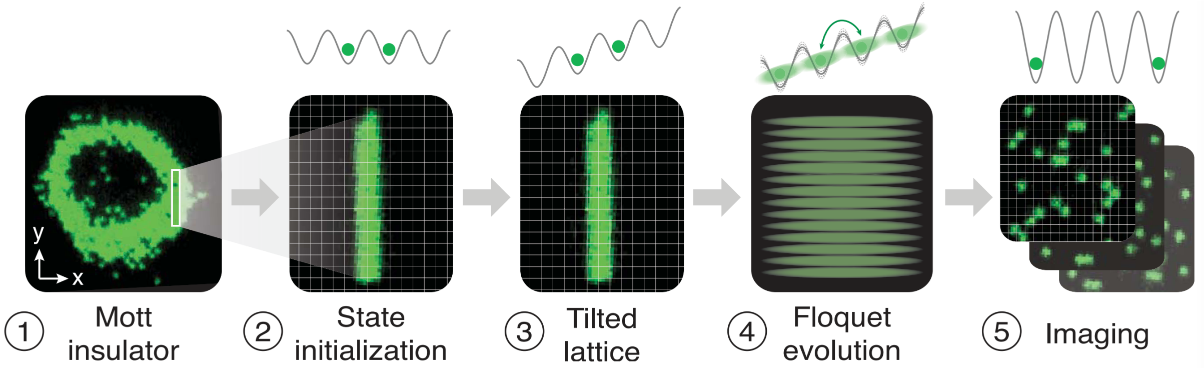

Figure 3.9: Experimental sequence implemented in Ref. [15]: (1-2) Initialize two columns of atoms from a Mott insulator of ^{87}Rb; (3) Suppress tunneling by tilting the lattice; (4) Apply 3-tone modulation to induce tunneling and let the system evolve; (5) Perform projective measurement by fluorescence imaging. Image taken from Ref. [15]

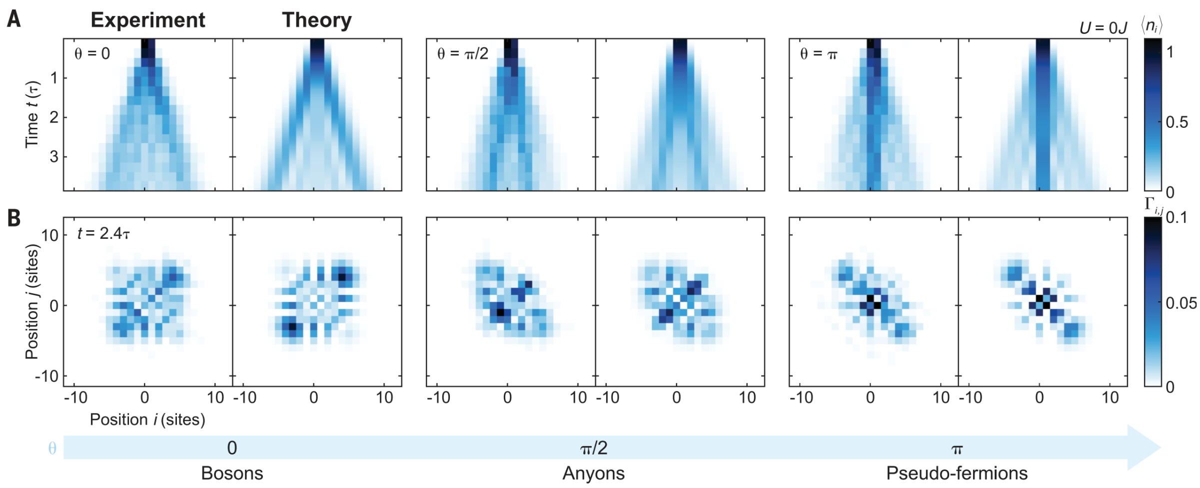

Figure 3.10: Quantum walks of two anyons for $U = 0$. (A) Density profile of two-particle quantum walks for various θ. (B) Density-density correlator $\Gamma_{i,j}$ [Eq. (3.18)] at $t = 2.40(5)\tau$ for various θ. Figure taken from Ref. [15].

is done to obtain the expectation values of specific observables.

The experimental setup is used to study two different situations. First, they consider a system where there is no interaction in $\hat{H}_\theta$, $U = 0$. Under this condition, they analyze the anyonic behavior of bosons undergoing simultaneous quantum walks by measuring their quantum correlations. The state is initialized as $\hat{b}_0^\dagger \hat{b}_1^\dagger |0\rangle = |...0110...\rangle$, and then it is let to evolve for various periods of time measured in units of $\tau \equiv \hbar/J$, the tunneling time. After a certain evolution time, the trajectory of such initial state is captured, and then averaged over all copies of the system. In this way, they are capable of getting the density distributions presented in Fig. 3.10(A). The statistics are characterized by the density-density correlator,

$$\Gamma_{i,j} = \langle \hat{b}_j^\dagger \hat{b}_i^\dagger \hat{b}_i \hat{b}_j \rangle, \tag{3.18}$$

which represents the probability to find one particle on site i and another on site j.

Results in Fig. 3.10(B) show that for $\theta = 0$ bosonic bunching (i.e., the statistical tendency of bosons to stick together) appears, since the dominant matrix elements of $\Gamma_{i,j}$ are the diagonal ones, $i = j$. This is in accordance with Bose-Einstein statistics. On the opposite case, when $\theta = \pi$, the dominant matrix elements are the anti-diagonal ones, with $i = -j$, which is a manifestation of anti-bunching behavior, characteristic of fermions. However, in this case it is remarkable that also significant values for the diagonal matrix elements emerge. This reflects the fact that anyons with $\theta = \pi$ behave as pseudofermions, as it has already been mentioned. Thus, they behave like bosons on-site, leading to enhanced weights along the diagonal of $\Gamma_{i,j}$. For fractional phase, $\theta = \pi/2$, the correlation matrix $\Gamma_{i,j}$ shows intermediate levels of bunching and anti-bunching, as a result of fractional statistics.

More conclusions can be drawn from Fig. 3.10(A), where the density distribution images are presented. Results are characterized by a bimodal structure, leading to a conical shape that narrows for increasing values of the statistical angle θ. This structure can be understood if one thinks of the evolution of the initial Fock state as an interferometric phenomenon, as illustrated in Fig. 3.11. The experiment is initiated with the Fock state $|..., 0, 1, 1, 0, ...\rangle$, and then tunneling is induced. A rightward tunneling event leads to two possible configurations, which correspond to a boson tunneling to an adjacent site. In the first case, the leftmost boson tunnels to its right adjacent site, where the other boson is located, leading to a configuration whose corresponding Fock state is $|..., 0, 0, 2, 0, ...\rangle$. This distribution constitutes the starting point for another rightwards tunneling event where a phase $e^{-i\theta}$ is acquired, ending in the state $|..., 0, 0, 1, 1, ...\rangle$. On the other hand, starting from the initial state $|..., 0, 1, 1, 0, ...\rangle$ the rightmost boson may tunnel to its right neighbour site, which is initially unoccupied, thus yielding to the configuration $|..., 0, 1, 0, 1, ...\rangle$. Then, the final distribution $|..., 0, 0, 1, 1, ...\rangle$ is reached by another tunneling process to the right, with no global phase acquired at any point. One sees then that the two intermediate configurations lead, via rightward particle hopping, to the same final configuration $|..., 0, 0, 1, 1, ...\rangle$. A similar reasoning applies when considering leftward tunneling. The two transitional possibilities interfere distinctly depending on the value of θ. Thus, if $\theta = 0$, the interference is constructive, and therefore the probability of reaching the final states, in which the bosonic density has spread outwards, is enhanced, which is reflected as a homogeneous background and pronounced outer propagation fronts in the cone structure [see left panels in Fig. 3.11(A)]. On the contrary, for the case $\theta = \pi$, the interference is completely destructive, minimizing the probablity of spreading. Thus, the initial site populations tend to remain invariant in time, manifested as a marked central straight line in the density profile for pseudofermions [see right panels in Fig. 3.11(A)]. When the statistical angle takes intermediate values, as for instance $\pi/2$, the interference is also intermediate, characterized by a narrower cone in the density profile.

The interaction parameter U in Hamiltonian (3.13) can be experimentally controled in this setup by introducing a detuning in the sideband frequencies $(E \pm U_0)/\hbar$ of the driving fields, becoming instead $[E \pm (U_0 - U)]/\hbar$. While this is not straightforward to see, it follows by performing a time dependent unitary transformation (i.e., a change of reference frame) of the driven tilted system, by which it turns into (3.13), as discussed in the supplemental material of Ref. [15]. The presence of interactions leads to asymmetric transport in the density profile of two anyons undergoing quantum walks, as can be appreciated from Fig. 3.12. In this case, two intermediate statistical angles with opposite sign are studied, corresponding to $\theta = \pm\pi/2$. These two cases show distributions that seem to be related by a reflection about the center of the lattice, since the density profile shows transport toward the right when $\theta = -\pi/2$ and $U/J = 1.9(4)$, whereas for $\theta = \pi/2$ the direction of

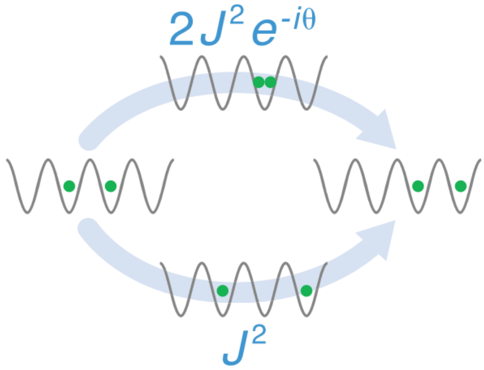

Figure 3.11: Interferometric picture of the Fock state evolution. Figure taken from [15].

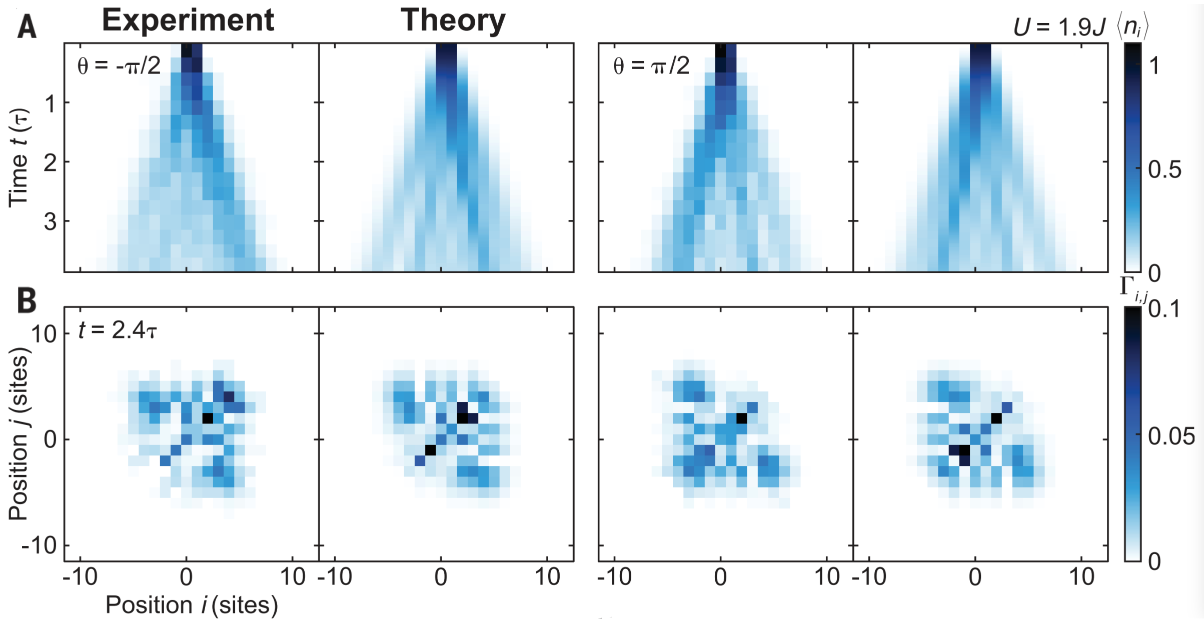

Figure 3.12: Quantum walks of two anyons for $U \neq 0$ and $\theta = -\pi/2$ (left panels) and $\theta = \pi/2$ (right panels). (A) Density profile of two-particle quantum walks. (B) Density-density correlator $\Gamma_{i,j}$ at $t = 2.40(5)\tau$. Figure taken from Ref. [15].

transport is toward the left.

Asymmetric transport is a paradigmatic feature of the anyonic statistics, and could be naturally expected due to the breaking of parity symmetry in Hamiltonian (3.13), by which tunneling events towards left and right acquire different phases and are not equivalent. In the theoretical study of Ref. [24], it is observed that transport is not only asymmetric with θ, but also with U, as depicted in Fig. 3.13. This fact is explained by demonstrating the relations

$$\langle \hat{n}_j(t) \rangle_{+U} = \langle \hat{n}_{j'}(t) \rangle_{-U}, \tag{3.19}$$

$$\langle \hat{n}_j(t) \rangle_{+\theta} = \langle \hat{n}_{j'}(t) \rangle_{-\theta}, \tag{3.20}$$

where sites j and j' are related by the parity operator Π.

Therefore, it can be stated that by reversing the sign of the statistical angle θ or interaction strength U, anyons also reverse their preferred propagation direction.

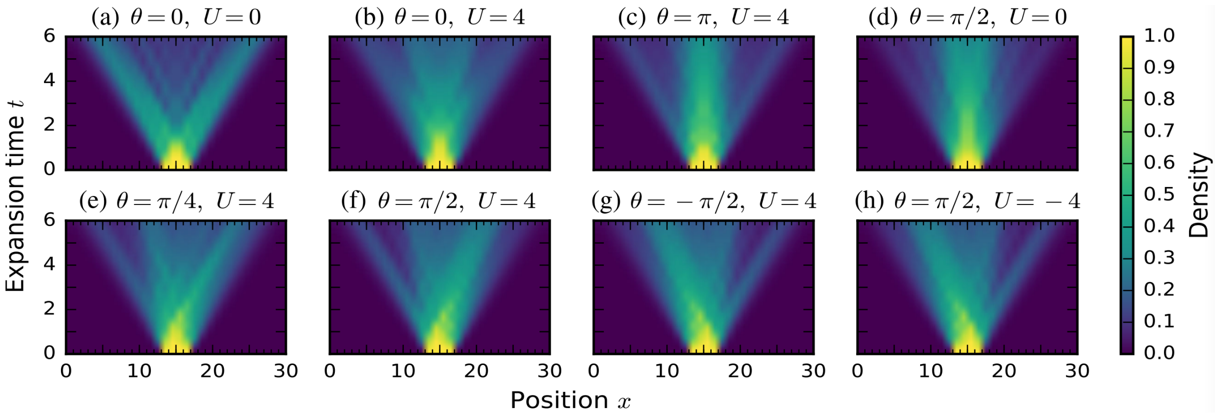

Figure 3.13: Anyonic transport as a function of θ and U, where one can observe the predicted transformation of the asymmetric transport under sign reversal of θ or U, according to Eqs. (3.19) and (3.20). Figure taken from Ref. [24].

4 | Physical properties of the anyonic ground state

The aim of this chapter is to study the ground state of the Anyonic-Hubbard model. In particular, we conduct the first study of the ground state structure in Fock space via multifractality, as well as its applicability to monitor Mott insulating and superfluid phases in anyonic matter. For this purpose, we first use an analytical approach using *mean-field theory* to characterize the ground state phase diagram. Additionally, in the strong interacting regime, perturbation theory is applied to obtain an analytical expression for the ground state and its generalized fractal dimensions. These expressions are compared against numerical results, and then such results are used to determine the emergence of a phase transition in the ground state, as well as the critical point for which it occurs.

4.1 Superfluid to Mott insulator transition: Mean-field calculation

Using an analogous procedure to the one described in Ref. [23], we perform an analytic calculation in order to determine the position of the critical point for which the transition from a superfluid to a Mott insulator phase in the ground state can be observed. For this purpose, we make use of the *mean-field approximation*, where some operators on the Hamiltonian are substituted by their expectation values [36].

Mean-field approximation starts from the assumption that second order fluctuations of the bosonic creation and annihilation operators are negligible [36],

$$(\hat{b}_j - \langle \hat{b}_j \rangle)(\hat{b}_i^\dagger - \langle \hat{b}_i^\dagger \rangle) \approx 0, \quad i \neq j, \tag{4.1}$$

which is equivalent to stating that the product $\hat{b}_j^\dagger \hat{b}_i$ of such operators is decoupled

$$\hat{b}_j^\dagger \hat{b}_i \approx \hat{b}_j^\dagger \langle \hat{b}_i \rangle + \hat{b}_i \langle \hat{b}_j^\dagger \rangle - \langle \hat{b}_i \rangle \langle \hat{b}_j^\dagger \rangle. \tag{4.2}$$

We start from the Anyonic-Hubbard Hamiltonian written in terms of bosonic operators, and formulate it in the Grand canonical ensemble, as we did in Sec. 2.2.2. Hence, we will use the Hamiltonian of Eq. (3.13) and add a term that allows the total particle number to vary, according to the chemical potential μ. Thus, the Hamiltonian we work with is

$$\hat{K}_\theta = -J \sum_{j=1}^{L} (\hat{b}_j^\dagger \hat{b}_{j+1} e^{i\theta \hat{n}_j} + e^{-i\theta \hat{n}_j} \hat{b}_{j+1}^\dagger \hat{b}_j) + \frac{U}{2} \sum_{j=1}^{L} \hat{n}_j (\hat{n}_j - 1) - \mu \sum_{j=1}^{L} \hat{n}_j. \tag{4.3}$$

We can separate the total Hamiltonian in two parts, $\hat{H}_0$ and $\hat{H}_1$, $\hat{H}_1 \equiv \hat{H}_J$ being the tunneling term, and $\hat{H}_0$ all remaining terms, $\hat{H}_0 = \hat{K}_\theta - \hat{H}_J$. Thus,

$$\hat{K}_\theta = \hat{H}_0 + \hat{H}_1. \tag{4.4}$$

The mean-field approximation will be used in the tunneling term, which entails the following substitutions,

$$\begin{aligned} \hat{b}_j^\dagger e^{i\theta\hat{n}_j}\hat{b}_{j+1} &\longrightarrow \langle \hat{b}_j^\dagger e^{i\theta\hat{n}_j}\rangle \hat{b}_{j+1} + \langle \hat{b}_{j+1}\rangle \hat{b}_j^\dagger e^{i\theta\hat{n}_j}, \\ e^{-i\theta\hat{n}_j}\hat{b}_j\hat{b}_{j+1}^\dagger &\longrightarrow \langle e^{-i\theta\hat{n}_j}\hat{b}_j\rangle \hat{b}_{j+1}^\dagger + \langle \hat{b}_{j+1}^\dagger\rangle e^{-i\theta\hat{n}_j}\hat{b}_j, \end{aligned}$$

where the expectation values are taken in the ground state of the system, which is so far unknown.

Then, in the mean-field approximation, the tunneling term takes the form

$$\hat{H}_1 \approx -J\sum_{j=1}^{L}\left(\langle \hat{b}_j^\dagger e^{i\theta\hat{n}_j}\rangle \hat{b}_{j+1} + \langle \hat{b}_{j+1}\rangle \hat{b}_j^\dagger e^{i\theta\hat{n}_j} + \langle e^{-i\theta\hat{n}_j}\hat{b}_j\rangle \hat{b}_{j+1}^\dagger + \langle \hat{b}_{j+1}^\dagger\rangle e^{-i\theta\hat{n}_j}\hat{b}_j\right). \tag{4.5}$$

Recall that, since periodic boundary conditions are being assumed, the Hamiltonian $\hat{H}_\theta$, and thus $\hat{K}_\theta$, exhibits translational invariance. Consequently, the ground state is also invariant under spatial translations, and hence the expectation values of $\hat{b}_j$ and $\hat{b}_{j+1}$ are the same. Similarly, $\langle \hat{b}_j e^{i\theta\hat{n}_j}\rangle = \langle \hat{b}_{j+1} e^{i\theta\hat{n}_{j+1}}\rangle$. This fact allows writing

$$\begin{aligned} \hat{H}_1 &\approx -J\sum_{j=1}^{L}(\langle \hat{b}_j^\dagger e^{i\theta\hat{n}_j}\rangle \hat{b}_{j+1} + \langle \hat{b}_j\rangle \hat{b}_j^\dagger e^{i\theta\hat{n}_j} + \langle e^{-i\theta\hat{n}_j}\hat{b}_j\rangle \hat{b}_{j+1}^\dagger + \langle \hat{b}_j^\dagger\rangle e^{-i\theta\hat{n}_j}\hat{b}_j) &(4.6)\\ &= -J\sum_{j=1}^{L}(\langle \hat{b}_{j-1}^\dagger e^{i\theta\hat{n}_{j-1}}\rangle \hat{b}_j + \langle \hat{b}_j\rangle \hat{b}_j^\dagger e^{i\theta\hat{n}_j} + \langle e^{-i\theta\hat{n}_{j-1}}\hat{b}_{j-1}\rangle \hat{b}_j^\dagger + \langle \hat{b}_j^\dagger\rangle e^{-i\theta\hat{n}_j}\hat{b}_j) &(4.7)\\ &= -J\sum_{j=1}^{L}(\langle \hat{b}_j^\dagger e^{i\theta\hat{n}_j}\rangle \hat{b}_j + \langle \hat{b}_j\rangle \hat{b}_j^\dagger e^{i\theta\hat{n}_j} + \langle e^{-i\theta\hat{n}_j}\hat{b}_j\rangle \hat{b}_j^\dagger + \langle \hat{b}_j^\dagger\rangle e^{-i\theta\hat{n}_j}\hat{b}_j), &(4.8) \end{aligned}$$

where in order to obtain (4.7) from (4.6) we renamed some indices $j \longrightarrow j-1$ (recall we have periodic boundary conditions), and we made use of the ground state translational invariance to get (4.8) from (4.7). At this point, we define

$$\lambda \equiv \langle \hat{b}_j^\dagger e^{i\theta\hat{n}_j}\rangle \quad \text{and} \quad \beta \equiv \langle \hat{b}_j^\dagger\rangle, \tag{4.9}$$

so that $\hat{H}_1$ takes the form

$$\begin{aligned} \hat{H}_1 &\approx -J\sum_{j=1}^{L}(\lambda\ \hat{b}_j + \lambda^*\ \hat{b}_j^\dagger + \beta\ e^{-i\theta\hat{n}_j}\hat{b}_j + \beta^*\ \hat{b}_j^\dagger e^{i\theta\hat{n}_j}) &(4.10)\\ &= -J\sum_{j=1}^{L}\left((\lambda + \beta\ e^{-i\theta\hat{n}_j})\hat{b}_j + \hat{b}_j^\dagger(\lambda^* + \beta^*\ e^{i\theta\hat{n}_j})\right). &(4.11) \end{aligned}$$

We would like to note that, for the purpose of simplifying the operations, this calculation was attempted using only one mean-field parameter $\alpha \equiv \langle \hat{b}_j\rangle = \langle \hat{b}_{j+1}\rangle$, leaving the exponential $e^{-i\theta\hat{n}_j}$ out of the expectation values. However, this method resulted not to be valid, and thus the two parameters λ and β had to be considered.

Therefore, the total Hamiltonian in this approximation corresponds to a Hamiltonian in which the sites are decoupled, and thus it can be written as the sum of terms regarding to each of the lattice sites j,

$$\hat{K}_\theta \approx \sum_{j=1}^{L}[\hat{H}_0^{(j)} + \hat{H}_1^{(j)}], \tag{4.12}$$

where

$$\hat{H}_0^{(j)} = \frac{U}{2}\hat{n}_j(\hat{n}_j - 1) - \mu\hat{n}_j, \tag{4.13}$$

$$\hat{H}_1^{(j)} = -J\left((\lambda + \beta\ e^{-i\theta\hat{n}_j})\hat{b}_j + \hat{b}_j^\dagger(\lambda^* + \beta^*\ e^{i\theta\hat{n}_j})\right). \tag{4.14}$$

Thus, the eigenstates of the total Hamiltonian $\hat{K}_\theta$ are just tensor products of the form

$$|\phi\rangle = \bigotimes_j |\varphi^{(j)}\rangle, \tag{4.15}$$

where $|\varphi^{(j)}\rangle$ are the eigenstates of $\hat{H}_0^{(j)} + \hat{H}_1^{(j)}$.

The ground state will be a Mott insulator in the case $\hat{H}_1 = 0$. Consequently, the Mott insulator phase is defined by the conditions

$$\lambda = 0, \tag{4.16}$$

$$\beta = 0, \tag{4.17}$$

since in this case the entire Hamiltonian is the pure interaction Hamiltonian that one recovers in the $J/U \to 0$ limit, and for a given μ, the ground state of each $\hat{H}_0^{(j)}$ is the state with ν bosons, $|\nu\rangle$, such that

$$\nu - 1 < \mu/U < \nu, \quad \nu \in \mathbb{N}, \tag{4.18}$$

as we discussed in Sec. 2.2.2.

However, λ and β are defined as expectation values on the ground state, but such ground state is unknown. In the mean-field approximation the entrance into the superfluid phase is signaled by $\lambda \neq 0$ and $\beta \neq 0$. Then, one may estimate the transition point using a perturbative treatment controlled by the mean-field parameters contained in $\hat{H}_1$, i.e., assuming $|\lambda|, |\beta| \ll 1$. For the purpose of calculating the ground state, we will make use of non-degenerate perturbation theory, which states, for a Hamiltonian of the form

$$\hat{\mathcal{H}} = \hat{\mathcal{H}}_0 + \alpha\ \hat{\mathcal{H}}_1, \quad \alpha \ll 1, \tag{4.19}$$

that the ground state may be written as

$$|\xi_{gs}\rangle = |\xi^{(0)}\rangle + \alpha|\xi^{(1)}\rangle + \mathcal{O}\left(\alpha^2\right), \tag{4.20}$$

where $|\xi^{(0)}\rangle \equiv |\psi_0\rangle$ is the ground state of $\hat{\mathcal{H}}_0$, and in terms of the eigenenergies and eigenstates of the latter, $\hat{\mathcal{H}}_0|\psi_m\rangle = E_m|\psi_m\rangle$,

$$|\xi^{(1)}\rangle = \sum_{m\neq 0} \frac{\langle\psi_m|\hat{\mathcal{H}}_1|\psi_0\rangle}{E_m - E_0}|\psi_m\rangle. \tag{4.21}$$

Since we already argued that our Hamiltonian is the sum of single-site Hamiltonians, we can restrain our calculations to just one site j. For this reason, we consider the single-site Hamiltonian [see Eq. (4.12)] measured in units of U,

$$\frac{\hat{K}_\theta^{(j)}}{U} \approx \frac{\hat{H}_0^{(j)}}{U} + \frac{\hat{H}_1^{(j)}}{U}, \tag{4.22}$$

In this case, the 0−th order of (4.20) then corresponds to the ground state of $\hat{H}_0^{(j)}/U$, which we already argued is $|\nu\rangle$. Thus,

$$|\xi^{(0)}\rangle = |\nu\rangle. \tag{4.23}$$

In order to get $|\xi^{(1)}\rangle$, we will make use of Eq. (4.21), recalling that the perturbative parameters, λ and β, appear in $\hat{H}_1^{(j)}$, which leads to

$$|\xi^{(1)}\rangle = \frac{J}{U}\left(\frac{\sqrt{\nu+1}(\lambda^* + \beta^*\ e^{i\theta\nu})}{\nu - \mu/U}|\nu+1\rangle + \frac{\sqrt{\nu}(\lambda + \beta\ e^{-i\theta(\nu-1)})}{\mu/U - \nu + 1}|\nu-1\rangle\right). \tag{4.24}$$

With the purpose of simplifying our notation, we define $\tilde{\mu} \equiv \mu/U$ and $\tilde{J} \equiv J/U$.

The ground state is, consequently,

$$\begin{aligned}|\xi_{gs}\rangle =&|\nu\rangle + \tilde{J}\left(\frac{\sqrt{\nu+1}(\lambda^* + \beta^*\ e^{i\theta\nu})}{\nu - \tilde{\mu}}|\nu+1\rangle + \frac{\sqrt{\nu}(\lambda + \beta\ e^{-i\theta(\nu-1)})}{\tilde{\mu} - \nu + 1}|\nu-1\rangle\right) \\ &+ \mathcal{O}(\lambda^2, \beta^2).\end{aligned} \tag{4.25}$$

According to the definitions of λ and β,

$$\begin{aligned}\lambda &= \langle\xi_{gs}|\hat{b}_j^\dagger\ e^{i\theta\hat{n}_j}|\xi_{gs}\rangle \\ &= \tilde{J}\left(\frac{\nu(\lambda\ e^{i\theta(\nu-1)} + \beta)}{\tilde{\mu} - \nu + 1} + \frac{(\nu+1)(\lambda\ e^{i\theta\nu} + \beta)}{\nu - \tilde{\mu}}\right) + \mathcal{O}(\lambda^2, \beta^2),\end{aligned} \tag{4.26}$$

$$\begin{aligned}\beta &= \langle\xi_{gs}|\hat{b}_j^\dagger|\xi_{gs}\rangle \\ &= \tilde{J}\left(\frac{\nu(\lambda + \beta\ e^{-i\theta(\nu-1)})}{\tilde{\mu} - \nu + 1} + \frac{(\nu+1)(\lambda + \beta\ e^{-i\theta\nu})}{\nu - \tilde{\mu}}\right) + \mathcal{O}(\lambda^2, \beta^2),\end{aligned} \tag{4.27}$$

which define a set of self-consistent relations. The system can be expressed in the form

$$\begin{pmatrix} \lambda \\ \beta \end{pmatrix} = \begin{pmatrix} \Lambda_{11} & \Lambda_{12} \\ \Lambda_{21} & \Lambda_{22} \end{pmatrix}\begin{pmatrix} \lambda \\ \beta \end{pmatrix}. \tag{4.28}$$

Thus, forcing the eigenvalues of Λ, $\alpha_\pm$, to obey $|\alpha_\pm| > 1$ the solution of the system converges to non-vanishing values of λ and β, which establish the limit between the Mott-insulator and the superfluid phases. In other words, the condition $\min\{|\alpha_+|, |\alpha_-|\} = 1$ gives the values of J/U for each μ/U that delimit the Mott-insulator and superfluid regimes.

Alternatively, to find the critical J/U that, for each μ/U, determines the border between the Mott insulating and the superfluid phases, the system of equations defined by (4.26) and (4.27) may be explicitly solved. One may select one of the two equations, for instance (4.27), and manipulate both sides so as to leave, on one side, all the dependence on λ and on the other, all the dependence on β. Thus, one finds a relation between λ and β of the form

$$\beta = -\tilde{J}\frac{e^{i\theta\nu}(1+\tilde{\mu})}{-\tilde{J}e^{-i\theta}(\tilde{\mu}-\nu)\nu + \tilde{J}(1+\tilde{\mu}-\nu)(1+\nu) + e^{i\theta}(\nu-\tilde{\mu}-1)(\nu-\tilde{\mu})}\lambda. \tag{4.29}$$

The latter expression is then substituted in the remaining equation, (4.26), obtaining an expression for λ that is independent of β. Afterwards, one just needs to impose $\lambda \neq 0$, since that is the condition for which the Mott insulating phase is left. This condition leads to two possible solutions of J/U from which one has to select the one that, for each value of θ, ν and μ/U, corresponds to the lower value of the tunneling strength that makes the system leave the Mott insulating phase, i.e., the most restricting one, reading

$$\tilde{J} = \frac{\left[\sqrt{f(\theta,\tilde{\mu},\nu) - 4(\tilde{\mu}-\nu)(1+\tilde{\mu}-\nu)\nu(1+\nu)\sin^2(\theta/2)} - |f(\theta,\tilde{\mu},\nu)|\right]}{4\sin^2(\theta/2)\nu(\nu+1)}, \tag{4.30}$$

where

$$f(\theta,\tilde{\mu},\nu) = (1+\tilde{\mu}-\nu)(1+\nu)\cos(\theta\nu) - \nu(\tilde{\mu}-\nu)\cos\left(\theta(\nu-1)\right). \tag{4.31}$$

Figure 4.1 shows the phase boundaries obtained from this procedure, and provides evidence that the Mott lobes obtained using the mean-field approximation persist for non vanishing values of the statistical angle θ. They are compared against the results for $\theta = 0$, already discussed in Sec. 2.2.2. The panels in Fig. 4.1 also include the coordinates of the maximum value of J/U for which the system behaves as a Mott insulator for each integer density ν, which show in every case that the critical value $(J/U)_c$ is greater when $\theta \neq 0$ than in the case $\theta = 0$. However, there is not a monotonic tendency for this critical value when θ increases, as it can be seen in Fig. 4.2. Similarly, larger densities seem to imply lower critical points, as is the case for $\theta = 0$, however this is not the case for all values of θ.

Mean-field predictions are not very accurate in one-dimensional systems. Further numerical studies of the anyonic ground state phase diagram have actually shown that the mean-field approximation fails to describe qualitatively correctly the evolution of $(J/U)_c$ with θ and ν [22].

4.2 Multifractality in the Anyonic-Hubbard ground state

Our purpose now consists in studying the structural properties of the ground state of the Anyonic-Hubbard model. Since it is already known that the multifractal properties of the states provide information regarding their structure, we make use of the generalized fractal dimensions defined in Sec. 2.3 to carry out such study. In the following, we draw on

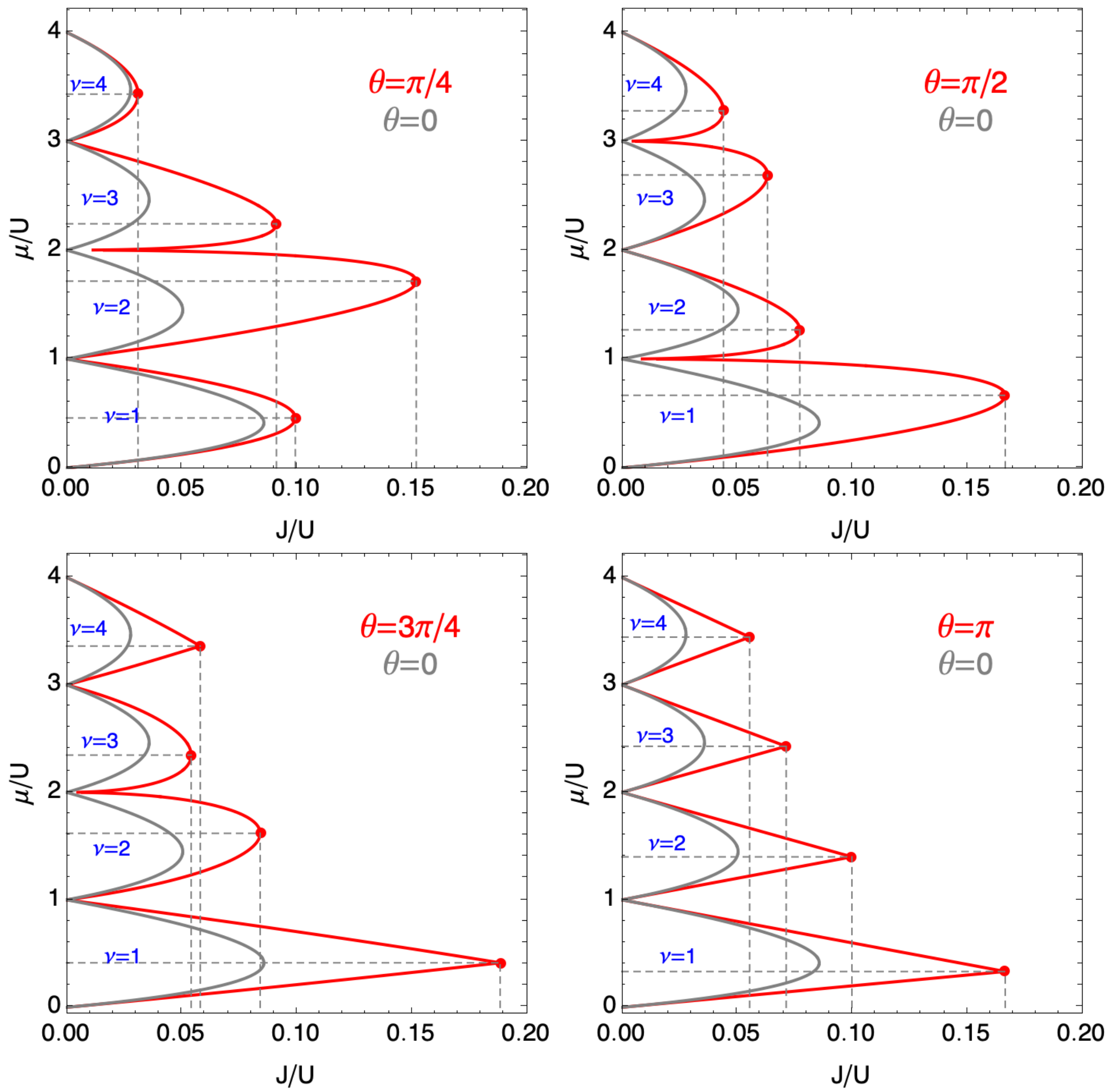

Figure 4.1: Mott lobes for different values of $\theta \neq 0$ obtained using mean-field theory [Eq. (4.30)], compared to the lobes corresponding to $\theta = 0$. Dashed lines indicate the coordinates for which the critical value $(J/U)_c$ (red circles) is found for each integer density ν.

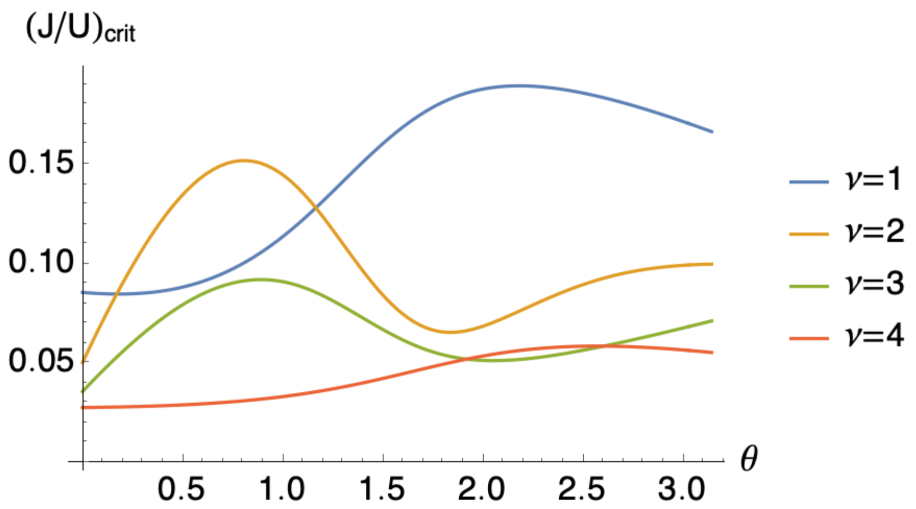

Figure 4.2: Critical points $(J/U)_c$ for the Mott insulator to superfluid phase transition obtained from mean-field theory as a function of the statistical angle θ for different integer densities ν.

exact diagonalization to numerically solve the Hamiltonian $\hat{H}_\theta$ [Eq. (3.13)] for different values of the statistical angle. Making use of parallel execution on HPC facilities, we can obtain the ground state in systems with Hilbert space dimensions $\mathcal{N} \leq 4.5 \times 10^9$, corresponding to $L = 18$ at unit density. The specifications on the numerical methods used and resources required are displayed in Appendix C.

We would like to remark that, for all of our simulations, we work in the on-site Fock basis $\{|\mathbf{n}\rangle\}$, defined in Eq. (2.94).

4.2.1 Ground state structure and multifractality versus J/U for different values of θ

We numerically obtain the ground state of the system for various system sizes and statistical angles and calculate the values of the generalized fractal dimensions $\tilde{D}_q$, defined in Eq. (2.126), to verify whether they provide useful information regarding the structure of such ground state. As it was explained in Sec. 2.3, a multifractal state is characterized for having values of the generalized fractal dimensions between 0 and 1, for any q. Thus, the evolution of the values of $\tilde{D}_q$ with q and L will reveal the potential multifractality of the anyonic ground state.

Figure 4.3 shows different fractal dimensions, namely $\tilde{D}_1$, $\tilde{D}_2$ and $\tilde{D}_\infty$ as functions of J/U for different values of the statistical angle θ, different lattice sizes and density $\nu = 1$. For all values of θ, the qualitative behavior observed is the same. As $J/U \to 0$ the exact ground state is expected to converge to the single Fock state, $|\mathbf{n}\rangle = |\mathbf{1}\rangle$, for any θ, as discussed in Sec. 2.2.2, and hence the GFDs in this limit vanish for any L. As J/U is increased, the values of $\tilde{D}_q$ rise relatively slowly (notice the logscale for J/U in Fig. 4.3), and eventually they undergo a pronounced surge for values of J/U of order $J/U \approx 0.1$. It is remarkable that the value of J/U for which the pronounced tendency change for the values of $\tilde{D}_q$ occurs is the same independently of the statistical angle and the lattice size. This accelerated growth of the GFDs occurs up to values of J/U close to unity, where a convergence starts to emerge. Eventually, the GFDs approach values closer to unity for

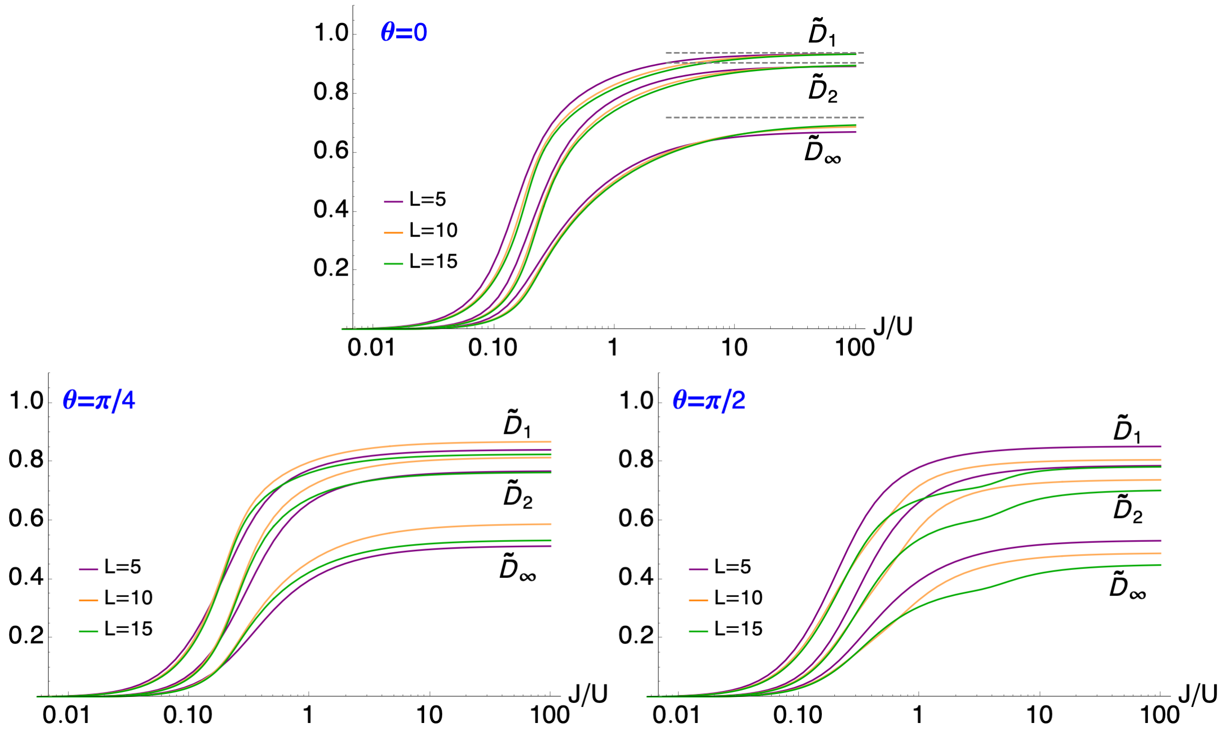

Figure 4.3: Generalized fractal dimensions $\tilde{D}_1$, $\tilde{D}_2$ and $\tilde{D}_\infty$ versus J/U for different lattice sizes and statistical angles, for fixed integer density $\nu = 1$. The dashed lines in the panel for $\theta = 0$ correspond to the analytical calculation of the different $q-$dependent fractal dimensions D_q in the weakly interacting limit [28].

$J/U \to \infty$. This should also be expected, since this limit is dominated by the tunneling term, which naturally induces mixing of the on-site Fock basis $\{|\mathbf{n}\rangle\}$, and therefore the ground state should tend to delocalize to a certain degree.

The case $\theta = 0$ provides particularly useful information, since it is the only one for which analytical expressions for the fractal dimensions D_q in the ground state can be obtained, under certain conditions. For instance, for the case $J/U \to \infty$, one can deduce equations for D_q, which show a non-trivial dependency on the values of q [28], as indicated by dashed lines in the upper panel of Fig. 4.3. Thus, for the case $\theta = 0$ and in the limit $J/U \to \infty$, multifractality in the ground state is ensured. From Fig. 4.3, we can learn that the GFDs for $q = 1, 2$ and ∞ follow independent trajectories, and upon increasing system size they approach different values as J/U grows. In order to conclude on the multifractal character of the ground state, a proper extrapolation towards $L \to \infty$ would be required. However, our results for finite systems, in combination with what is known for $\theta = 0$ [28], provide good numerical evidence that the anyonic ground state exhibits multifractality in Fock space for any value of the statistical angle.

For the purpose of confirming the relation between the change in generalized fractal dimensions and the structure of the ground state, we use a system with $L = N = 7$, whose Hilbert space dimension is $\mathcal{N} = 1716$. Then we choose, for a fixed value of θ, different values of J/U and study whether a variation in the structure of the ground state can be observed. The corresponding intensities $|\varphi_{j(\mathbf{n})}|^2$ as functions of the index $j(\mathbf{n})$ of each basis Fock state $|\mathbf{n}\rangle$ are shown in Fig. 4.4, and provide evidence that the pronounced change in the generalized fractal dimensions is associated with changes in the structure of the ground state. In fact, one can see that for almost vanishing values of J/U there is one intensity which is very close to unity for all the values of θ, whereas the rest of them are almost negligible, leading to a highly localized state in Fock space, as expected from the associated values of $\tilde{D}_1$, which are close to zero. When increasing the value of J/U to 0.2, one observes that the state still seems rather localized, since there is a reduced group of basis states with noticeable intensities. However, in spite of observing the presence of one intensity that stands out over the rest, its value is no longer so close to unity, and thus there are other amplitudes that importantly contribute to the expansion of the state (i.e., which are not negligible). Since this behavior is observed for all the values of θ shown, one can state that for every statistical angle the state is starting to delocalize, which is in accordance with the intermediate values of $\tilde{D}_1 \approx 0.4$ that appear in all cases. On the other hand, when approaching high values of J/U, the opposite limit is visible: The state is rather delocalized in Fock space independently of θ, having many smaller intensities of comparable magnitude. We emphasize that the observed structure for large J/U corresponds to non-trivial values of $\tilde{D}_q$ below 1.

Consequently, it can be stated that a noticeable change in the ground state structure of the anyonic system occurs for any choice of the statistical phase when exceeding a certain value of J/U, which correlates with a rise in the values of the generalized fractal dimensions in the same range of J/U.

In the following sections, we will study to which extent the values of J/U for which the abrupt change in the generalized fractal dimensions occurs may be related to the critical region of the Mott insulator to superfluid phase transition.

4.2.2 Perturbation theory

Up to this point, we have been able to relate changes in the structure of the ground state with changes in the generalized fractal dimensions from numerical results. Our purpose is now to get an approximate analytical expression for the ground state and use it to derive one for the generalized fractal dimensions valid in the regime of strong interactions. This will help us to understand better the effect of θ for small tunneling strength. In order to achieve this, we make use of *standard perturbation theory.* During the present section, we will work with a system with integer density ν and, as we have been doing so far, we will consider periodic boundary conditions.

The total Hamiltonian reads

$$\frac{\hat{H}_\theta}{U} = \left(\hat{H}_{\text{int}} - \frac{J}{U}\hat{H}_{\text{tun}}\right), \tag{4.32}$$

where

$$\hat{H}_{\text{int}} = \frac{1}{2}\sum_{j=1}^{L} \hat{n}_j(\hat{n}_j - 1), \tag{4.33}$$

$$\hat{H}_{\text{tun}} = \sum_{j=1}^{L} (\hat{b}_j^\dagger \hat{b}_{j+1} e^{i\theta\hat{n}_j} + e^{-i\theta\hat{n}_j}\hat{b}_{j+1}^\dagger \hat{b}_j). \tag{4.34}$$

In the limit of strong interactions, $J/U \ll 1$, one may obtain an approximate expression

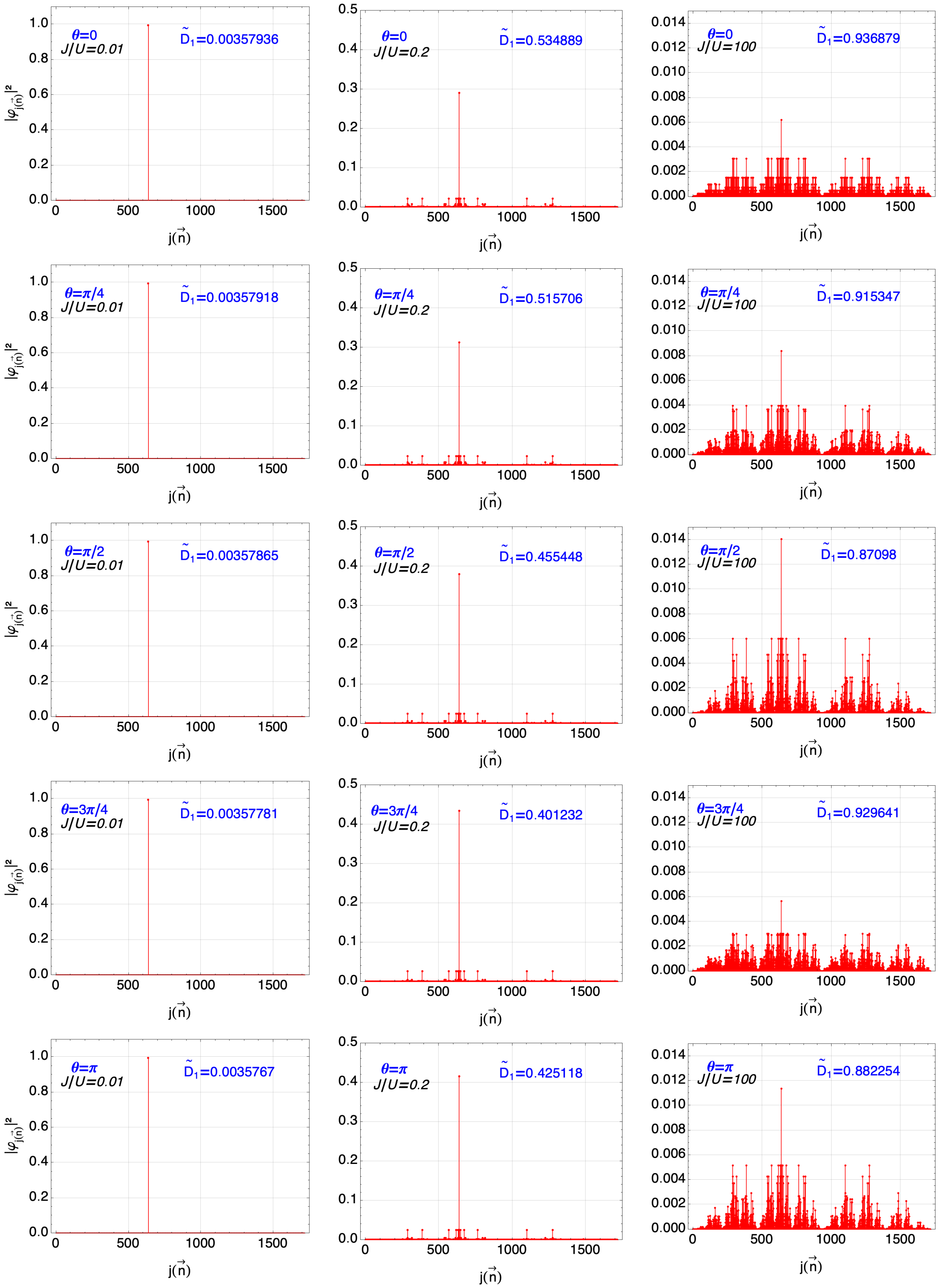

Figure 4.4: Ground state intensities $|\varphi_{j(\mathbf{n})}|^2$ versus basis index for $j(\mathbf{n})$ $L = N = 7$ and different values of θ (increasing from top to bottom) and J/U (increasing from left to right) with their corresponding value of $\tilde{D}_1$, as indicated.

for the ground state, which reads

$$|\phi_{gs}\rangle = |\phi^{(0)}\rangle - \frac{J}{U}|\phi^{(1)}\rangle + \left(\frac{J}{U}\right)^2 |\phi^{(2)}\rangle + \mathcal{O}\left[\left(\frac{J}{U}\right)^3\right]. \tag{4.35}$$

Each contribution follows from

$$|\phi^{(0)}\rangle = |\phi_0\rangle, \tag{4.36}$$

$$|\phi^{(1)}\rangle = \sum_{|\mathbf{n}\rangle \neq |\phi_0\rangle} \frac{\langle \mathbf{n}|\hat{H}_{\text{tun}}|\phi_0\rangle}{\epsilon_0 - \epsilon_{\mathbf{n}}} |\mathbf{n}\rangle, \tag{4.37}$$

$$\begin{aligned} |\phi^{(2)}\rangle = & \sum_{|\mathbf{n}\rangle \neq |\phi_0\rangle} \sum_{|\mathbf{k}\rangle \neq |\phi_0\rangle} \frac{\langle \mathbf{n}|\hat{H}_{\text{tun}}|\mathbf{k}\rangle \langle \mathbf{k}|\hat{H}_{\text{tun}}|\phi_0\rangle}{(\epsilon_0 - \epsilon_{\mathbf{n}})(\epsilon_0 - \epsilon_{\mathbf{k}})} |\mathbf{n}\rangle \\ & - \sum_{|\mathbf{n}\rangle \neq |\phi_0\rangle} \frac{\langle \mathbf{n}|\hat{H}_{\text{tun}}|\phi_0\rangle \langle \phi_0|\hat{H}_{\text{tun}}|\phi_0\rangle}{(\epsilon_{\mathbf{n}} - \epsilon_0)^2} |\mathbf{n}\rangle - \sum_{|\mathbf{n}\rangle \neq |\phi_0\rangle} \frac{1}{2} \frac{|\langle \phi_0|\hat{H}_{\text{tun}}|\mathbf{n}\rangle|^2}{(\epsilon_0 - \epsilon_{\mathbf{n}})^2} |\phi_0\rangle, \end{aligned} \tag{4.38}$$

where $|\phi_0\rangle$ is the ground state of the unperturbed Hamiltonian, $\hat{H}_{\text{int}}$, which is already known to be the state of ν bosons per site,

$$|\phi_0\rangle = |\nu, \ldots, \nu, \ldots, \nu\rangle, \tag{4.39}$$

with energy $\epsilon_0 = L\nu(\nu-1)/2$, and $\epsilon_{\mathbf{n}} = \sum_{j=1}^{L} n_j(n_j-1)/2$ and $|\mathbf{n}\rangle$ denote, respectively, the eigenenergies and eigenstates (the on-site Fock states) of $\hat{H}_{\text{int}}$.

Up to second order in perturbation theory the ground state takes the form

$$\begin{aligned} |\phi_{gs}\rangle = & \left[1 - \tilde{J}^2\ L\ \nu(\nu+1)\right] |\phi_0\rangle \\ & + \tilde{J}\sqrt{\nu(\nu+1)} \sum_{j=1}^{L} \left[e^{i\theta\nu}|\phi_0\rangle^{+1_j}_{-1_{j+1}} + e^{-i\theta(\nu-1)}|\phi_0\rangle^{+1_{j+1}}_{-1_j}\right] \\ & + \tilde{J}^2 \sum_{j=1}^{L} e^{i2\theta\nu}\sqrt{\nu(\nu+1)}\ [\ (\nu+1) + e^{-i\theta}\nu\ ]|\phi_0\rangle^{+1_j}_{-1_{j+2}} \\ & + \tilde{J}^2 \sum_{j=1}^{L} \frac{\sqrt{\nu(\nu+1)(\nu+2)(\nu-1)}}{4} \left(e^{i\theta(2\nu+1)}|\phi_0\rangle^{+2_j}_{-2_{j+1}} + e^{-i\theta(2\nu-3)}|\phi_0\rangle^{+2_{j+1}}_{-2_j}\right) \\ & + \tilde{J}^2 \sum_{j=1}^{L} \frac{(\nu+1)\sqrt{\nu(\nu-1)}}{3}[e^{i\theta} + e^{i2\theta}]|\phi_0\rangle^{+1_{j+2,j}}_{-2_{j+1}} \\ & + \tilde{J}^2 \sum_{j=1}^{L} e^{-i\theta(2\nu-1)}\sqrt{\nu(\nu+1)}[(1+e^{i\theta})\nu + 1]|\phi_0\rangle^{+1_{j+2}}_{-1_j} \\ & + \tilde{J}^2 \sum_{j=1}^{L} \frac{\nu\sqrt{(\nu+1)(\nu+2)}}{3}[e^{i\theta} + e^{i2\theta}]|\phi_0\rangle^{+2_{j+1}}_{-1_{j+2,j}} \\ & + \tilde{J}^2 \sum_{j=1}^{L} \frac{\nu(\nu+1)}{2} \sum_{i\neq j, j\pm 1}^{L} \left[e^{i2\theta\nu}|\phi_0\rangle^{+1_{j,i}}_{-1_{j+1,i+1}} + e^{-i2\theta(\nu-1)}|\phi_0\rangle^{+1_{j+1,i+1}}_{-1_{j,i}} + 2e^{i\theta}|\phi_0\rangle^{+1_{j,i+1}}_{-1_{j+1,i}}\right] \\ & + \mathcal{O}\left(\tilde{J}^3\right), \end{aligned} \tag{4.40}$$

where the notation $|\phi_0\rangle^{+n_l}_{-m_k}$ represents the state $|\phi_0\rangle$ with n added bosons in site l and m subtracted bosons in site k. Similarly, the state denoted by $|\phi_0\rangle^{+n_{l,p}}_{-m_{k,r}}$ is the one in which m bosons have been subtracted from sites k and r and n bosons have been added to sites l and p. For instance, the state $|\phi_0\rangle^{+1_i}_{-1_j}$ is

$$|\phi_0\rangle^{+1_i}_{-1_j} \equiv |\nu, \ldots, \underbrace{\nu - 1}_{j}, \ldots, \underbrace{\nu + 1}_{i}, \ldots, \nu\rangle, \tag{4.41}$$

and the state $|\phi_0\rangle^{+2_k}_{-1_{i,j}}$ is

$$|\phi_0\rangle^{+2_k}_{-1_{i,j}} \equiv |\nu, \ldots, \underbrace{\nu - 1}_{j}, \ldots, \underbrace{\nu - 1}_{i}, \ldots, \underbrace{\nu + 2}_{k}, \ldots \nu\rangle. \tag{4.42}$$

An explicit calculation of $|\phi_{gs}\rangle$ is shown in Appendix B. Recall that, in order to simplify the notation, we defined $\tilde{J} = J/U$.

Note that Eq. (4.40) indicates that L cannot take arbitrarily high values in order for the expression to be acceptable, since from a certain value of L the first amplitude would give an intensity greater than unity, which violates the normalization condition. In addition, expression (4.40) shows that the contribution to the ground state corresponding to $|\phi_0\rangle$ is independent of θ, in contrast to the rest of the amplitudes. The latter expansion for $|\phi_{gs}\rangle$ in the limit $\theta \to 0$ reproduces correctly the known results in perturbation theory for the standard Bose-Hubbard Hamiltonian reported in Ref. [27].

On the basis of the result in Eq. (4.40), the analytical expression for the intensities of the ground state in the on-site Fock basis can be obtained from the amplitudes of the orthogonal states contributing to the expansion of $|\phi_{gs}\rangle$. After the calculation of these intensities, one can see that some of them participate more than once, their multiplicity being determined by the system size L, as shown in Table 4.1. Moreover, the first intensity shows a dependence on L, and thus the range of J/U values for which its perturbative expression is valid will be different as a function of the lattice size. In addition, one can see that not all intensities depend on θ. Lastly, it is noticeable that some intensities only contribute for $\nu > 1$, namely those derived from the amplitudes of states for which two hopping processes from the same site have occurred.

We will check the validity of the perturbative result for $L = N = 5$ and $L = N = 7$, by obtaining the intensities using exact diagonalization. The first step consists in fixing a value of J/U and represent the exact and the perturbation theory intensities as functions of the statistical angle θ, as depicted in Fig. 4.5. Results for both system sizes show agreement with perturbation theory for the lowest values of J/U, as expected, since perturbation theory hinges on the approximation $J/U \ll 1$, and hence its validity is supposed to last while this regime is held. When approaching values of J/U closer to 1, the concordance starts to be mitigated. In fact, for $J/U = 0.1$ differences between both methods start to be noticeable, which means we are leaving the perturbative regime. The dependence on the system size of the perturbation theory results appears for greater values of J/U, which could be expected in view of Eq. (4.40), where the only dependence on L appears on the amplitude corresponding to $|\phi_0\rangle$ and, as it is multiplied by $(J/U)^2$, it is expected to be more relevant for significant values of J/U. From these plots, one can also state that perturbation theory result matches perfectly with exact diagonalization for low values of J/U independently of the statistical phase.

Intensity $|\langle \mathbf{n}|\phi_{gs}\rangle|^2$	Multiplicity
$1-2\tilde{J}^2\ L\ \nu(\nu+1)$	1
$\tilde{J}^2\ \nu(\nu+1)$	$2L$
$\tilde{J}^4\ \nu(\nu+1)\,[1+2\nu(1+\nu)(1+\cos\theta)]$	$2L$
$\tilde{J}^4\nu^2(\nu+1)^2$	$2L(L-3)$
$\frac{2}{9}\tilde{J}^4\nu^2(1+\nu)(2+\nu)(1+\cos\theta)$	L
$\frac{2}{9}\tilde{J}^4\nu(\nu-1)(1+\nu)^2(1+\cos\theta)$	L
$\frac{1}{16}\tilde{J}^4\nu(\nu-1)(1+\nu)(2+\nu)$	$2L$

Table 4.1: Intensities contributing to $|\phi_{gs}|^2$ calculated from perturbation theory up to second order according to the expansion (4.40), with their corresponding multiplicities.

The validity of perturbation theory is most conveniently analyzed when the statistical angle is fixed and the dominant intensities are represented as functions of J/U, as presented in Fig. 4.6. The results are in accordance with the previous perspective, as for each of the statistical angles shown, the agreement between both methods is reasonable, in relative terms, for $J/U \lesssim 10^{-1}$, and thereafter larger deviations start to appear. It is also remarkable that the dependence on the lattice size is hardly visible in these plots: In this case, results are shown up to $J/U = 0.15$ (which is close to the limit for which perturbation theory is valid), and because we already know that the dependence on L for the intensities is proportional to $(J/U)^2$, it is reasonable to think that in the shown regime of J/U the dependence on L will not be noticeable.

Once an analytical expression for the ground state is achieved, it is possible to derive the generalized fractal dimensions for such state in the strongly interacting regime, where we restrict ourselves to the case $q \geq 1$ for simplicity. From the notions learnt in Sec. 2.3, one knows that the first step to obtain the GFDs is to calculate the moments R_q, given by Eq. (2.120). Thus, in view of the intensities of Tab. 4.1, one can straightforwardly obtain

$$R_q = 1 - 2q\ L\nu(\nu+1)\tilde{J}^2 + \tilde{J}^{2q}[\nu(\nu+1)]^q\ \delta_{q,1} + \mathcal{O}(\tilde{J}^3), \quad q \geq 1. \tag{4.43}$$

Note that the last term of (4.43) only participates in the expansion for $q = 1$, because otherwise it would provide contributions of higher order than $\tilde{J}^2$.

Once we have obtained an expression for R_q, one may insert it in (2.126) and expand up to second order in $\tilde{J}$ to calculate the GFDs in the strong interacting regime. Thus, using the expansion $\log(1+x) = x + \mathcal{O}(x^2)$, one obtains

$$\tilde{D}_q = \frac{-\tilde{J}^2 2q\ L\nu(\nu+1) + \tilde{J}^{2q}\ 2L[\nu(\nu+1)]^q\ \delta_{q,1}}{(1-q)\log\mathcal{N}} + \mathcal{O}(\tilde{J}^3), \quad q \geq 1. \tag{4.44}$$

At this point, the last step to calculate each of the generalized fractal dimensions is to particularize for the desired value of q. For instance, for $q = 1$ and according to (2.127),

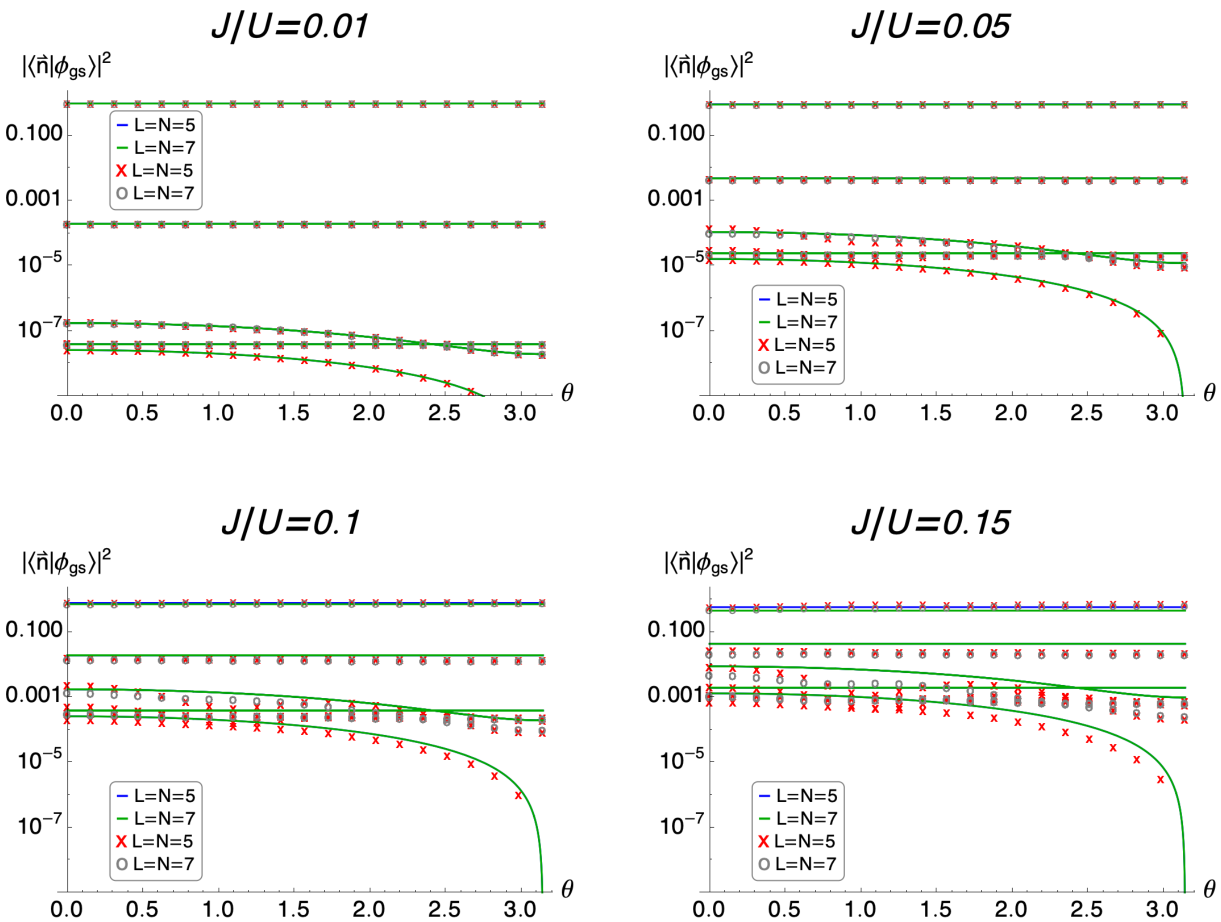

Figure 4.5: Ground state intensities calculated using perturbation theory (lines, corresponding to the intensities shown in Table 4.1) and exact diagonalization (symbols) for fixed values of J/U, and sizes $L = N = 5$ and $L = N = 7$, as a function of θ.

one only has to take the limit $q \to 1$ in the latter expression, which gives

$$\tilde{D}_1 = \frac{2\tilde{J}^2\ L\nu(\nu+1)}{\log \mathcal{N}} \left(1 - 2\log(\tilde{J}) - \log[\nu(\nu+1)]\right) + \mathcal{O}(\tilde{J}^3). \tag{4.45}$$

As one can see, the expression for $\tilde{D}_1$ up to order $\tilde{J}^2$ (and in general for every q) does not exhibit any dependence on θ, which means higher orders in $\tilde{J}$ in the expansion of the ground state would be required to observe an analytical θ dependence. However, the mentioned lack of dependence on θ for small J/U confirms the fact that the Mott insulating phase, which we know to emerge in this regime for $\theta = 0$, also persists for any non vanishing statistical angle.

Analogously, following Eq. (2.129), the expression for $\tilde{D}_\infty$ gives

$$\tilde{D}_\infty = \frac{2\tilde{J}^2\ L\ \nu(\nu+1)}{\log \mathcal{N}} + \mathcal{O}\left(\tilde{J}^3\right), \tag{4.46}$$

where we used that, in the strong interaction regime and under the condition that L cannot take arbitrarily high values, the maximum intensity contributing to the ground

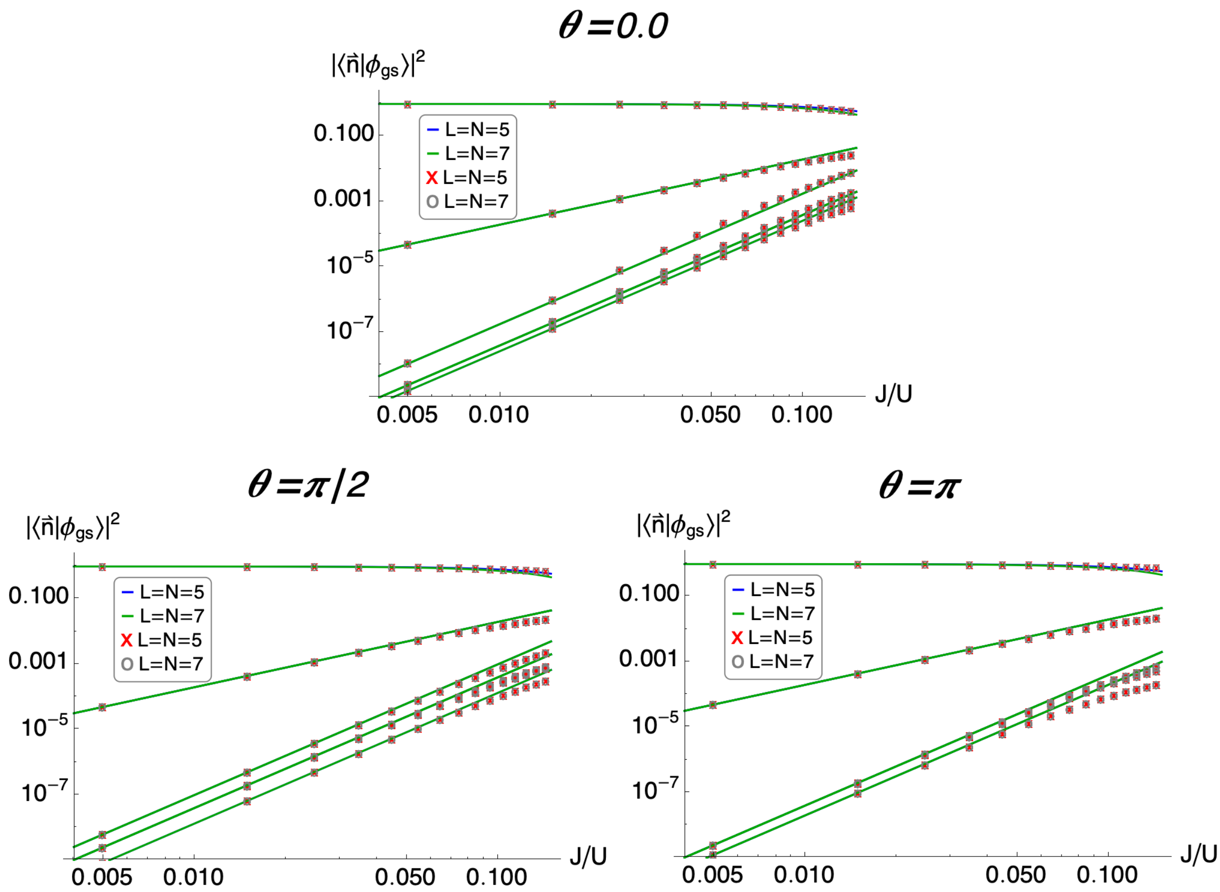

Figure 4.6: Ground state intensities calculated using perturbation theory (lines, corresponding to the intensities shown in Table 4.1) and exact diagonalization (symbols) for fixed values of θ, and sizes $L = N = 5$ and $L = N = 7$, as a function of J/U.

state is given by

$$|\psi_j|^2_{max} = 1 - 2\tilde{J}^2\ L\nu(\nu+1) + \mathcal{O}\left(\tilde{J}^3\right). \tag{4.47}$$

In Fig. 4.7, we show $\tilde{D}_1$ and $\tilde{D}_\infty$ as functions of J/U using perturbation theory (lines) and exact diagonalization (symbols), for two system sizes, $L = N = 7$ ($\mathcal{N} = 1716$) and $L = N = 17$ ($\mathcal{N} = 1\ 166\ 803\ 110$). One can conclude from the plot that for low J/U perturbation theory gives a fair description of the numerical data for all values of θ. On the other hand, for $J/U \gtrsim 0.05$ the exact results start to depart from the analytical prediction. However, it can be seen that the numerical data for $\tilde{D}_1$ and $\tilde{D}_\infty$ show a monotonic decrease with θ, i.e., the larger statistical angle, the smaller the fractal dimensions for the same value of J/U. This behavior indicates that θ induces a slightly stronger localization in Fock space as one starts leaving the strongly interacting regime, which could indicate that larger tunneling strength might be required to leave the Mott insulating regime for larger θ, resulting in greater values of the critical point for higher statistical angles. The dependence on the lattice size does not seem to play an important role in the perturbation theory validity regime for the GFDs since, for both systems studied in Fig. 4.7, the accordance between exact diagonalization and perturbation analytical predictions do not show noticeable differences, despite having very uneven Hilbert space dimensions.

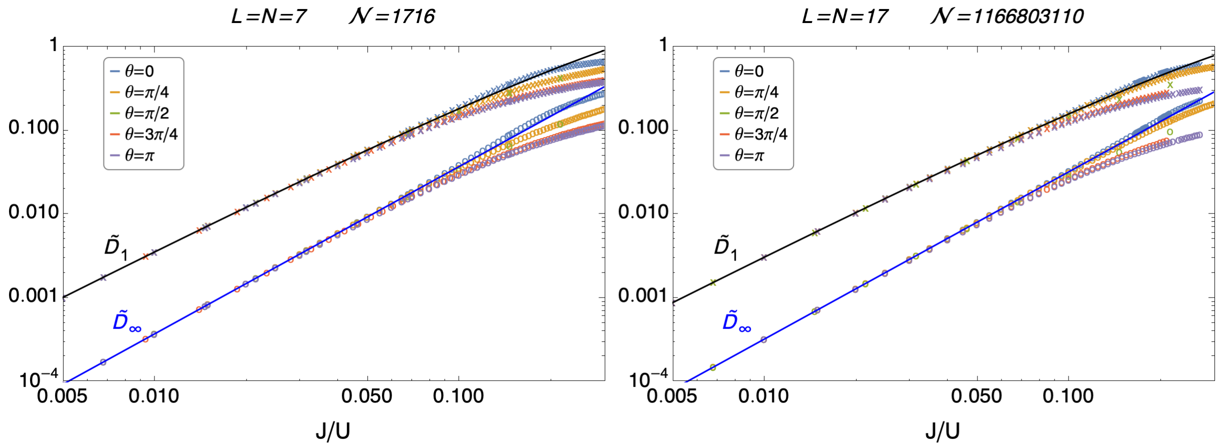

Figure 4.7: $\tilde{D}_1$ and $\tilde{D}_\infty$ comparison between perturbation theory [lines, Eqs. (4.45), (4.46)] and exact numerical results (symbols) for different θ values as a function of J/U, for $L = N = 7$ and $L = N = 17$.

4.2.3 Evolution of the generalized fractal dimensions with particle density and statistical angle

So far we have discussed the evolution of the generalized fractal dimensions with J/U and θ for different system sizes restricted to unit density, $\nu = 1$. Here, we study the evolution of the GFDs with ν as well. For this purpose, we will fix the lattice size to $L = 7$ and calculate, using exact diagonalization, the generalized fractal dimensions for different numbers of bosons, ranging from 1 to 25.

Figure 4.8 shows the value of $\tilde{D}_1$ as a function of the density ν and of J/U, for different statistical angles. The density plots show, for every θ, a suppression of $\tilde{D}_1$ when integer densities are approached, as can be seen from the blue colored regions. However, this suppression is not present for every value of J/U, but it is visible for $J/U \lesssim 0.1$. Beyond this point, $\tilde{D}_1$ starts to increase, reaching noticeable higher values. Therefore, for integer densities the ground state is localized in Fock space for low J/U and starts to delocalize when the tunneling strength is increased. Moreover, the J/U range with low $\tilde{D}_1$ narrows for higher integer densities. These behaviors are generally observed for every statistical angle, although some specific θ features emerge, that we discuss below. Additionaly, for non-integer densities, intermediate values of $\tilde{D}_1$ emerge without an abrupt change as J/U rises.

The analysis for fixed L permits to observe a distinct behavior in the evolution of $\tilde{D}_1$ which could be correlated with the emergence of a Mott insulating phase (characterized by enhanced localization in Fock space) for integer densities and low values of J/U, and the existence of a superfluid phase (concomitant with delocalization in Fock space) for larger J/U values for integer ν or for any non-integer density irrespective of J/U. This conclusion holds for any value of the statistical phase.

These results constitute the first evidence that the existence of different macroscopic phases for lattice anyons can be revealed by the Fock space structure of the system's ground state, hence generalizing the observations reported in Ref. [28] for bosons.

For the purpose of having a better understanding of the behavior of the ground state structure with the statistical angle, we proceed to study some cuts of the density plots

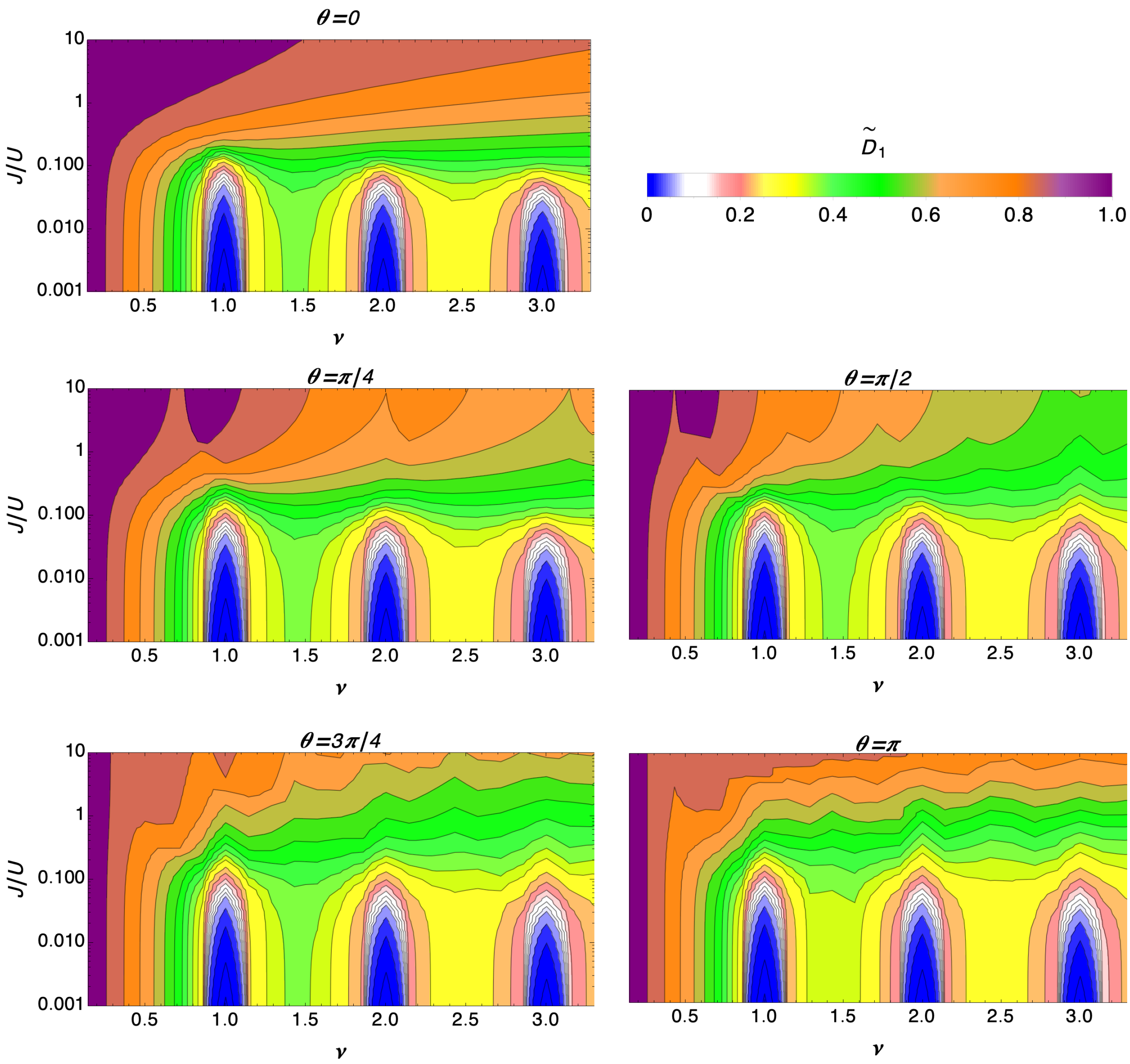

Figure 4.8: Density plots of $\tilde{D}_1$ as a function of J/U and the density ν, for different statistical angles and $L = 7$. The plots are obtained using 25 different values of J/U ranging from 0.001 to 10, equally spaced in logarithmic scale, and using a first order interpolation.

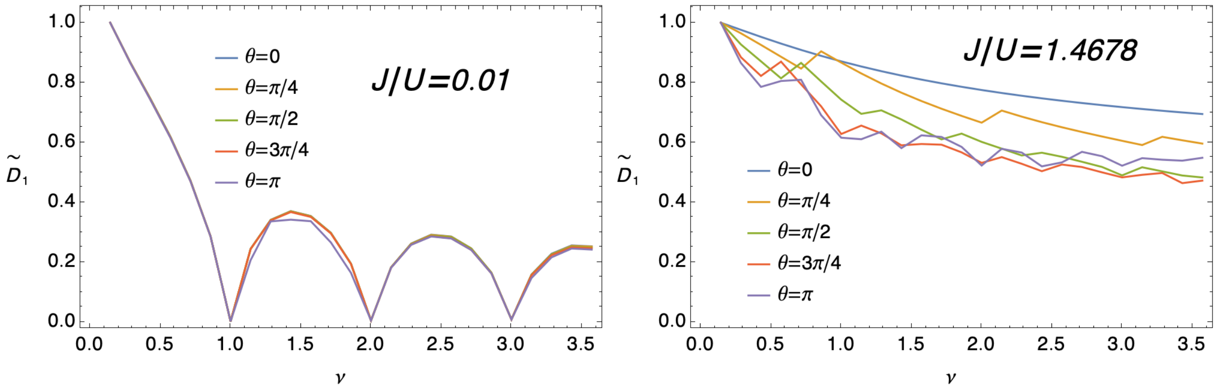

Figure 4.9: $\tilde{D}_1$ versus density ν for $L = 7$ and different J/U values and statistical angles, as indicated.

presented above. We select two fixed values of J/U that are expected to reveal different structures in Fock space, these values being $J/U = 0.01$ and $J/U = 1.4678$, as shown in Fig. 4.9. Results for the lower value of J/U show a deep suppression of the generalized fractal dimension at integer densities, independently of the statistical angle. This drop of $\tilde{D}_1$ is associated with the Mott-insulating phase, emerging at integer densities. On the other hand, in the right panel with $J/U = 1.4678$, one sees that the suppression of the generalized fractal dimension for integer densities disappears, which means the Mott-insulating regime has been left. However, each of the statistical angles show different values of $\tilde{D}_1$. Indeed, higher values of θ give mostly lower values of $\tilde{D}_1$ which implies that, for a fixed density and increasing θ, larger values of J/U are needed for the ground state to reach the same degree of delocalization in Fock space.

We perform a vertical cut in the previous density plots, at $\nu = 1$ for various θ. Then, using two different system sizes, corresponding to $L = 7$ and $L = 17$, we study the evolution of $\tilde{D}_1$ as a function of J/U, shown in Fig. 4.10. Since in both panels logarithmic scale in both axes is used, one can see that the generalized fractal dimension $\tilde{D}_1$ shows two asymptotic tendencies in its evolution: The power-law regime for $J/U \lesssim 0.1$ described by perturbation theory [Eq. (4.45)] and characterized by $\tilde{D}_1 \ll 1$, and the asymptotic convergence of $\tilde{D}_1$ towards values comparable to unity for $J/U > 1$. These tendencies are distinctly visible independently of L and, in principle, the crossover between such limiting behaviors could be qualitatively identified with the transitioning from Mott insulating to superfluid phases in a finite system. Regarding the values of θ, one can see the same tendency that we have been observing in the previous plots: Greater statistical angles require higher tunneling strengths for $\tilde{D}_1$ to undergo the mentioned crossover, leading to a need of larger J/U values for the ground state to become delocalized. Thus, this new point of view also supports the conclusion that, at least for $\nu = 1$, higher critical points $(J/U)_c$ should be needed for larger statistical angles in order for the ground state to leave the Mott insulating phase.

In order to obtain a complete description of the evolution of the generalized fractal dimensions with the system parameters, one must also vary continuously the statistical phase. We choose two integer densities, namely $\nu = 1$ and 2, and obtain the values of $\tilde{D}_1$ as functions of J/U and the statistical angle θ. Additionally, this time we consider hard-wall boundary conditions. Results are shown in Fig. 4.11, accompanied by the estimations of the critical points reported in Refs. [22, 23, 39] as well as the mean-field approximation

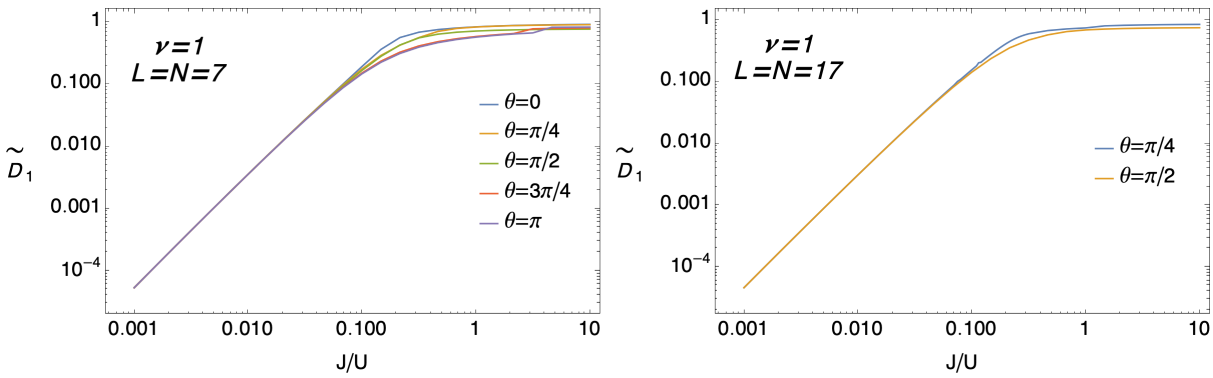

Figure 4.10: $\tilde{D}_1$ versus J/U for different statistical angles and lattice sizes, for $\nu = 1$.

prediction for the critical point (derived in Sec. 4.1 and displayed in Fig. 4.2) . The plot corresponding to $\nu = 1$ shows that for low J/U the values of $\tilde{D}_1$ are suppressed for any statistical angle, indicating that the ground state remains localized independently of θ for sufficiently low tunneling strengths, as expected. When approaching greater values of J/U, the GFD starts to grow, reaching higher magnitudes for lower statistical angles at a fixed tunneling strength. One can see that the numerical predictions for the critical point tend to follow the $\tilde{D}_1$ isolines indicating that, in order to leave the Mott insulating phase, certain values of the GFD have to be reached, as we had concluded previously. The mean-field prediction also shows an interesting behavior, since despite markedly deviating from the numerical values of $(J/U)_c$, it seems to follow approximately the tendency of the isolines.

On the other hand, for $\nu = 2$, a certain lobular structure of $\tilde{D}_1$ emerges with the statistical angle, and for fixed values of J/U the dependence of the GFD on θ becomes clearly non-monotonic (in fact oscillatory). Moreover, we cannot conclude that the numerical predictions for $(J/U)_c$ adjust to our expectations, since they do not seem to follow the isolines of $\tilde{D}_1$, as they did in the previous case. Interestingly, the mean field prediction reproduces rather faithfully the behavior of the $\tilde{D}_1$ isolines. This observation suggests that further studies for $\nu > 1$ are needed to confirm the validity of the numerical estimations of the critical point as a function of θ reported in Ref. [22], as well as to verify if mean-field approximation provides a better qualitative description of the evolution of the critical point for one-dimensional anyons than expected.

4.3 Mott insulator to superfluid transition via multifractality: Estimation of the critical point

In the previous sections, we have demonstrated that multifractality in Fock space emerges for the ground state of the anyonic system, and we have given evidence that the evolution of the GFDs with the relative tunneling strength and density also contain qualitative features of the transition between a Mott insulator and a superfluid phase. Now we analyze whether the changes in $\tilde{D}_q$ permit to perform a quantitative estimation of the critical point of the transition.

A recent work has proven the relation between abrupt changes in the values of the GFDs and the phase transition from Mott insulator to superfluid in the standard Bose-Hubbard

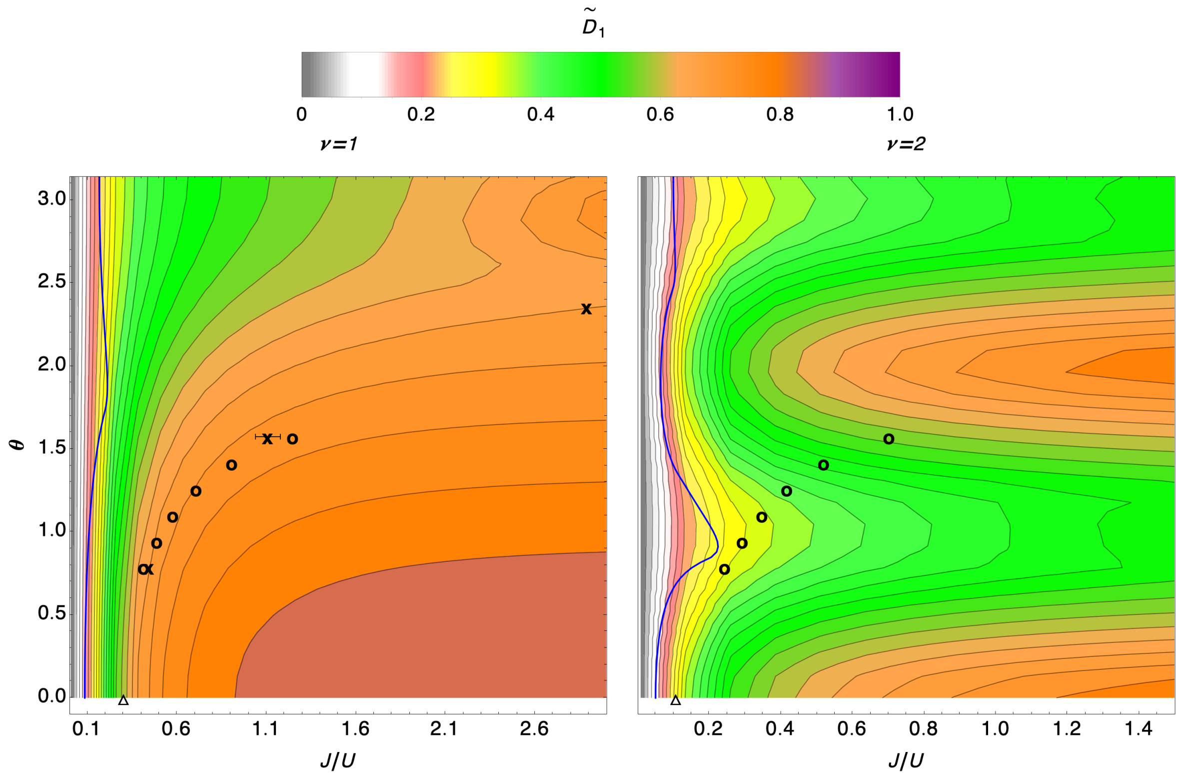

Figure 4.11: $\tilde{D}_1$ versus J/U and θ for integer densities $\nu = 1$ and $\nu = 2$ and $L = 7$. The data is formed by a series of 25 values of θ ranging from 0 to π and 25 values of J/U. Symbols correspond to the estimations of the critical point reported in Refs. [22] (circles), [39] (triangles) and [23] (crosses), whereas the blue line corresponds to the mean-field prediction of the critical point. In this case, hard wall boundary conditions are considered.

Hamiltonian [28]. In this study, they manage to determine the critical point of the transition at unit density from the evolution of the fractal dimensions $\tilde{D}_2$ and $\tilde{D}_\infty$. Our aim now is to verify whether the method used for this determination is also valid for the anyonic system, i.e., for non-vanishing statistical angles.

In order to present the method put forward in Ref. [28], we first use it to characterize the transition in the case $\theta = 0$ from the evolution of $\tilde{D}_1$. This will serve to describe the technical details and provide a new and independent estimation of the critical point $(J/U)_c$ for $\nu = 1$.

The procedure to follow is based upon the fact that while the mere value of the GFDs is not enough to determine the critical point of the transition, their derivatives with respect to the tunneling strength J/U encode that information. As J/U grows from the Mott insulator regime, the derivative of the GFDs is found to reach a single maximum at a certain value $(J/U)^*$ that converges to the critical point $(J/U)_c$ when the thermodynamic limit is reached.

We start by obtaining the values of $\tilde{D}_1$ for an appropriate range of J/U within the Mott insulating phase close to where the critical point is expected to be found. Here, we obtain $\tilde{D}_1$ in a dense grid of values of $J/U \in [0, 0.27]$ considering system sizes $L \in [5, 18]$, as shown by symbols in the upper panel of Fig. 4.12, where it can be seen that for every

$L = N$	m	n	Number of points	$(J/U)^*$	χ^2
5	5	3	73	0.117	8.114×10^{-9}
6	4	6	73	0.127	2.180×10^{-9}
7	4	6	73	0.135	3.312×10^{-9}
8	4	6	73	0.141	4.082×10^{-9}
9	4	6	73	0.147	4.160×10^{-9}
10	4	6	73	0.151	3.614×10^{-9}
11	4	6	73	0.155	2.759×10^{-9}
12	4	6	73	0.159	1.942×10^{-9}
13	4	6	73	0.162	1.443×10^{-9}
14	4	6	73	0.165	1.392×10^{-9}
15	4	6	73	0.167	1.803×10^{-9}
16	4	6	73	0.169	2.662×10^{-9}
17	4	6	73	0.171	3.808×10^{-9}
18	4	6	73	0.174	5.226×10^{-9}

Table 4.2: Information on the Padé fits of Fig. 4.12, including the expansion orders $\{m, n\}$ and the position of the maximum $(J/U)^*$ of the fit first derivative.

lattice size the tendency of $\tilde{D}_1$ with J/U is the same, since the GFD starts at almost vanishing values for low tunneling strengths, and then increases, with the greater systems having higher associated values of $\tilde{D}_1$ for fixed J/U.

Then, in order to optimize the numerical calculation of the derivative of $\tilde{D}_1$ with respect to J/U, we first fit the data to a *Padé approximant*, which can be later differenciated. This is achieved by numerically finding integers $\{m, n\}$ that give the best fit of the $\tilde{D}_1$ numerical data to the expression

$$P_{m,n}\left(\frac{J}{U}\right) = \frac{\sum_{j=0}^{m} a_j \left(\frac{J}{U}\right)^j}{1 + \sum_{j=1}^{n} b_j \left(\frac{J}{U}\right)^j}. \tag{4.48}$$

Since our data has the numerical uncertainty associated with exact diagonalization only, we assume them to have vanishing errors. For this reason, we will consider the best fit to be the one with the lowest number of parameters, $n + m + 1$, that yields $\chi^2 \leq 10^{-8}$. We have checked that all fits fulfilling this condition provide a faithful description of the data and the same value for the position $(J/U)^*$ of the maximum of the derivative. The best fits to the data are shown by lines overlaying the symbols in Fig. 4.12, and the corresponding derivatives are also displayed as solid lines. One can see that the values of the derivative of $\tilde{D}_1$ reach a single maximum and then decrease, taking higher values for smaller systems. Details on the fits as well as the values of $(J/U)^*$ are provided in Table 4.2.

Recall that, as learnt in Sec. 2.2.2, one of the magnitudes that helps to characterize the Mott insulating and superfluid phases is the correlation length, ξ, which takes finite system size independent values in the MI phase, and diverges at the transition point in the thermodynamic limit, according to (2.113). Since we are working with finite size systems, the correlation length can only take values up to the system size. Now, our central hypothesis is that the maximum of the derivative of $\tilde{D}_1$, i.e., the point at which

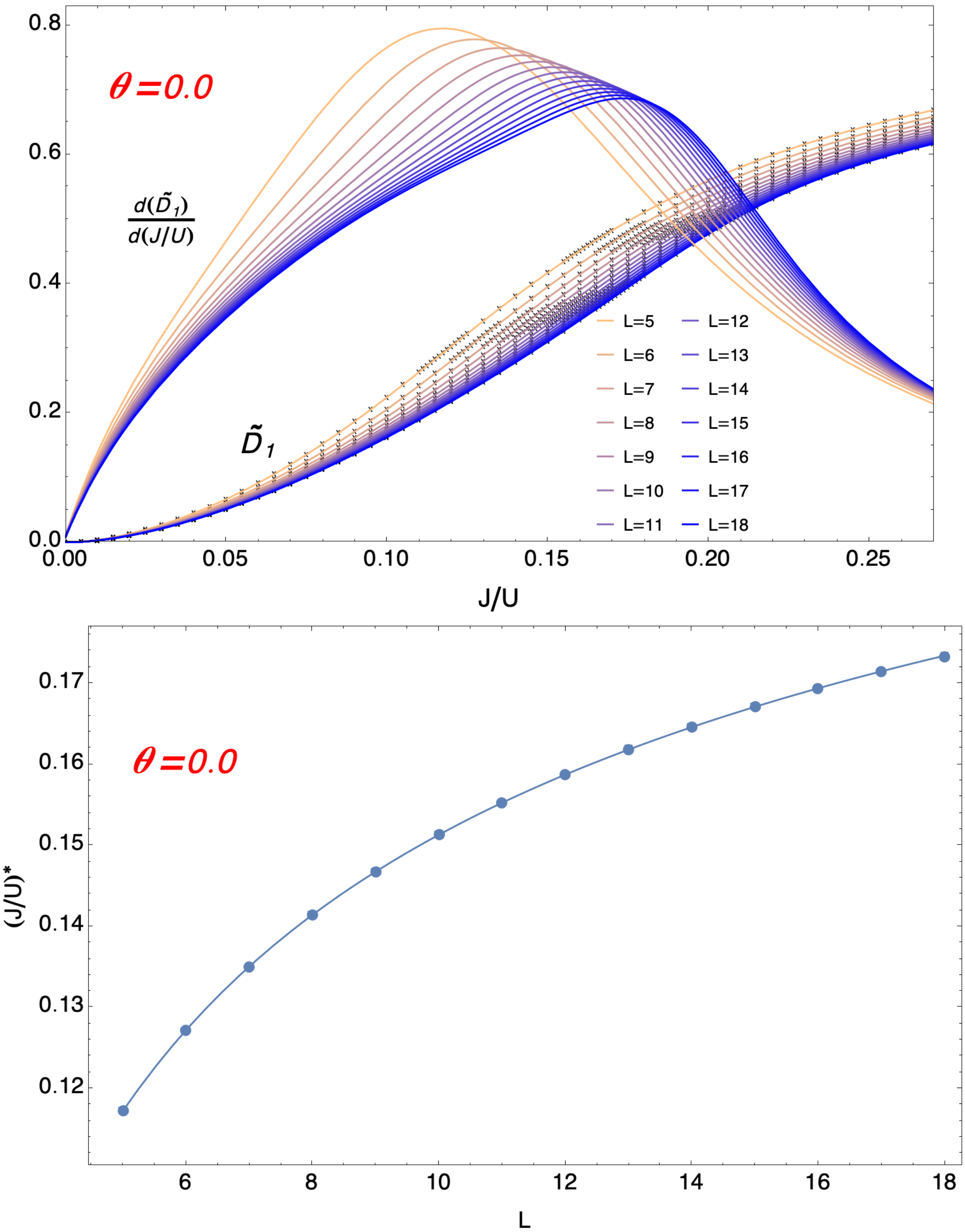

Figure 4.12: (Upper panel) Numerically obtained $\tilde{D}_1$ (crosses) versus J/U for $L \in [5, 18]$ and $\theta = 0$ together with the best Padé fits [Eq. (4.48)] (solid lines overlaying symbols) and their corresponding derivatives (solid lines), whose value has been scaled by the factor 0.2 for optimal visualization. (Lower panel) Scaling of the position of the maximum of $\frac{d(\tilde{D}_1)}{d(J/U)}$ (dots) versus L for $\theta = 0$, where the solid line corresponds to the fit to (4.50) with parameters $(J/U)_c = 0.304 \pm 0.012$, $b = 2.818 \pm 0.318$ and $l_q = 0.007 \pm 0.004$, yielding $\chi^2 = 0.255$.

$\tilde{D}_1$ grows the fastest, corresponds to the $(J/U)^*$ value at which the correlation length becomes comparable to the system size, $\xi \propto L$, i.e., according to (2.112),

$$\exp\left(\frac{c}{\sqrt{(J/U)_c - (J/U)^*}}\right) = k\ L, \tag{4.49}$$

for constant k and c. Therefore, one has that the scaling of $(J/U)^*$ should be governed by

$$(J/U)^*(L) = (J/U)_c - \frac{b^2}{\log^2(L/|l_q|)}, \tag{4.50}$$

for suitable parameters $(J/U)_c$, b and l_q.

In order to make use of the scaling law (4.50), one needs to specify the uncertainty of the $(J/U)^*$ values. Here, we assume that the precision is determined by the finite spacing $\Delta_{(J/U)}$ of the grid of J/U values used to calculate $\tilde{D}_1$. Correspondingly, we take the standard uncertainty to be $\sigma_{(J/U)^*} = \Delta_{(J/U)}/\sqrt{12}$. For the $\theta = 0$ data, we sample $\tilde{D}_1$ with $\Delta_{(J/U)} = 1.25 \times 10^{-3}$ in the region around the maximum of the derivative.

The scaling fit of $(J/U)^*$ versus L is shown in the bottom panel of Fig. 4.12 (solid line), accompanied by the data used for the fit (symbols) and their uncertainties (which are contained within symbol size), where we see that the law (4.50) provides a statistically acceptable description of the data. The resulting estimation of the transition critical point is

$$\left(\frac{J}{U}\right)_c^{\theta=0} = 0.304 \pm 0.012, \tag{4.51}$$

which is in excellent agreement with the results of Ref. [28] as well as with previous theoretical and experimental estimations (see Sec. 2.2.2), despite the fact that our analysis uses rather small system sizes.

Given that the previous method is applicable for the case of $\theta = 0$, our aim now is to verify whether it gives valid results for $\theta \neq 0$. For this purpose, we will begin with small statistical angles, as for instance $\theta = 0.02\pi$ by following an analogous procedure to the latter one. Thus, we first select a set of values of J/U, for which $\tilde{D}_1$ is numerically obtained, corresponding to the crosses in the left panel of Fig. 4.13, and fitted to a Padé approximant, represented by solid lines in the same figure. The fit is differentiated for the purpose of estimating the $(J/U)^*$ value for which the derivative, whose value is represented, for each lattice size, in the right panel of the same figure. The uncertainties for $(J/U)^*$ are also shown in the plot, and correspond to standard uncertainty associated with the new spacing of the grid, being in this case $\sigma_{(J/U)} = \Delta_{(J/U)}/\sqrt{12} = 5 \times 10^{-3}/\sqrt{12}$. The specifications on the Padé fits are given, for each lattice size $L \in [5, 17]$, in Table 4.3.

We observe that the values of $(J/U)^*$ for $\theta = 0.02\pi$ follow a monotonic increase with L, in accordance with the behavior of the scaling law (4.50), which provides a statistically acceptable description of the data and the sought estimation for the critical point

$$\left(\frac{J}{U}\right)_c^{\theta=0.02\pi} = 0.293 \pm 0.046. \tag{4.52}$$

The latter result, within the uncertainty range, is in agreement with the expected ten-

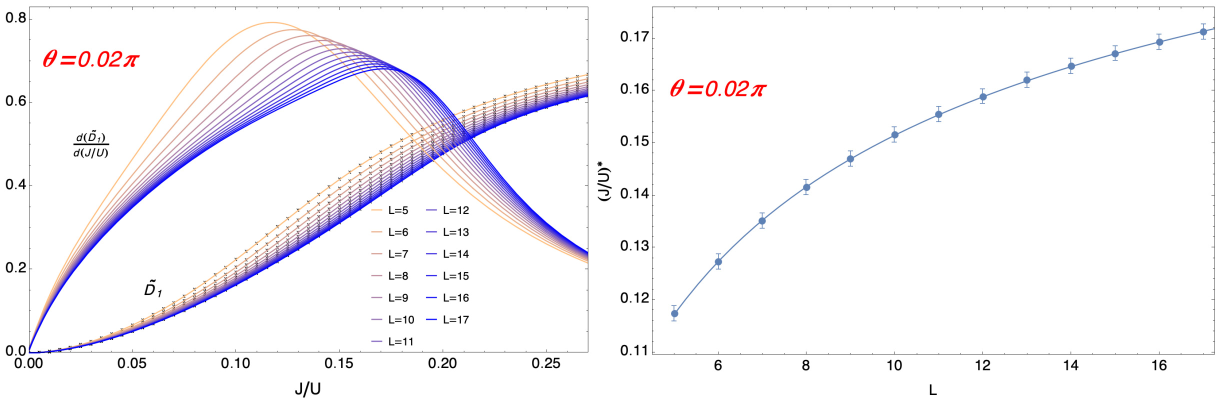

Figure 4.13: (Left panel) Numerically obtained $\tilde{D}_1$ (crosses) versus J/U for $L \in [5, 17]$ and $\theta = 0.02\pi$ together with the best Padé fits [Eq. (4.48)] (solid lines overlaying symbols) and their corresponding derivatives (solid lines), whose value has been scaled by the factor 0.2 for optimal visualization. (Right panel) Scaling of the position of the maximum of $\frac{d(\tilde{D}_1)}{d(J/U)}$ (dots) versus L for $\theta = 0.02\pi$, where the solid line corresponds to the fit to (4.50) with parameters $(J/U)_c = 0.293 \pm 0.046$, $b = 2.549 \pm 1.198$ and $l_q = -0.012 \pm 0.024$, yielding $\chi^2 = 0.044$.

$L = N$	m	n	Number of points	$(J/U)^*$	χ^2
5	4	5	57	0.117	1.082×10^{-8}
6	4	6	57	0.127	2.448×10^{-9}
7	4	6	57	0.135	3.773×10^{-9}
8	4	6	57	0.142	4.724×10^{-9}
9	4	6	57	0.147	4.895×10^{-9}
10	4	6	57	0.152	4.314×10^{-9}
11	4	6	57	0.156	3.319×10^{-9}
12	5	5	57	0.159	3.126×10^{-9}
13	4	6	57	0.162	1.643×10^{-9}
14	4	6	57	0.165	1.449×10^{-9}
15	4	6	57	0.167	1.769×10^{-9}
16	4	6	57	0.169	2.542×10^{-9}
17	4	6	57	0.171	3.654×10^{-9}

Table 4.3: Information on the Padé fits of Fig. 4.13, including the expansion orders $\{m, n\}$ and the position of the maximum $(J/U)^*$ of the fit first derivative.

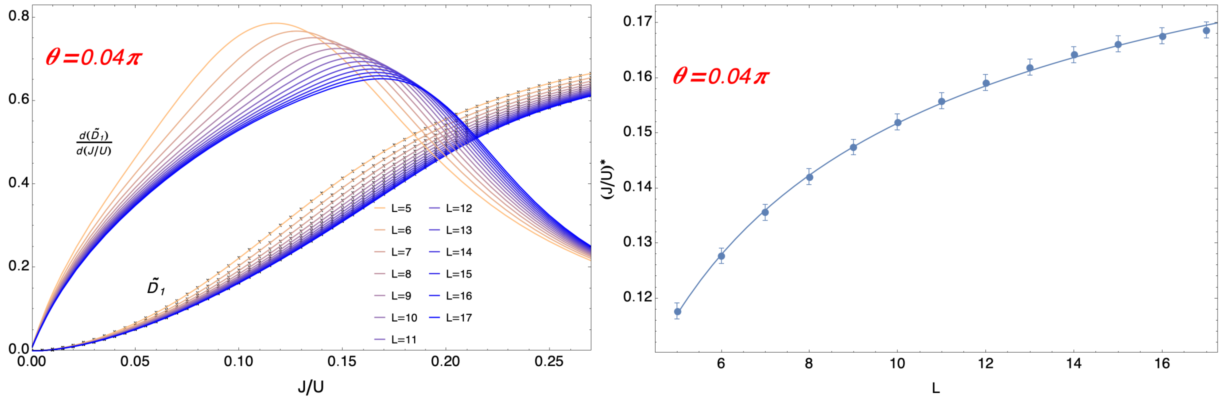

Figure 4.14: (Left panel) Numerically obtained $\tilde{D}_1$ (crosses) versus J/U for $L \in [5, 17]$ and $\theta = 0.04\pi$ together with the best Padé fits [Eq. (4.48)] (solid lines overlaying symbols) and their corresponding derivatives (solid lines), whose value has been scaled by the factor 0.2 for optimal visualization. (Right panel) Scaling of the position of the maximum of $\frac{d(\tilde{D}_1)}{d(J/U)}$ (dots) versus L for $\theta = 0.04\pi$, where the solid line corresponds to the fit to (4.50) with parameters $(J/U)_c = 0.244 \pm 0.022$, $b = 1.431 \pm 0.482$ and $l_q = 0.090 \pm 0.092$, yielding $\chi^2 = 1.287$.

dency, since for such small θ its value should be fairly similar to the one for $\theta = 0$.

After this point, we keep increasing the value of θ, and use $\theta = 0.04\pi$. The results for the numerical values of $\tilde{D}_1$ for lattice sizes $L \in [5, 17]$ as functions of J/U are depicted by crosses in the left panel of Fig. 4.14, accompanied by their corresponding Padé fits and the resulting derivatives in solid lines. The Padé fits allow us to obtain the tunneling strength giving a maximum increasing tendency of $\tilde{D}_1$, $(J/U)^*$, as in the previous cases. These values and their uncertainties (which coincide with those for $\theta = 0.02\pi$), as well as the fit to Eq. (4.50), are depicted in the right panel of Fig. 4.14. In this case, the $(J/U)^*$ data can also be reliably described by the proposed scaling law, and the estimated critical point reads

$$\left(\frac{J}{U}\right)_c^{\theta=0.04\pi} = 0.244 \pm 0.022. \tag{4.53}$$

One can see that, despite the uncertainty, the critical point seems to be emerging for decreasing values of the tunneling strength for increasing statistical angles, in contradistinction to what we would expect from previous studies [22].

We performed the previous analysis for increasing statistical angles, corresponding to $\theta = 0.06\pi$, 0.08π and 0.1π. Unfortunately, in these cases, estimations for the critical point cannot be obtained. In order to see this, we show the tunneling strength $(J/U)^*$ with their associated uncertainties as a function of L for each statistical angle in Fig. 4.15. We remark that, for $\theta \geq 0.02\pi$, the data uncertainties coincide. For low statistical angles, $\theta \in [0, 0.04\pi]$, the tendency for $(J/U)^*$ is in accordance with our expectations for the scaling [Eq. (4.50)], since it is monotonically increasing with L. On the other hand, greater values of θ show a deviation of this behavior, exhibiting a non-monotonic dependence on L. Indeed, an oscillatory tendency seems to emerge as the statistical angle is increased, which we believe could be a finite size effect.

In view of our results, we can conclude that within the range of system sizes available to exact diagonalization the method to estimate $(J/U)_c$ for anyons is restricted to very

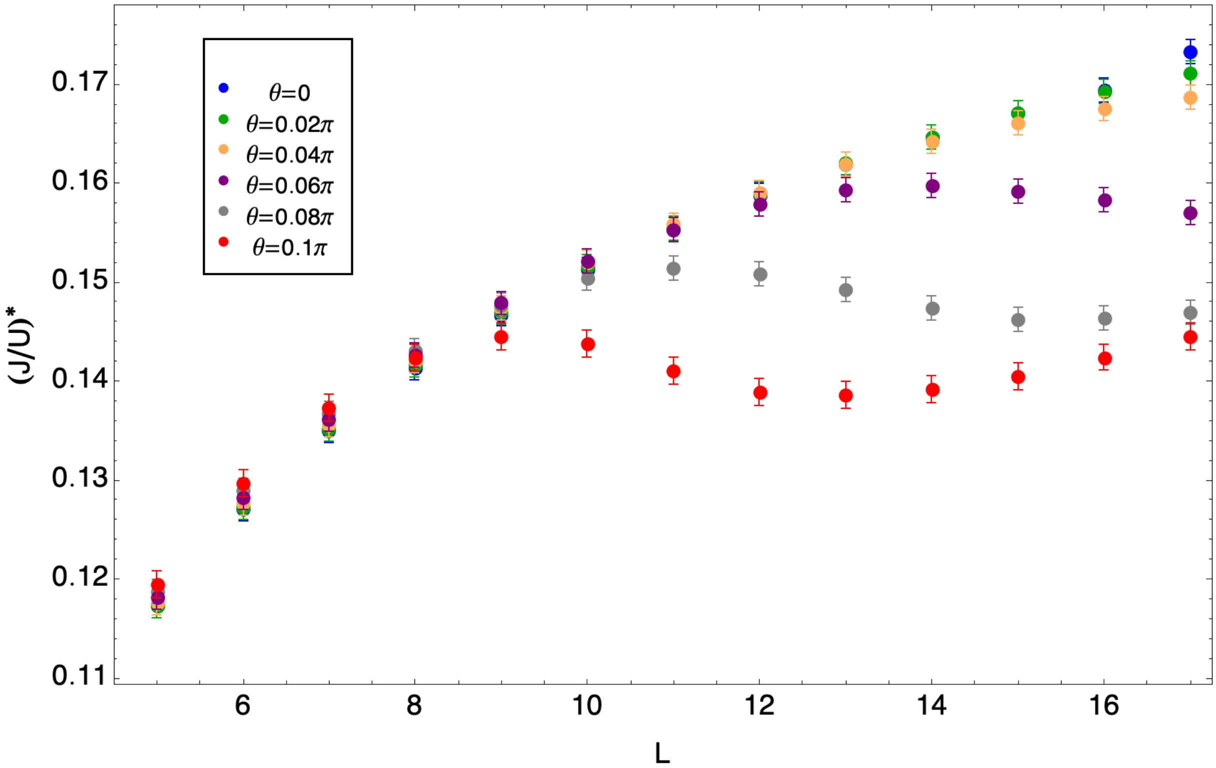

Figure 4.15: Position of the maximum for the derivative of $\tilde{D}_1$ as function of L with the corresponding uncertainties, for several values of the statistical angle θ.

small statistical angles. Other techniques would need to be used to calculate $\tilde{D}_q$ for larger systems in order to decide whether the observed behavior of $(J/U)^*$ is due to finite size effects or whether the anyonic system may follow a different scaling law to the one proposed in (4.50).

5 | Conclusions

In this work, we discussed several aspects regarding quantum many-body systems. First, we acquired the main notions necessary to understand the second quantization formalism, and use them to derive the Bose-Hubbard Hamiltonian. For the latter model, we described the two macroscopical phases that can be observed as functions of the ratio between the tunneling and interaction strength, as well as of the chemical potential.

We discussed the possibility of fractional statistics in dimensions lower than three, giving rise to anyons. Using a Jordan-Wigner transformation, we managed to obtain a modified version of the Bose-Hubbard model with occupation-dependent tunneling strengths that effectively represents the physics of the Anyonic-Hubbard model and that can be experimentally implemented.

We were able to obtain an analytical expression for the border delimiting the Mott insulator and superfluid phases in the Anyonic-Hubbard model by making use of the mean-field approximation.

Subsequently, we performed a series of numerical simulations for the modified Bose-Hubbard model (which we recall reproduces the physics of the Anyonic-Hubbard model). First, we used three different lattice sizes $L = 5$, $L = 10$ and $L = 15$ and, at fixed density $\nu = 1$, we obtain the values of the generalized fractal dimensions (GFDs) $\tilde{D}_1$, $\tilde{D}_2$ and $\tilde{D}_\infty$ as functions of the tunneling strength, for different statistical angles. For each statistical angle, we could observe that the generalized fractal dimensions $\tilde{D}_q$ of the ground state take different values as functions of q as L grows, providing strong evidence of the existence of multifractality in the ground state of the Anyonic-Hubbard model. For every lattice size L and q value, the behavior of the GFDs is the same as a function of J/U: They begin taking close to zero values in the strongly interacting regime, which are associated with a localized structure in Fock space of the ground state, and increase up to values closer to unity in the weakly interacting limit, leading to a noticeably delocalized structure in Fock space. The mentioned structure of the ground state in the different regimes was then verified by visualizing directly the intensities associated with the corresponding basis states.

Afterwards, we proceeded to derive an analytical expression for the ground state that is expected to be valid in the strongly interacting limit, using standard perturbation theory. The perturbative result was confirmed to give a fair description of the ground state for $J/U \lesssim 0.1$ for all statistical angles and system sizes considered. The derived form of the ground state allowed obtaining analytical expressions for the generalized fractal dimensions $\tilde{D}_1$ and $\tilde{D}_\infty$ in the strongly interacting regime. Both expressions are independent of θ up to second order in the tunneling strength, which confirms the fact that the Mott insulating phase persists for non vanishing statistical angle, since for $\theta = 0$

it is already known to exist.

The analysis of the evolution of $\tilde{D}_1$ with particle density ν and J/U, shown in the density plots for the $L = 7$, reveals that, for $\theta = 0$, a suppression of $\tilde{D}_1$ emerges at integer densities for $J/U \lesssim 0.1$, indicating a Mott insulating character. For larger tunneling strengths or non-integer densities, the generalized fractal dimensions reach larger values, indicating delocalization of the ground state which correlates with the existence of a superfluid phase. For non vanishing statistical angle $\theta = \pi/4, \pi/2, 3\pi/4, \pi$, a similar qualitative behavior is observed, which provides the first evidence that the existence of different macroscopic phases can be revealed by the structure in Fock space of the anyonic system's ground state. Furthermore, the data revealed that an increase of the statistical angle θ implies larger J/U values to achieve the same degree of delocalization at integer density, which suggests that the critical point $(J/U)_c$ of the transition should grow with θ.

When θ is changed continuously at fixed integer density, the analysis of $\tilde{D}_1$ as a function of statistical angle and tunneling strength shows that the estimations for the critical points reported in the literature for $\nu = 1$ follow qualitatively the $\tilde{D}_1$ isolines as θ varies, in accordance with our previous observations. However, for $\nu = 2$ the estimations for $(J/U)_c$ reported in Ref. [22] do not follow at all the tendency of the $\tilde{D}_1$ isolines. Surprisingly, the mean-field prediction for the critical point reproduces correctly the behavior of the $\tilde{D}_1$ isolines with θ. This suggests that a deeper analysis is required to verify whether the already proposed values of the critical point are correct, as well as if the mean-field approximation provides a better qualitative prediction of the transition in one-dimensional systems than expected.

Finally, we verified whether the structure of the ground state encodes information of the critical point of the Mott insulator to superfluid transition. Using the generalized fractal dimension $\tilde{D}_1$ at fixed integer density $\nu = 1$, we managed to do a scaling fit with the lattice size L of the (J/U) value at which a maximum of the derivative of $\tilde{D}_1$ could be found for the case $\theta = 0$. This allowed us to obtain a new and independent estimation of the critical point for the Bose-Hubbard system, $(J/U)_c^{\theta=0} = 0.304 \pm 0.012$, which is in perfect agreement with the results found in the literature. This analysis was extended to non-vanishing values of θ, leading to $(J/U)_c^{\theta=0.02\pi} = 0.293 \pm 0.046$, which follows the expected behavior within the uncertainty. However, for larger values of θ, a decreasing tendency for $(J/U)_c$ began to be observed, namely $(J/U)_c^{\theta=0.04\pi} = 0.244 \pm 0.022$, which does not agree with our expectations. In fact, it was seen that the evolution of the $(J/U)^*$ value with the system size L happens to be monotonically increasing with L only up to $\theta = 0.04\pi$, and afterwards, $\theta \in [0.06\pi, 0.1\pi]$, an oscillatory behavior starts to develop, which could be a finite size effect.

Therefore, for the range of system sizes accesible to exact diagonalization, the method based on the scaling of the $\tilde{D}_1$ derivative to estimate the critical point of the Mott insulator to superfluid phase transition in the anyonic system can only be applied for very small statistical angles. Larger systems would be needed to conclude whether this limitation is simply a finite size effect or a modification of the proposed scaling law for $(J/U)^*$ is necessary in the anyonic case.

Bibliography

[1] P. Coleman, *Introduction to Many-Body Physics* (Cambridge University Press, 2015).

[2] A. L. Fetter and J. D. Walecka, *Quantum Theory of Many-particle Systems*, 2003rd ed. (Dover Publications, Inc., 2003).

[3] I. Bloch, J. Dalibard, and S. Nascimbène, *Quantum simulations with ultracold quantum gases*, Nature Physics **8**, 267–276 (2012).

[4] I. Bloch, J. Dalibard, and W. Zwerger, *Many-body physics with ultracold gases*, Reviews of Modern Physics **80**, 885–964 (2008).

[5] C. Gross and I. Bloch, *Quantum simulations with ultracold atoms in optical lattices*, Science **357**, 995–1001 (2017).

[6] M. Greiner and S. Fölling, *Condensed-matter physics: optical lattices.*, Nature **453**, 736–738 (2008).

[7] G. Boéris, L. Gori, M. D. Hoogerland, A. Kumar, E. Lucioni, L. Tanzi, M. Inguscio, T. Giamarchi, C. D'Errico, G. Carleo, G. Modugno, and L. Sanchez-Palencia, *Mott transition for strongly interacting one-dimensional bosons in a shallow periodic potential*, Physical Review A **93**, 011601 (2016).

[8] M. Greiner, O. Mandel, T. Esslinger, T. W. Hänsch, and I. Bloch, *Quantum phase transition from a superfluid to a Mott insulator in a gas of ultracold atoms*, Nature **415**, 39–44 (2002).

[9] T. Stöferle, H. Moritz, C. Schori, M. Köhl, and T. Esslinger, *Transition from a strongly interacting 1d Superfluid to a Mott insulator*, Physical Review Letters **92**, 130403 (2004).

[10] W. S. Bakr, J. I. Gillen, A. Peng, S. Fölling, and M. Greiner, *A quantum gas microscope for detecting single atoms in a Hubbard-regime optical lattice*, Nature **462**, 74–77 (2009).

[11] C. Gross and W. Bakr, *Quantum gas microscopy for single atom and spin detection*, Nature Physics **17**, 1316 (2021).

[12] W. S. Bakr, A. Peng, M. E. Tai, R. Ma, J. Simon, J. I. Gillen, S. Folling, L. Pollet, and M. Greiner, *Probing the superfluid-to-Mott insulator transition at the single-atom level*, Science **329**, 547–550 (2010).

[13] D. Greif, M. F. Parsons, A. Mazurenko, C. S. Chiu, S. Blatt, F. Huber, G. Ji, and M. Greiner, *Site-resolved imaging of a fermionic mott insulator*, Science **351**, 953–957 (2016).

[14] M. F. Parsons, A. Mazurenko, C. S. Chiu, G. Ji, D. Greif, and M. Greiner, *Site-resolved measurement of the spin-correlation function in the fermi-hubbard model*, Science **353**, 1253–1256 (2016).

[15] J. Kwan, P. Segura, Y. Li, S. Kim, A. V. Gorshkov, A. Eckardt, B. Bakkali-Hassani, and M. Greiner, *Realization of one-dimensional anyons with arbitrary statistical phase*, Science **386**, 1055–1060 (2024).

[16] S. Dhar, B. Wang, M. Horvath, A. Vashisht, Y. Zeng, M. B. Zvonarev, N. Goldman, Y. Guo, M. Landini, and H.-C. Nägerl, *Observing anyonization of bosons in a quantum gas*, Nature **642**, 53–57 (2025).

[17] F. Wilczek, *Quantum mechanics of fractional-spin particles*, Physical Review Letters **49**, 957–959 (1982).

[18] J. M. Leinaas and J. Myrheim, *On the theory of identical particles*, Il Nuovo Cimento B Series 11 **37**, 1–23 (1977).

[19] G. S. Canright and S. M. Girvin, *Fractional statistics: Quantum possibilities in two dimensions*, Science **247**, 1197–1205 (1990).

[20] M. Greiter and F. Wilczek, *Fractional statistics*, Annual Review of Condensed Matter Physics **15**, 131–157 (2024).

[21] F. D. M. Haldane, *"Fractional statistics" in arbitrary dimensions: A generalization of the Pauli principle*, Physical Review Letters **67**, 937–940 (1991).

[22] J. Arcila-Forero, R. Franco, and J. Silva-Valencia, *Critical points of the anyon-Hubbard model*, Physical Review A **94**, 013611 (2016).

[23] T. Keilmann, S. Lanzmich, I. McCulloch, and M. Roncaglia, *Statistically induced phase transitions and anyons in 1d optical lattices*, Nature Communications **2**, 361 (2011).

[24] F. Liu, J. R. Garrison, D.-L. Deng, Z.-X. Gong, and A. V. Gorshkov, *Asymmetric particle transport and light-cone dynamics induced by anyonic statistics*, Physical Review Letters **121**, 250404 (2018).

[25] F. Lange, S. Ejima, and H. Fehske, *Strongly repulsive anyons in one dimension*, Physical Review A **95**, 063621 (2017).

[26] D. J. Luitz, F. Alet, and N. Laflorencie, *Universal behavior beyond multifractality in quantum many-body systems*, Physical Review Letters **112**, 057203 (2014).

[27] J. Lindinger, *Multifractal properties of the ground state of the Bose-Hubbard model*, Msc thesis, Albert-Ludwigs-Universität Freiburg (2017).

[28] J. Lindinger, A. Buchleitner, and A. Rodríguez, *Many-body multifractality throughout bosonic superfluid and Mott insulator phases*, Physical Review Letters **122**, 106603 (2019).

[29] L. Pausch, E. G. Carnio, A. Rodríguez, and A. Buchleitner, *Chaos and ergodicity across the energy spectrum of interacting bosons*, Physical Review Letters **126**, 150601 (2021).

[30] L. Pausch, *Eigenstate structure and quantum chaos in the Bose-Hubbard Hamiltonian*, Ph.D. thesis, Albert-Ludwigs-Universität Freiburg (2022).

[31] L. Pausch, E. G. Carnio, A. Buchleitner, and A. Rodríguez, *Chaos in the bose-hubbard model and random two-body hamiltonians*, New Journal of Physics **23**, 123036 (2021).

[32] L. Pausch, A. Buchleitner, E. G. Carnio, and A. Rodríguez, *Optimal route to quantum chaos in the Bose–Hubbard model*, Journal of Physics A: Mathematical and Theoretical **55**, 324002 (2022).

[33] P. M. Clavero and A. Rodríguez, *Characterization of the chaotic phase in the tilted Bose-Hubbard model*, Physical Review E **111**, 064214 (2025).

[34] K. Mayer, *Matter-wave Scattering from Interacting Bosons in Optical Lattices*, Ph.D. thesis, Albert-Ludwigs-Universität Freiburg (2014).

[35] M. P. A. Fisher, P. B. Weichman, G. Grinstein, and D. S. Fisher, *Boson localization and the superfluid-insulator transition*, Physical Review B **40**, 546–570 (1989).

[36] K. V. Krutitsky, *Ultracold bosons with short-range interaction in regular optical lattices*, Physics Reports **607**, 1–101 (2016).

[37] M. A. Cazalilla, R. Citro, T. Giamarchi, E. Orignac, and M. Rigol, *One dimensional bosons: From condensed matter systems to ultracold gases*, Reviews of Modern Physics **83**, 1405–1466 (2011).

[38] J. Carrasquilla, S. R. Manmana, and M. Rigol, *Scaling of the gap, fidelity susceptibility, and Bloch oscillations across the superfluid-to-Mott-insulator transition in the one-dimensional Bose-Hubbard model*, Physical Review A **87**, 043606 (2013).

[39] S. Ejima, H. Fehske, and F. Gebhard, *Dynamic properties of the one-dimensional Bose-Hubbard model*, Europhysics Letters **93**, 30002 (2011).

[40] R. Ma, M. E. Tai, P. M. Preiss, W. S. Bakr, J. Simon, and M. Greiner, *Photon-assisted tunneling in a biased strongly correlated bose gas*, Physical Review Letters **107**, 095301 (2011).

[41] C. Weitenberg and J. Simonet, *Tailoring quantum gases by floquet engineering*, Nature Physics **17**, 1342–1348 (2021).

[42] S. Balay, S. Abhyankar, M. Adams, S. Benson, J. Brown, P. Brune, K. Buschelman, E. Constantinescu, L. Dalcin, A. Dener, V. Eijkhout, J. Faibussowitsch, W. Gropp, V. Hapla, T. Isaac, P. Jolivet, D. Karpeev, D. Kaushik, M. Knepley, F. Kong, S. Kruger, D. May, L. McInnes, R. Mills, L. Mitchell, T. Munson, J. Roman, K. Rupp, P. Sanan, J. Sarich, B. Smith, S. Zampini, H. Zhang, and J. Zhang, *PETSc/TAO Users Manual (Rev. 3.20)*, Tech. Rep. (Argonne National Laboratory (ANL), 2023).

[43] V. Hernandez, J. E. Roman, and V. Vidal, *Slepc: A scalable and flexible toolkit for the solution of eigenvalue problems*, ACM Transactions on Mathematical Software **31**, 351–362 (2005).

A | Anyonic-Hubbard Hamiltonian in terms of bosonic operators. Jordan-Wigner transformation.

In this Appendix we detail the process by which one can write the Anyonic-Hubbard Hamiltonian in terms of bosonic operators with occupation-dependent tunneling strength, provided that it ensures the commutation relations given in Eq. (3.4).

We begin by proving that the Jordan-Wigner transformation in (3.12) leads to the desired anyonic algebra in Eq. (3.4). For this purpose, we will first calculate the product of the operators $\hat{a}_i \hat{a}_j^\dagger$. Taking $i < j$ and making use of the relation given by the Jordan-Wigner transformation,

$$\hat{a}_j = \hat{b}_j \exp\left(i\theta \sum_{i=1}^{j-1} \hat{n}_i\right) \tag{A.1}$$

and its self-adjoint

$$\hat{a}_j^\dagger = \exp\left(-i\theta \sum_{i=1}^{j-1} \hat{n}_i\right) \hat{b}_j^\dagger, \tag{A.2}$$

we have

$$\hat{a}_i \hat{a}_j^\dagger = \hat{b}_i \underbrace{\exp\left(i\theta \sum_{k=1}^{i-1} \hat{n}_k\right)}_{\equiv \mathrm{A}} \underbrace{\exp\left(-i\theta \sum_{s=1}^{j-1} \hat{n}_s\right)}_{\equiv \mathrm{B}} \hat{b}_j^\dagger = \hat{b}_i \; e^A e^B \; \hat{b}_j^\dagger. \tag{A.3}$$

Recall the Baker–Campbell–Hausdorff (BCH) formula, which states

$$e^X e^Y = e^Z, \quad \text{with } Z = X + Y + \frac{1}{2}[X,Y] + \frac{1}{12}[X,[X,Y]] + ... \,. \tag{A.4}$$

According to the latter expression, and since the bosonic number operators $\hat{n}_i$ commute, one has $e^A e^B = e^{A+B}$. Thus,

$$\hat{a}_i \hat{a}_j^\dagger = \hat{b}_i \; e^{A+B} \; \hat{b}_j^\dagger = \hat{b}_i \exp\left[i\theta \left(\sum_{k=1}^{i-1} \hat{n}_k - \sum_{s=1}^{j-1} \hat{n}_s\right)\right] \hat{b}_j^\dagger. \tag{A.5}$$

Since we have taken $i < j$, the terms inside the exponential will cancel up to the $i-$th position. Thus,

$$\hat{a}_i\hat{a}_j^\dagger = \hat{b}_i \; e^{A+B} \; \hat{b}_j^\dagger = \hat{b}_i \exp\left[i\theta\left(-\sum_{k=i}^{j-1}\hat{n}_k\right)\right]\hat{b}_j^\dagger = \hat{b}_i \; e^{-\hat{n}_i}e^{-\sum_{k=i+1}^{j-1}i\theta\hat{n}_k} \; \hat{b}_j^\dagger, \tag{A.6}$$

where we have separated the exponential of the terms $k = i$ from the rest, and we have used the BCH formula again. Because number operators always commute, one can commute the two exponentials,

$$\hat{a}_i\hat{a}_j^\dagger = \hat{b}_i \; e^{-\sum_{k=i+1}^{j-1}i\theta\hat{n}_k}e^{-i\theta\hat{n}_i} \; \hat{b}_j^\dagger, \tag{A.7}$$

At this point, one can see that, since the index k is always larger than i, and the index i is lower than j, the bosonic commutation relations lead to $[\hat{n}_i, \hat{b}_j^\dagger] = [\hat{n}_k, \hat{b}_i] = 0$, and the creation and annihilation operators commute with the exponentials multiplying them. Consequently, our expression can be rewritten as

$$\hat{a}_i\hat{a}_j^\dagger = e^{-\sum_{k=i+1}^{j-1}i\theta\hat{n}_k} \; \hat{b}_i\hat{b}_j^\dagger \; e^{-i\theta\hat{n}_i}. \tag{A.8}$$

With analogous reasonings, we calculate $\hat{a}_j^\dagger\hat{a}_i$. Using the Jordan-Wigner relation,

$$\hat{a}_j^\dagger\hat{a}_i = \underbrace{\exp\left(-i\theta\sum_{s=1}^{j-1}\hat{n}_s\right)}_{\equiv \mathrm{C}}\hat{b}_j^\dagger\hat{b}_i \underbrace{\exp\left(i\theta\sum_{k=1}^{i-1}\hat{n}_k\right)}_{\equiv \mathrm{D}}\hat{b}_j^\dagger = \; e^{C} \; \hat{b}_j^\dagger\hat{b}_i \; e^{D}. \tag{A.9}$$

Since the index s takes values always lower than j and k is always lower than i, one can commute each of the exponentials with the operators they are accompanied by, obtaining

$$\hat{a}_j^\dagger\hat{a}_i = \hat{b}_j^\dagger \; e^{C}e^{D} \; \hat{b}_i. \tag{A.10}$$

The BCH formula indicates that the product of exponentials $e^C e^D$ equals e^{C+D}, so that

$$\hat{a}_j^\dagger\hat{a}_i = \hat{b}_j^\dagger \; \exp\left(-i\theta\sum_{s=1}^{j-1}\hat{n}_s + i\theta\sum_{k=1}^{i-1}\hat{n}_k\right)\hat{b}_i, \tag{A.11}$$

where the terms in the argument of the exponential cancel out up to the $i-$th term, and thus

$$\hat{a}_j^\dagger\hat{a}_i = \hat{b}_j^\dagger \; \exp\left(-i\theta\sum_{k=i}^{j-1}\hat{n}_k\right)\hat{b}_i = \hat{b}_j^\dagger \; e^{-i\theta\hat{n}_i}e^{-i\theta\sum_{k=i+1}^{j-1}\hat{n}_k}\hat{b}_i. \tag{A.12}$$

Again, since i and k are always lower than j, the operators $\hat{n}_i$ and $\hat{n}_k$ commute with $\hat{b}_j^\dagger$. Thus, the product of exponentials and $\hat{b}_j^\dagger$ can be commuted,

$$\hat{a}_j^\dagger\hat{a}_i = e^{-i\theta\hat{n}_i}e^{-i\theta\sum_{k=i+1}^{j-1}\hat{n}_k} \; \hat{b}_j^\dagger\hat{b}_i, \tag{A.13}$$

and the two exponentials can be interchanged,

$$\hat{a}_j^\dagger\hat{a}_i = e^{-i\theta\sum_{k=i+1}^{j-1}\hat{n}_k}e^{-i\theta\hat{n}_i} \; \hat{b}_j^\dagger\hat{b}_i. \tag{A.14}$$

Multiplying the latter expression by $f(\theta) \equiv e^{-i\theta \; \mathrm{sgn}(j-i)}$, which in the present case where

$i < j$, equals to $e^{-i\theta}$, one obtains

$$e^{-i\theta}\hat{a}_j^\dagger \hat{a}_i = e^{-i\theta} e^{-i\theta \sum_{k=i+1}^{j-1} \hat{n}_k} e^{-i\theta \hat{n}_i}\ \hat{b}_j^\dagger \hat{b}_i = e^{-i\theta \sum_{k=i+1}^{j-1} \hat{n}_k} e^{-i\theta(\hat{n}_i+1)}\ \hat{b}_j^\dagger \hat{b}_i, \tag{A.15}$$

where we used that $e^{i\theta}$ is just a phase and thus commutes with all operators.

Bringing back the result obtained in (A.8), we can calculate the result of $\hat{a}_i\hat{a}_j^\dagger - f(\theta)\hat{a}_j^\dagger \hat{a}_i$,

$$\hat{a}_i\hat{a}_j^\dagger - f(\theta)\hat{a}_j^\dagger \hat{a}_i = e^{-i\theta \sum_{k=i+1}^{j-1} \hat{n}_k}\ \hat{b}_i \hat{b}_j^\dagger\ e^{-\hat{n}_i} - e^{-i\theta \sum_{k=i+1}^{j-1} \hat{n}_k} e^{-i\theta(\hat{n}_i+1)}\ \hat{b}_j^\dagger \hat{b}_i \tag{A.16}$$

$$= e^{-i\theta \sum_{k=i+1}^{j-1} \hat{n}_k} \left(\hat{b}_i \hat{b}_j^\dagger\ e^{-i\theta\hat{n}_i} - e^{-i\theta(\hat{n}_i+1)}\ \hat{b}_j^\dagger \hat{b}_i\right). \tag{A.17}$$

Using that $i < j$, one has that $[\hat{b}_i, \hat{b}_j^\dagger] = 0$, which allows rewriting the product $\hat{b}_i \hat{b}_j^\dagger\ e^{-i\theta\hat{n}_i}$ as

$$\hat{b}_i \hat{b}_j^\dagger\ e^{-i\theta\hat{n}_i} = \hat{b}_i e^{-i\theta\hat{n}_i} \hat{b}_j^\dagger = e^{-i\theta\hat{n}_i} e^{+i\theta\hat{n}_i} \hat{b}_i e^{-i\theta\hat{n}_i} \hat{b}_j^\dagger. \tag{A.18}$$

Now, one can make use of the operator expansion theorem,

$$e^X Y e^{-X} = Y + [X, Y] + \frac{1}{2!}[X, [X, Y]] + \frac{1}{3!}[X[X[X, Y]]] + ... \tag{A.19}$$

and of $[\hat{n}_i, \hat{b}_i] = -\hat{b}_i$ to rewrite the previous term as

$$\hat{b}_i \hat{b}_j^\dagger\ e^{-i\theta\hat{n}_i} = e^{-i\theta\hat{n}_i} \hat{b}_i e^{-i\theta} \hat{b}_j^\dagger = e^{-i\theta(\hat{n}_i+1)} \hat{b}_i \hat{b}_j^\dagger. \tag{A.20}$$

Using this result, one has

$$\hat{a}_i\hat{a}_j^\dagger - f(\theta)\hat{a}_j^\dagger \hat{a}_i = e^{-i\theta \sum_{k=i+1}^{j-1} \hat{n}_k} \left(e^{-i\theta(\hat{n}_i+1)} \hat{b}_i \hat{b}_j^\dagger - e^{-i\theta(\hat{n}_i+1)}\ \hat{b}_j^\dagger \hat{b}_i\right) \tag{A.21}$$

$$= e^{-i\theta \sum_{k=i+1}^{j-1} \hat{n}_k} e^{-i\theta(\hat{n}_i+1)} \left(\hat{b}_i \hat{b}_j^\dagger - \hat{b}_j^\dagger \hat{b}_i\right) \tag{A.22}$$

$$= e^{-i\theta \sum_{k=i+1}^{j-1} \hat{n}_k} e^{-i\theta(\hat{n}_i+1)}\ [\hat{b}_i, \hat{b}_j] = 0, \tag{A.23}$$

since $[\hat{b}_i, \hat{b}_j] = 0$. Thus, we have proven

$$\hat{a}_i\hat{a}_j^\dagger = e^{-i\theta} \hat{a}_j^\dagger \hat{a}_i, \tag{A.24}$$

which corresponds to the commutation relation (3.4a) for anyons for the case $i < j$.

A completely analogous procedure will lead us to

$$\hat{a}_i\hat{a}_j = e^{i\theta} \hat{a}_j \hat{a}_i, \tag{A.25}$$

for $i < j$, which obeys the anyonic commutation relation dictated by Eq. (3.4b).

For the case $i = j$, one can straightforwardly obtain the new form of $\hat{a}_j^\dagger \hat{a}_j$, which reads

$$\hat{a}_j^\dagger \hat{a}_j = \exp\left(-i\theta \sum_{i=1}^{j-1} \hat{n}_i\right) \hat{b}_j^\dagger \hat{b}_j \exp\left(i\theta \sum_{i=1}^{j-1} \hat{n}_i\right).$$

Again, since the sums only include up to $i = j$, the operators $\hat{b}_j^{(\dagger)}$ commute with the exponentials, leading to

$$\hat{a}_j^\dagger \hat{a}_j = \hat{b}_j^\dagger \hat{b}_j \exp\left(-i\theta \sum_{i=1}^{j-1} \hat{n}_i\right) \exp\left(i\theta \sum_{i=1}^{j-1} \hat{n}_i\right),$$

where $\hat{b}_j^\dagger \hat{b}_j = \hat{n}_j$, and due to the fact that number operators always commute, the product of the exponentials is the exponential of the sum,

$$\hat{a}_j^\dagger \hat{a}_j = \hat{n}_j e^0 = \hat{n}_j.$$

This is, $\hat{n}_j = \hat{a}_j^\dagger \hat{a}_j = \hat{b}_j^\dagger \hat{b}_j$

A completely analogous reason will derive the correct commutation relation for the case $j < i$, and thus will not be reproduced. This leaves us with one possibility left, $i = j$. In such case, the Jordan Wigner transformation leads to

$$\hat{a}_i \hat{a}_i^\dagger = \hat{b}_i \exp\left(i\theta \sum_{k=1}^{i-1} \hat{n}_k\right) \exp\left(-i\theta \sum_{s=1}^{i-1} \hat{n}_s\right) \hat{b}_i^\dagger = \hat{b}_i \exp\left(i\theta \sum_{k=1}^{i-1} \hat{n}_k - i\theta \sum_{s=1}^{i-1} \hat{n}_s\right) \hat{b}_i^\dagger. \tag{A.26}$$

Since $j = i$, all of the terms inside the exponential cancel out, giving

$$\hat{a}_i \hat{a}_i^\dagger = \hat{b}_i \hat{b}_i^\dagger. \tag{A.27}$$

Similarly, we obtain

$$\hat{a}_i^\dagger \hat{a}_i = \hat{b}_i \hat{b}_i, \tag{A.28}$$

and hence $[\hat{a}_i, \hat{a}_i^\dagger] = [\hat{b}_i, \hat{b}_i^\dagger] = \mathbb{I}$, in agreement with (3.4a).

Once we have demonstrated that the commutation relations are ensured by the Jordan-Wigner transformation, we are in a position to derive the expression of the AHH in terms of bosonic operators. We start from the Anyonic-Hubbard Hamiltonian,

$$\hat{H}^a = -J \sum_{j=1}^{L} (\hat{a}_j^\dagger \hat{a}_{j+1} + \hat{a}_{j+1}^\dagger \hat{a}_j) + \frac{U}{2} \sum_{j=1}^{L} \hat{a}_j^\dagger \hat{a}_j (\hat{a}_j^\dagger \hat{a}_j - 1), \tag{A.29}$$

and we use Eqs. (A.1) and (A.2) with $\hat{n}_j = \hat{b}_j^\dagger \hat{b}_j$.

Let us write the tunneling term first. For this purpose, we will obtain the product $\hat{a}_j^\dagger \hat{a}_{j+1}$ in terms of the bosonic operators:

$$\hat{a}_j^\dagger \hat{a}_{j+1} = \exp\left(-i\theta \sum_{i=1}^{j-1} \hat{n}_i\right) \hat{b}_j^\dagger \hat{b}_{j+1} \exp\left(i\theta \sum_{i=1}^{j} \hat{n}_i\right).$$

As the first exponential only includes sites from $i = 1$ to $i = j - 1$, it commutes with both $\hat{b}_j^\dagger$ and $\hat{b}_{j+1}$, since $[\hat{n}_l, \hat{b}_k] = -\delta_{lk} \hat{b}_l$ and $[\hat{n}_l, \hat{b}_k^\dagger] = \delta_{lk} \hat{b}_l^\dagger$. Therefore,

$$\hat{a}_j^\dagger \hat{a}_{j+1} = \hat{b}_j^\dagger \hat{b}_{j+1} \exp\left(-i\theta \sum_{i=1}^{j-1} \hat{n}_i\right) \exp\left(i\theta \sum_{i=1}^{j} \hat{n}_i\right).$$

Recalling $[\hat{n}_l, \hat{n}_k] = 0$ the BCH formula [Eq. (A.4)], one has

$$\hat{a}_j^\dagger \hat{a}_{j+1} = \hat{b}_j^\dagger \hat{b}_{j+1} \exp\left(-i\theta \sum_{i=1}^{j-1} \hat{n}_i \; + i\theta \sum_{i=1}^{j} \hat{n}_i\right) = \hat{b}_j^\dagger \hat{b}_{j+1} \exp\left(i\theta \hat{n}_j\right). \tag{A.30}$$

Taking the adjoint of the latter expression, one gets

$$\left(\hat{a}_j^\dagger \hat{a}_{j+1}\right)^\dagger = \hat{a}_{j+1}^\dagger \hat{a}_j = \exp\left(-i\theta \hat{n}_j\right) \hat{b}_{j+1}^\dagger \hat{b}_j. \tag{A.31}$$

Then, the tunneling term takes the form

$$\hat{H}_J = -J \sum_{j=1}^{L} (\hat{b}_j^\dagger \hat{b}_{j+1} e^{i\theta \hat{n}_j} + e^{-i\theta \hat{n}_j} \hat{b}_{j+1}^\dagger \hat{b}_j). \tag{A.32}$$

Recalling our previous results, the interaction term takes the same form in terms of the anyonic and bosonic operators. Consequently, the Hamiltonian can be rewritten as

$$\hat{H} = -J \sum_{j=1}^{L} (\hat{b}_j^\dagger \hat{b}_{j+1} e^{i\theta \hat{n}_j} + e^{-i\theta \hat{n}_j} \hat{b}_{j+1}^\dagger \hat{b}_j) + \frac{U}{2} \sum_{j=1}^{L} \hat{n}_j (\hat{n}_j - 1). \tag{A.33}$$

Therefore, it has been proven that the AHH can be written in terms of bosonic creation and annihilation operators and a tunneling strength that is dependent on the occupation number.

B | Perturbation theory calculation of the ground state

This Appendix presents the calculation of the ground state $|\phi_{gs}\rangle$ in perturbation theory, using the Hamiltonian

$$\frac{\hat{H}_\theta}{U} = \hat{H}_{\text{int}} - \tilde{J}\hat{H}_{\text{tun}} = \frac{1}{2}\sum_{j=1}^{L}\hat{n}_j(\hat{n}_j - 1) - \tilde{J}\sum_{j=1}^{L}(\hat{b}_j^\dagger\hat{b}_{j+1}e^{i\theta\hat{n}_j} + e^{-i\theta\hat{n}_j}\hat{b}_{j+1}^\dagger\hat{b}_j). \tag{B.1}$$

Recall that, up to second order in the tunneling strength $\tilde{J} \equiv J/U$, the ground state is given by

$$|\phi_{gs}\rangle = |\phi^{(0)}\rangle - \tilde{J}|\phi^{(1)}\rangle + \tilde{J}^2|\phi^{(2)}\rangle + \mathcal{O}(\tilde{J}^3), \tag{B.2}$$

where each of the contributions reads

$$|\phi^{(0)}\rangle = |\phi_0\rangle, \tag{B.3}$$

$$|\phi^{(1)}\rangle = \sum_{|\mathbf{n}\rangle\neq|\phi_0\rangle}\frac{\langle\mathbf{n}|\hat{H}_{\text{tun}}|\phi_0\rangle}{\epsilon_0 - \epsilon_\mathbf{n}}|\mathbf{n}\rangle, \tag{B.4}$$

$$\begin{aligned}|\phi^{(2)}\rangle = &\sum_{|\mathbf{n}\rangle\neq|\phi_0\rangle}\sum_{|\mathbf{k}\rangle\neq|\phi_0\rangle}\frac{\langle\mathbf{n}|\hat{H}_{\text{tun}}|\mathbf{k}\rangle\langle\mathbf{k}|\hat{H}_{\text{tun}}|\phi_0\rangle}{(\epsilon_0 - \epsilon_\mathbf{n})(\epsilon_0 - \epsilon_\mathbf{k})}|\mathbf{n}\rangle \\ &- \sum_{|\mathbf{n}\rangle\neq|\phi_0\rangle}\frac{\langle\mathbf{n}|\hat{H}_{\text{tun}}|\phi_0\rangle\langle\phi_0|\hat{H}_{\text{tun}}|\phi_0\rangle}{(\epsilon_\mathbf{n} - \epsilon_0)^2}|\mathbf{n}\rangle - \sum_{|\mathbf{n}\rangle\neq|\phi_0\rangle}\frac{1}{2}\frac{|\langle\phi_0|\hat{H}_{\text{tun}}|\mathbf{n}\rangle|^2}{(\epsilon_0 - \epsilon_\mathbf{n})^2}|\phi_0\rangle.\end{aligned} \tag{B.5}$$

In the latter expression, the states $|\mathbf{n}\rangle$ are the eigenstates of $\hat{H}_{\text{int}}$, whose corresponding eigenenergy is denoted by $\epsilon_\mathbf{n}$.

Recall that $|\phi_0\rangle$ denotes the ground state of the unperturbed Hamiltonian $\hat{H}_{\text{int}}$, which is already known to be the state with ν bosons per site,

$$|\phi_0\rangle = |\nu, \nu, ..., \nu\rangle, \tag{B.6}$$

and ϵ_0 is the corresponding eigenenergy of the Hamiltonian $\hat{H}_{\text{int}}$ of such ground state, $\epsilon_0 \equiv \langle\phi_0|\hat{H}_{\text{int}}|\phi_0\rangle = L\nu(\nu - 1)/2$.

Let us calculate the rest of the contributions order by order.

B.1 First-order correction

We calculate the first order contribution to the ground state, $|\phi^{(1)}\rangle$, following Eq. (B.4). For this purpose, first we calculate $\hat{H}_{\text{tun}}|\phi_0\rangle$,

$$
\begin{aligned}
\hat{H}_{\text{tun}}|\phi_0\rangle &= \sum_{j=1}^{L}(\hat{b}_j^\dagger \hat{b}_{j+1} e^{i\theta\hat{n}_j} + e^{-i\theta\hat{n}_j}\hat{b}_{j+1}^\dagger \hat{b}_j)|\phi_0\rangle \\
&= \sum_{j=1}^{L}(e^{i\theta\nu}\sqrt{\nu}\sqrt{\nu+1}|\phi_0\rangle_{-1_{j+1}}^{+1_j} + e^{-i\theta(\nu-1)}\sqrt{\nu}\sqrt{\nu+1}|\phi_0\rangle_{-1_j}^{+1_{j+1}}) \\
&= \sum_{j=1}^{L}(e^{i\theta\nu}\sqrt{\nu}\sqrt{\nu+1}|\phi_0\rangle_{-1_{j+1}}^{+1_j} + e^{-i\theta(\nu-1)}\sqrt{\nu}\sqrt{\nu+1}|\phi_0\rangle_{-1_{j-1}}^{+1_j}),
\end{aligned}
\tag{B.7}
$$

where we renamed indices making use of periodic boundary conditions to obtain the last line. Moreover, the notation $|\phi_0\rangle_{-m_k}^{+n_l}$ represents the state $|\phi_0\rangle$ with n added bosons in site l and m subtracted bosons from site k. Similarly, the state denoted by $|\phi_0\rangle_{-m_{k,r}}^{+n_{l,p}}$ will be the one in which m bosons have been subtracted from sites k and r and n bosons have been added in sites l and p, as defined in Eqs. (4.41) and (4.42).

In view of Eq. (B.7) one can see that, because Fock states with different occupation numbers in the same site are orthogonal, the only contributing $|\mathbf{n}\rangle$ states to the matrix element $\langle\mathbf{n}|\hat{H}_{\text{tun}}|\phi_0\rangle$ will be those of the form $|\phi_0\rangle_{-1_{j\pm1}}^{+1_j}$. These states share the same expectation value of $\hat{H}_{\text{int}}$,

$$
\begin{aligned}
{}_{+1_{j\pm1}}^{+1_j}\langle\phi_0|\hat{H}_{\text{int}}|\phi_0\rangle_{-1_{j\pm1}}^{+1_j} &= {}_{+1_{j\pm1}}^{+1_j}\langle\phi_0|\frac{1}{2}\sum_{j=1}^{L}\hat{n}_j(\hat{n}_j-1)|\phi_0\rangle_{-1_{j\pm1}}^{+1_j} \\
&= \frac{1}{2}\left(\sum_{j=1}^{L}n_j(n_j-1)\right){}_{+1_{j\pm1}}^{+1_j}\langle\phi_0|\phi_0\rangle_{-1_{j\pm1}}^{+1_j} \\
&= \frac{1}{2}\left(\sum_{j=1}^{L}n_j(n_j-1)\right) \\
&= \frac{1}{2}\left(\sum_{j=1}^{L-2}\nu(\nu-1)+(\nu+1)\nu+(\nu-1)(\nu-2)\right) \\
&= \frac{1}{2}\left((L-2)\nu(\nu-1)+(\nu+1)\nu+(\nu-1)(\nu-2)\right) \\
&= \frac{1}{2}\left(L\nu(\nu-1)+2\right) = \epsilon_0+1,
\end{aligned}
\tag{B.8}
$$

where $L\nu(\nu-1)/2 = \langle\phi_0|\hat{H}_{\text{int}}|\phi_0\rangle \equiv \epsilon_0$. Thus, the expression (B.4) yields

$$\begin{aligned}
|\phi^{(1)}\rangle =& \sum_{k=1}^{L} \frac{{}^{+1_k}_{+1_{k\pm1}}\langle\phi_0|\hat{H}_{\text{tun}}|\phi_0\rangle}{\epsilon_0-\epsilon_0-1}|\phi_0\rangle^{+1_k}_{-1_{k\pm1}} \\
=& -\sum_{k=1}^{L} {}^{+1_k}_{+1_{k\pm1}}\langle\phi_0|\sum_{j=1}^{L}(e^{i\theta\nu}\sqrt{\nu}\sqrt{\nu+1}|\phi_0\rangle^{+1_j}_{-1_{j+1}})|\phi_0\rangle^{+1_k}_{-1_{k\pm1}} \\
& -\sum_{k=1}^{L} {}^{+1_k}_{+1_{k\pm1}}\langle\phi_0|\sum_{j=1}^{L}(e^{-i\theta(\nu-1)}\sqrt{\nu}\sqrt{\nu+1}|\phi_0\rangle^{+1_j}_{-1_{j-1}})\ |\phi_0\rangle^{+1_k}_{-1_{k\pm1}} \\
=& -\sum_{k=1}^{L}\delta_{j,k}\sum_{j=1}^{L}(e^{i\theta\nu}\sqrt{\nu}\sqrt{\nu+1})|\phi_0\rangle^{+1_k}_{-1_{k+1}} \\
& -\sum_{k=1}^{L}\delta_{j,k}\sum_{j=1}^{L}(e^{-i\theta(\nu-1)}\sqrt{\nu}\sqrt{\nu+1})\ |\phi_0\rangle^{+1_k}_{-1_{k-1}} \\
=& -\sum_{j=1}^{L}\left(e^{i\theta\nu}\sqrt{\nu}\sqrt{\nu+1}|\phi_0\rangle^{+1_j}_{-1_{j-1}} + e^{-i\theta(\nu-1)}\sqrt{\nu}\sqrt{\nu+1}|\phi_0\rangle^{+1_j}_{-1_{j+1}}\right).
\end{aligned} \tag{B.9}$$

Consequently, the first-order contribution to the ground state reads

$$|\phi^{(1)}\rangle = -\sqrt{\nu}\sqrt{\nu+1}\sum_{j=1}^{L}\left(e^{i\theta\nu}|\phi_0\rangle^{+1_j}_{-1_{j-1}} + e^{-i\theta(\nu-1)}\ |\phi_0\rangle^{+1_j}_{-1_{j+1}}\right). \tag{B.10}$$

B.2 Second-order correction

In order to obtain the second-order correction to the ground state in perturbation theory, one must make use of Eq. (B.5), which consists of three terms.

One can anticipate that the second term will not contribute to the correction, since it is proportional to the matrix element $\langle\phi_0|\hat{H}_{\text{tun}}|\phi_0\rangle$ and, since $\hat{H}_{\text{tun}}|\phi_0\rangle$ gives a linear combination of states orthogonal to $|\phi_0\rangle$, one has that $\langle\phi_0|\hat{H}_{\text{tun}}|\phi_0\rangle = 0$.

Let us obtain the first term, which reads

$$|\phi_1^{(2)}\rangle \equiv \sum_{|\mathbf{n}\rangle\neq|\phi_0\rangle}\sum_{|\mathbf{k}\rangle\neq|\phi_0\rangle}\frac{\langle\mathbf{n}|\hat{H}_{\text{tun}}|\mathbf{k}\rangle\langle\mathbf{k}|\hat{H}_{\text{tun}}|\phi_0\rangle}{(\epsilon_0-\epsilon_{\mathbf{n}})(\epsilon_0-\epsilon_{\mathbf{k}})}|\mathbf{n}\rangle = \sum_{|\mathbf{n}\rangle\neq|\phi_0\rangle}\frac{\sum_{|\mathbf{k}\rangle\neq|\phi_0\rangle}\langle\mathbf{n}|\hat{H}_{\text{tun}}|\mathbf{k}\rangle\langle\mathbf{k}|\hat{H}_{\text{tun}}|\phi_0\rangle}{(\epsilon_0-\epsilon_{\mathbf{n}})(\epsilon_0-\epsilon_{\mathbf{k}})}|\mathbf{n}\rangle. \tag{B.11}$$

The presence of the matrix element $\langle\mathbf{k}|\hat{H}_{\text{tun}}|\phi_0\rangle$ restricts the possibilities for our states $|\mathbf{k}\rangle$ to those of the form $|\phi_0\rangle^{+1_j}_{-1_{j\pm1}}$, for which we already know that the expectation values of the interaction term are equal to ϵ_0+1. Hence, the coefficient $\epsilon_0-\epsilon_{\mathbf{k}}$ in the denominator can be directly substituted by -1.

Since we already know that $\langle\phi_0|\hat{H}_{\text{tun}}|\phi_0\rangle = 0$, the sum over $\mathbf{k}$ can be extended to the whole Fock space, since the $|\mathbf{k}\rangle = |\phi_0\rangle$ contribution will add a zero to the sum. Thus,

$$|\phi_1^{(2)}\rangle = -\sum_{|\mathbf{n}\rangle\neq|\phi_0\rangle}\frac{\sum_k\langle\mathbf{n}|\hat{H}_{\text{tun}}|\mathbf{k}\rangle\langle\mathbf{k}|\hat{H}_{\text{tun}}|\phi_0\rangle}{(\epsilon_0-\epsilon_{\mathbf{n}})}|\mathbf{n}\rangle, \tag{B.12}$$

but we know that Fock states verify Eq. (2.6), hence

$$|\phi_1^{(2)}\rangle = \sum_{|\mathbf{n}\rangle\neq|\phi_0\rangle} \frac{\langle \mathbf{n}|\hat{H}_{\text{tun}}^2|\phi_0\rangle}{(\epsilon_0-\epsilon_{\mathbf{n}})}|\mathbf{n}\rangle. \tag{B.13}$$

In order to determine the states $|\mathbf{k}\rangle$ contributing to the latter expression, we obtain the result of $\hat{H}_{\text{tun}}^2|\phi_0\rangle$,

$$\begin{aligned}\hat{H}_{\text{tun}}^2|\phi_0\rangle =&\sum_{i=1}^{L}\sum_{j=1}^{L}(\hat{b}_j^\dagger\hat{b}_{j+1}e^{i\theta\hat{n}_j}+e^{-i\theta\hat{n}_j}\hat{b}_{j+1}^\dagger\hat{b}_j)(\hat{b}_i^\dagger\hat{b}_{i+1}e^{i\theta\hat{n}_i}+e^{-i\theta\hat{n}_i}\hat{b}_{i+1}^\dagger\hat{b}_i)|\phi_0\rangle \\ =&\sum_{j,i=1}^{L}(\hat{b}_j^\dagger\hat{b}_{j+1}e^{i\theta\hat{n}_j}\hat{b}_i^\dagger\hat{b}_{i+1}e^{i\theta\hat{n}_i}+\hat{b}_j^\dagger\hat{b}_{j+1}e^{i\theta\hat{n}_j}e^{-i\theta\hat{n}_i}\hat{b}_{i+1}^\dagger\hat{b}_i \\ &+e^{-i\theta\hat{n}_j}\hat{b}_{j+1}^\dagger\hat{b}_j\hat{b}_i^\dagger\hat{b}_{i+1}e^{i\theta\hat{n}_i}+e^{-i\theta\hat{n}_j}\hat{b}_{j+1}^\dagger\hat{b}_je^{-i\theta\hat{n}_i}\hat{b}_{i+1}^\dagger\hat{b}_i)|\phi_0\rangle.\end{aligned} \tag{B.14}$$

At this point, one can rename some indices to rewrite the latter expression as

$$\begin{aligned}\hat{H}_{\text{tun}}^2|\phi_0\rangle =& \sum_{j,i=1}^{L}(\hat{b}_j^\dagger\hat{b}_{j+1}e^{i\theta\hat{n}_j}\hat{b}_i^\dagger\hat{b}_{i+1}e^{i\theta\hat{n}_i}+\hat{b}_j^\dagger\hat{b}_{j+1}e^{i\theta\hat{n}_j}e^{-i\theta\hat{n}_i}\hat{b}_{i+1}^\dagger\hat{b}_i \\ &+e^{-i\theta\hat{n}_i}\hat{b}_{i+1}^\dagger\hat{b}_i\hat{b}_j^\dagger\hat{b}_{j+1}e^{i\theta\hat{n}_j}+e^{-i\theta\hat{n}_j}\hat{b}_{j+1}^\dagger\hat{b}_je^{-i\theta\hat{n}_i}\hat{b}_{i+1}^\dagger\hat{b}_i)|\phi_0\rangle.\end{aligned} \tag{B.15}$$

Now, we proceed to write each term of the sum depending on the relation between the indices i and j.

- Case $i=j$

$$\begin{aligned}&\sum_{j=1}^{L}(\hat{b}_j^\dagger\hat{b}_{j+1}e^{i\theta\hat{n}_j}\hat{b}_j^\dagger\hat{b}_{j+1}e^{i\theta\hat{n}_j}+\hat{b}_j^\dagger\hat{b}_{j+1}e^{i\theta\hat{n}_j}e^{-i\theta\hat{n}_j}\hat{b}_{j+1}^\dagger\hat{b}_j \\ &\quad+e^{-i\theta\hat{n}_j}\hat{b}_{j+1}^\dagger\hat{b}_j\hat{b}_j^\dagger\hat{b}_{j+1}e^{i\theta\hat{n}_j}+e^{-i\theta\hat{n}_j}\hat{b}_{j+1}^\dagger\hat{b}_je^{-i\theta\hat{n}_j}\hat{b}_{j+1}^\dagger\hat{b}_j)|\phi_0\rangle \\ &=\sum_{j=1}^{L}(\hat{b}_j^\dagger\hat{b}_{j+1}e^{i\theta\hat{n}_j}\hat{b}_j^\dagger\hat{b}_{j+1}e^{i\theta\hat{n}_j}+\hat{n}_j\hat{b}_{j+1}\hat{b}_{j+1}^\dagger \\ &\quad+e^{-i\theta\hat{n}_j}\hat{n}_{j+1}\hat{b}_j\hat{b}_j^\dagger e^{i\theta\hat{n}_j}+e^{-i\theta\hat{n}_j}\hat{b}_{j+1}^\dagger\hat{b}_je^{-i\theta\hat{n}_j}\hat{b}_{j+1}^\dagger\hat{b}_j)|\phi_0\rangle \\ &=\sum_{j=1}^{L}e^{i\theta(2\nu+1)}\sqrt{\nu(\nu+1)(\nu-1)(\nu+2)}|\phi_0\rangle_{-2_{j+1}}^{+2_j} \\ &\quad+\sum_{j=1}^{L}e^{-i\theta(2\nu-3)}\sqrt{\nu(\nu+1)(\nu-1)(\nu+2)}|\phi_0\rangle_{-2_j}^{+2_{j+1}} \\ &\quad+\sum_{j=1}^{L}2\nu(\nu+1)|\phi_0\rangle,\end{aligned} \tag{B.16}$$

where, when required, we made use of the commutation relations in Eqs. (2.11).

- Case $i=j+1$

$$\sum_{j=1}^{L}(\hat{b}_j^\dagger\hat{b}_{j+1}e^{i\theta\hat{n}_j}\hat{b}_{j+1}^\dagger\hat{b}_{j+2}e^{i\theta\hat{n}_{j+1}}+\hat{b}_j^\dagger\hat{b}_{j+1}e^{i\theta\hat{n}_j}e^{-i\theta\hat{n}_{j+1}}\hat{b}_{j+2}^\dagger\hat{b}_{j+1}$$
$$+e^{-i\theta\hat{n}_{j+1}}\hat{b}_{j+2}^\dagger\hat{b}_{j+1}\hat{b}_j^\dagger\hat{b}_{j+1}e^{i\theta\hat{n}_j}+e^{-i\theta\hat{n}_j}\hat{b}_{j+1}^\dagger\hat{b}_je^{-i\theta\hat{n}_{j+1}}\hat{b}_{j+2}^\dagger\hat{b}_{j+1})|\phi_0\rangle$$
$$=\sum_{j=1}^{L}e^{i\theta(2\nu)}(\nu+1)\sqrt{\nu(\nu+1)}|\phi_0\rangle^{+1_j}_{-1_{j+2}}$$
$$+\sum_{j=1}^{L}e^{-i2\theta(\nu-1)}\nu\sqrt{\nu(\nu+1)}|\phi_0\rangle^{+1_{j+2}}_{-1_j}$$
$$+\sum_{j=1}^{L}e^{i\theta}(\nu+1)\sqrt{\nu(\nu-1)}\left(1+e^{i\theta}\right)|\phi_0\rangle^{+1_{j+2,j}}_{-2_{j+1}}. \tag{B.17}$$

- Case $i=j-1$

$$\sum_{j=1}^{L}(\hat{b}_j^\dagger\hat{b}_{j+1}e^{i\theta\hat{n}_j}\hat{b}_{j-1}^\dagger\hat{b}_je^{i\theta\hat{n}_{j-1}}+\hat{b}_j^\dagger\hat{b}_{j+1}e^{i\theta\hat{n}_j}e^{-i\theta\hat{n}_{j-1}}\hat{b}_j^\dagger\hat{b}_{j-1}$$
$$+e^{-i\theta\hat{n}_{j-1}}\hat{b}_j^\dagger\hat{b}_{j-1}\hat{b}_j^\dagger\hat{b}_{j+1}e^{i\theta\hat{n}_j}+e^{-i\theta\hat{n}_j}\hat{b}_{j+1}^\dagger\hat{b}_je^{-i\theta\hat{n}_{j-1}}\hat{b}_j^\dagger\hat{b}_{j-1})|\phi_0\rangle$$
$$=\sum_{j=1}^{L}e^{i\theta(2\nu-1)}\nu\sqrt{\nu(\nu+1)}|\phi_0\rangle^{+1_j}_{-1_{j+2}}$$
$$+\sum_{j=1}^{L}e^{i\theta}\nu\sqrt{(\nu+2)(\nu+1)}\left(1+e^{i\theta}\right)|\phi_0\rangle^{+2_{j+1}}_{-1_{j,j+2}}$$
$$+\sum_{j=1}^{L}e^{-i\theta(2\nu-1)}(\nu+1)\sqrt{\nu(\nu+1)}|\phi_0\rangle^{+1_{j+2}}_{-1_j}. \tag{B.18}$$

- Case $i\neq j$, $i\neq j\pm 1$

$$\sum_{j,i=1}^{L}(\hat{b}_j^\dagger\hat{b}_{j+1}e^{i\theta\hat{n}_j}\hat{b}_i^\dagger\hat{b}_{i+1}e^{i\theta\hat{n}_i}+\hat{b}_j^\dagger\hat{b}_{j+1}e^{i\theta\hat{n}_j}e^{-i\theta\hat{n}_i}\hat{b}_{i+1}^\dagger\hat{b}_i$$
$$+e^{-i\theta\hat{n}_i}\hat{b}_{i+1}^\dagger\hat{b}_i\hat{b}_j^\dagger\hat{b}_{j+1}e^{i\theta\hat{n}_j}+e^{-i\theta\hat{n}_j}\hat{b}_{j+1}^\dagger\hat{b}_je^{-i\theta\hat{n}_i}\hat{b}_{i+1}^\dagger\hat{b}_i)|\phi_0\rangle$$
$$=\sum_{j,i=1}^{L}(e^{i2\theta\nu}\nu(\nu+1)|\phi_0\rangle^{+1_{i,j}}_{-1_{i+1,j}}+\nu(\nu+1)e^{i\theta}|\phi_0\rangle^{+1_{i+1,j}}_{-1_{i,j+1}}+e^{-i2\theta(\nu-1)}|\phi_0\rangle^{+1_{i+1,j+1}}_{-1_{i,j}}. \tag{B.19}$$

Using the latter results, combined with the immediate calculation of the corresponding interaction expectation values, it is straightforward to check that

$$
\begin{aligned}
|\phi_1^{(2)}\rangle = &-\sum_{j=1}^{L} \frac{e^{i\theta(2\nu+1)}\nu(\nu+1)}{4}|\phi_0\rangle^{+2_j}_{-2_{j+1}} \\
&-\sum_{j=1}^{L} \frac{e^{-i\theta(2\nu-3)}\sqrt{\nu(\nu+1)(\nu+2)(\nu-1)}}{4}|\phi_0\rangle^{+2_{j+1}}_{-2_j} \\
&-\sum_{j=1}^{L} e^{i2\theta\nu}\sqrt{\nu(\nu+1)}\left((\nu+1)+e^{-i\theta}\nu\right)|\phi_0\rangle^{+1_j}_{-1_{j+2}} \\
&-\sum_{j=1}^{L} \frac{(\nu+1)\sqrt{\nu(\nu-1)}\left(e^{i\theta}+e^{i2\theta}\right)}{3}|\phi_0\rangle^{+1_{j,j+2}}_{-2_{j+1}} \\
&-\sum_{j=1}^{L} e^{-i\theta(2\nu-1)}\sqrt{\nu(\nu+1)}\left((\nu+1)+e^{-i\theta}\nu\right)|\phi_0\rangle^{-1_j}_{+1_{j+2}} \\
&-\sum_{j=1}^{L} \frac{\nu\sqrt{(\nu+2)(\nu+1)}\left(e^{i\theta}+e^{i2\theta}\right)}{3}|\phi_0\rangle^{+2_{j+1}}_{-1_{j,j+2}} \\
&-\sum_{j=1}^{L}\sum_{i\neq j,j\pm1} \frac{1}{2}e^{i2\theta\nu}\nu(\nu+1)|\phi_0\rangle^{-1_{j+1,i+1}}_{+1_{i,j}} \\
&-\sum_{j=1}^{L}\sum_{i\neq j,j\pm1} \frac{1}{2}e^{-i2\theta(\nu-1)}\nu(\nu+1)|\phi_0\rangle^{-1_{j,i}}_{+1_{i+1,j+1}} \\
&-\sum_{j=1}^{L}\sum_{i\neq j,j\pm1} \frac{1}{2}\nu(\nu+1)\left(2e^{i\theta}\right)|\phi_0\rangle^{-1_{j+1,i}}_{+1_{i+1,j}}.
\end{aligned} \tag{B.20}
$$

The third contribution to the second-order term is given by

$$
-\sum_{|\mathbf{n}\rangle\neq|\phi_0\rangle} \frac{1}{2}\frac{|\langle\phi_0|\hat{H}_{\mathrm{tun}}|\mathbf{n}\rangle|^2}{(\epsilon_0-\epsilon_{\mathbf{n}})^2}|\phi_0\rangle. \tag{B.21}
$$

In this case, one only needs to obtain the squared modulus of the coefficients in Eq. B.7, resulting in

$$
\begin{aligned}
-\sum_{|\mathbf{n}\rangle\neq|\phi_0\rangle} \frac{1}{2}\sum_{j=1}^{L}\frac{|\langle\phi_0|\hat{H}_{\mathrm{tun}}|\mathbf{n}\rangle|^2}{(\epsilon_0-\epsilon_{\mathbf{n}})^2}|\phi_0\rangle &= -\frac{1}{2}\left(|e^{i\theta}\nu\sqrt{\nu(\nu+1)}|^2+|e^{-i\theta(\nu-1)}\sqrt{\nu(\nu+1)}|^2\right)|\phi_0\rangle \\
&= -L\nu(\nu+1)|\phi_0\rangle.
\end{aligned} \tag{B.22}
$$

The combination of all the previous results lead to the final form of the ground state in perturbation theory,

$$
\begin{aligned}
|\phi_{gs}\rangle =& \Big[1 - \tilde{J}^2 \; L \; \nu(\nu+1)\Big] \, |\phi_0\rangle \\
&+ \tilde{J}\sqrt{\nu(\nu+1)} \sum_{j=1}^{L} \Big[e^{i\theta\nu} |\phi_0\rangle_{-1_{j+1}}^{+1_j} + e^{-i\theta(\nu-1)} |\phi_0\rangle_{-1_j}^{+1_{j+1}} \Big] \\
&+ \tilde{J}^2 \sum_{j=1}^{L} e^{i2\theta\nu} \sqrt{\nu(\nu+1)} \; [\; (\nu+1) + e^{-i\theta}\nu \;] |\phi_0\rangle_{-1_{j+2}}^{+1_j} \\
&+ \tilde{J}^2 \sum_{j=1}^{L} \frac{\sqrt{\nu(\nu+1)(\nu+2)(\nu-1)}}{4} \left(e^{i\theta(2\nu+1)} |\phi_0\rangle_{-2_{j+1}}^{+2_j} + e^{-i\theta(2\nu-3)} |\phi_0\rangle_{-2_j}^{+2_{j+1}} \right) \\
&+ \tilde{J}^2 \sum_{j=1}^{L} \frac{(\nu+1)\sqrt{\nu(\nu-1)}}{3} [e^{i\theta} + e^{i2\theta}] |\phi_0\rangle_{-2_{j+1}}^{+1_{j+2,j}} \\
&+ \tilde{J}^2 \sum_{j=1}^{L} e^{-i\theta(2\nu-1)} \sqrt{\nu(\nu+1)} [(1+e^{i\theta})\nu + 1] |\phi_0\rangle_{-1_j}^{+1_{j+2}} \\
&+ \tilde{J}^2 \sum_{j=1}^{L} \frac{\nu\sqrt{(\nu+1)(\nu+2)}}{3} [e^{i\theta} + e^{i2\theta}] |\phi_0\rangle_{-1_{j+2,j}}^{+2_{j+1}} \\
&+ \tilde{J}^2 \sum_{j=1}^{L} \frac{\nu(\nu+1)}{2} \sum_{i \neq j, j\pm1} \Big[e^{i2\theta\nu} |\phi_0\rangle_{-1_{j+1,i+1}}^{+1_{j,i}} + e^{-i2\theta(\nu-1)} |\phi_0\rangle_{-1_{j,i}}^{+1_{j+1,i+1}} + 2e^{i\theta} |\phi_0\rangle_{-1_{j+1,i}}^{+1_{j,i+1}} \Big] \\
&+ \mathcal{O}\left(\tilde{J}^3\right).
\end{aligned}
\tag{B.23}
$$

C | Numerical resources

In Tab. C.1, we indicate the computational resources required to calculate numerically, by exact diagonalization, the ground state of the modified Bose-Hubbard Hamiltonian [Eq.(3.13)] for different system sizes L at unit density, and where $\mathcal{N}$ denotes the dimensionality of Fock space. The code is written in Fortran 95 and makes use of the parallel libraries PETSc [42] and SLEPc [43] for long (64 bit) integers (due to the large values of $\mathcal{N}$). The code and the libraries were compiled with the Intel oneAPI (2025.0) compilers.

The execution took place in the HPC facilities provided by SCAYLE: Supercomputación Castilla y León (www.scayle.es/manual/es/hpc), financed by the European Regional Development Fund (ERDF), and the resources included in the table correspond to nodes with the Intel Shappire Rapids Architecture (2 Intel Xeon Platinum 8462Y processors, with 32×2 cores per node, operating frequency of 2.8 GH, and 1TB of RAM per node).

The code relies on MPI for parallel execution across multiple nodes, and the indicated execution times are typical running times to obtain the ground state for fixed system parameters under the condition $J/U \lesssim 1$ and any value of the statistical phase θ. For larger values of the relative tunneling strength J/U the running time may increase noticeably.

L	$\mathcal{N}$	Number of cores	Memory per core (MB)	Execution time (min)
11	352 716	1	1000	5
12	1 352 078	1	1600	5
13	5 200 300	4	3000	10
14	20 058 300	16	3000	10
15	77 558 760	32	6000	15
16	300 540 195	64	12 000	30
17	1 166 803 110	256	13 000	30
18	4 537 567 650	960	15 000	60

Table C.1: Computational resources required to obtain the ground state of Hamiltonian (3.13) for different L at unit density by exact diagonalization, using MPI and the libraries PETSc [42] and SLEPc [43].